AJUR

American Journal of
Undergraduate Research

Volume 19 | Issue 3 | December 2022

www.ajuronline.org

Print Edition ISSN 1536-4585
Online Edition ISSN 2375-8732

AJUR
American Journal of
Undergraduate Research

Volume 19 | Issue 3 | December 2022

American Journal of Undergraduate Research (AJUR) *is a national, independent, peer-reviewed, open-source, quarterly, multidisciplinary student research journal. Each manuscript of AJUR receives a DOI number. AJUR is archived by the US Library of Congress. AJUR was established in 2002, incorporated as a cheritable not-for-profit organization in 2018. AJUR is indexed internationally by EBSCO and Crossref with ISSNs of 1536-4585 (print) and 2375-8732 (web).*

Comparison of Genotypic and Phenotypic Predictions for Heavy Metal Resistance in *Salmonella enterica* and *Escherichia coli*

Jeevan Rivera-Díaz[a], *Haley Phillippi*[b], *Nyduta Mbogo*[c], *Erin M. Nawrocki*[c], *& Edward G. Dudley*[*c,d]

[a]*Department of Natural Sciences, University of Puerto Rico, Aguadilla, PR*
[b]*Department of Science and Mathematics, Mount Aloysius College, Cresson, PA*
[c]*Department of Food Science, The Pennsylvania State University, University Park, PA*
[d]*E. coli Reference Center, The Pennsylvania State University, University Park, PA*

https://doi.org/10.33697/ajur.2022.064

Students: jeevan.rivera@upr.edu, hmpst2@student.mtaloy.edu, nmm6190@psu.edu
Mentors: egd100@psu.edu, eqn5119@psu.edu*

ABSTRACT
Salmonella enterica and *Escherichia coli* are two pathogenic bacteria of worldwide importance that can infect the gastrointestinal tract. Contamination in the food supply chain is an area of concern. Animal feed may be supplemented with essential trace elements, which function as nutritional additives to promote growth & health and optimize production. Bacteria have acquired many metal resistance genes to adapt to the exposure of metals. In this study, our objectives were to evaluate in *S. enterica* and *E. coli*, the correlation between the resistance genotype and phenotype to certain heavy metals, and the ability of conjugative plasmids to transfer antimicrobial resistance genes (AMRGs) and heavy metal resistance genes (HMRGs). A total of 10 strains, five *S. enterica* and five *E. coli*, were used for this study. Minimal inhibitory concentrations (MICs) were determined for heavy metals: copper, silver, arsenic, and tellurite. The tested isolates showed resistance to copper (5/10; 50%), arsenic (7/10; 70%), and silver (9/10; 90%). Cohen's Kappa statistics were used to analyze genotype to phenotype agreements. Among the 10 strains sampled, the accordance between geno- and phenotypic heavy metal resistance was fair for copper (kappa = 0.4), none to slight for arsenic (kappa = 0.19) and tellurite (kappa = 0), and no agreement for silver (kappa = -0.19). The transfer of HMRGs was determined in a conjugation experiment performed for all five *Salmonella* strains as donors using mixed broth cultures. Transconjugants were obtained only from the genotypically tellurite-resistant strain PSU-3260, which yielded a transfer frequency of 10^{-3} transconjugants per donor. In such strain, the tellurite-resistant genes reside on an IncHI2-type plasmid that shares high DNA sequence identity with known HMRG-disseminating *Salmonella* plasmids. Our results indicated no considerable correlation between the geno- and phenotypic resistance towards heavy metals in the sampled *S. enterica* and *E. coli*. The necessity of research in this area is supported by the lack of standardized protocols and MIC clinical breakpoints for heavy metals.

KEYWORDS
Heavy metal; resistance; *Salmonella*; *E. coli*; agriculture; genotype; phenotype; MIC

INTRODUCTION

Salmonella enterica and *Escherichia coli* are two pathogenic bacteria of humans and animals that can infect the gastrointestinal tract. *E. coli* is a Gram-negative, facultative anaerobic bacillus found in the environment (including soil, water, and the gastrointestinal tract of warm-blooded animals), which can contaminate meat and produce. Though it is commonly part of the commensal intestinal flora, it can also be pathogenic, causing many diarrheal illnesses, including traveler's diarrhea and dysentery.[1] Shiga toxin-producing *E. coli* (STEC) is a pathotype of this species capable of causing bacillary dysentery, hemorrhagic colitis,[3] bloody diarrhea, hemolytic uremic syndrome (HUS), end-stage renal disease (ESRD), and even death.[2] STEC infections cause an estimated 265,000 illnesses, 3,600 hospitalizations, and about 30 deaths annually in the USA.[4]

S. enterica is a Gram-negative, facultative intracellular anaerobe of worldwide importance. Typically it is an orally acquired pathogen that can cause enteric fever, enterocolitis/diarrhea, and bacteremia, estimated to cause 1.3 billion disease cases annually.[5] Non-typhoidal *Salmonella* causes approximately 28% of foodborne illness-associated deaths.[6, 7] Also, it accounts for more than 93 million infections per year globally and over 1 million in the USA, thus being a leading cause of bacterial foodborne illness.[8]

Contamination in the food supply chain is an area of concern. Several outbreaks of *E. coli* and *Salmonella* arising from livestock have occurred in recent years. *E. coli* was responsible for an outbreak linked to ground beef which caused 209 reported cases in 2019.[9] Likewise, a backyard poultry-linked outbreak caused by *Salmonella* resulted in 1,135 illnesses, 273 hospitalizations, and two

deaths in 2021.[10] In the industry of commercial agriculture, heavy metals represent both mineral nutrients and potential contaminants.[11] Essential trace elements are commonly added to animal feed as nutritional additives to promote growth and health and optimize production.[11—14] These trace elements such as copper and zinc are required for hormone function, normal reproduction, vitamin synthesis, enzyme formation, and to support the integrity of the host immune system.[14] Yet, excessive exposure to undesirable levels of heavy metals damages the health of food-producing animals and the bioaccumulation of these metals could subsequently threaten consumers' health.[14] Apart from the heavy metals added intentionally, other metals such as mercury (Hg), lead (Pb), cadmium (Cd), and arsenic (As) occasionally contaminate animal feed.[14] Said animal feed contamination occurs through husbandry practices, soil ingestion, minor dietary ingredients, supplements, or spurious soil contamination in foliage.[15]

Bacteria have acquired many metal resistance genes through horizontal gene transfer and vertical evolution to adapt to the exposure of metals. [16, 17] There is co-resistance between resistance genes for antibiotics, metals,[14, 17, 18, 19] and disinfectants.[20, 21] Besides co-resistance (multiple resistance genes located on the same mobile element), co-selection of antimicrobial and heavy metal genes can also be mediated by cross-resistance (shared mechanisms of resistance), co-regulation (altered expression of resistance genes after exposure to toxic compounds), or biofilm formation.[14, 17, 18, 22, 23]

The growing evidence regarding antimicrobial resistance (AMR) co-selection among bacteria exposed to various heavy metals in animal diets has caused concern.[24, 25] The co-selection of genes providing resistance to heavy metals and antimicrobials of clinical importance, which pose a possible health hazard, requires further investigation.[17, 26] In addition, the correlation between genotypic and phenotypic resistance to heavy metals is not fully understood. Genotypic resistance can be screened, and most would assume that like AMR, there would be a correlation between geno- and phenotypic resistance. Yet, a better understanding of the correlation between genes and phenotypes will allow for better characterization of bacterial virulence factors. Additionally, the spread of resistance could be monitored by evaluating the plasmid transfer of these genes.

Therefore, in this study, our objectives were to evaluate in a small collection of *S. enterica* and *E. coli*: (1) the correlation between the presence of heavy metal resistance genes and the actual resistance to these metals; and (2) the ability of conjugative plasmids to transfer antimicrobial resistance genes (AMRGs) and heavy metal resistance genes (HMRGs).

MATERIALS AND METHODS

Bacterial strains and culture conditions

A total of 10 strains, five *Salmonella enterica* and five *Escherichia coli*, were used for this study (**Table 1**). These were selected from the NCBI Pathogen Detection database (*https://www.ncbi.nlm.nih.gov/pathogens*, accessed 4 October 2022). Strains were chosen upon availability and possession of resistance genes for the heavy metals in use. Whole genome sequencing (WGS), antimicrobial resistance (AMR), heavy metal resistance (HMR), and plasmid profiling were performed.[27] The presence of HMRGs was determined by analysis in the NCBI Pathogen Detection pipeline using the AMRFinderPlus tool with default parameters (*i.e.,* >90% identity and >50% coverage of the reference).[28]

Strains were maintained in 20% glycerol stocks at -80 ˚C for long-term storage and were routinely cultured in lysogeny broth (LB) and Mueller-Hinton (MH) agar at 37 ˚C. Sodium chloride was omitted from LB when supplemented with silver ($AgNO_3$), and so were their controls. Antibiotics were used at the following concentrations: nalidixic acid (30 μg/mL), chloramphenicol (12.5 μg/mL), kanamycin (25 μg/mL), ampicillin (50 μg/mL), and tetracycline (10 μg/mL). All media components were purchased from BD Difco (Franklin Lakes, NJ) and all chemicals from Millipore Sigma (St. Louis, MO) unless otherwise specified.

Heavy metal susceptibility testing and correlation analysis

All strains were cultured in MH broth overnight at 37 ˚C, then subcultured once and grown to mid-log phase. The bacterial suspension was diluted to 0.05 OD_{600} using MH broth. To determine the minimal inhibitory concentrations (MICs) for heavy metals, a standard broth microdilution procedure was conducted according to the Clinical and Laboratory Standards Institute,[29] with MH Broth and no-salt LB in an aerobic atmosphere. MH broth was supplemented separately with tellurite (Na_2TeO_3), copper ($CuSO_4$), and arsenic ($NaAsO_2$). Meanwhile, no-salt LB was supplemented only with silver ($AgNO_3$) since supplementing the MH broth with this metal caused the precipitation of such. MICs for silver, tellurite, and arsenic were done at two-fold dilutions with concentrations ranging from 0.016 to 8 mM. Copper MICs were done at two-fold dilutions from 0.063 to 32 mM. MICs were determined as the lowest concentration at which there was no visible growth after incubation for 24 hours at 37 ˚C. *S. enterica* reference strain LT2 was used as a benchmark to define the species' susceptibility towards heavy metals and to classify the test strains as resistant or susceptible.[12] DH5α, a common laboratory strain, was used as a reference for *E. coli*. This heavy metal susceptibility test was repeated with a pH adjustment performed on media containing silver, tellurite, and arsenic to pH 7.4, and copper to pH 7.2, using HCl and NaOH. Cohen's Kappa statistics were used to analyze genotype to phenotype agreements,[30] using Minitab Statistical Software (Version 17.1; 2010). Kappa coefficient values were interpreted as follows: ≤ 0 (no agreement),

0.01–0.20 (none to slight), 0.21–0.40 (fair), 0.41– 0.60 (moderate), 0.61–0.80 (substantial), and 0.81–1.00 (almost perfect agreement).[31] For the most part, upon the presence of a single resistance gene, the bacterial strains were interpreted as resistant. The exception was the presence of the gene *golT* in *Salmonella enterica* strains, which was excluded from the statistical analysis. Since the LT2 control and all *Salmonella enterica* strains have the same MIC values and genotype regarding this gene, it was not possible to establish with certainty that this gene confers resistance to copper in *Salmonella* strains. Likewise, the presence of a resistance operon was interpreted to confer the same level of resistance as a single resistance gene.

Conjugation assays

The transfer of HMRGs was determined in a conjugation experiment performed for all five *Salmonella* strains as donors using mixed broth cultures. Samples of the donors and recipient were grown overnight in MH broth. Overnight cultures were diluted to 0.1 OD_{600} using MH broth. 100 µL of the diluted donor were mixed with 1 mL of the diluted recipient culture. Two controls were made: one with donor only (100 µL of diluted donor culture and 1 mL of MH broth), and one with recipient only (1 mL of diluted recipient culture and 100 µL MH broth). They were incubated at 30 ˚C without shaking for 4 hours. Dilution series of mating mixtures were performed in 1X PBS through 10^9 and plated as follows: donor control on MH + heavy metal; recipient control on MH + Nal; and donor/recipient mixtures on MH + heavy metal + Nal to select for transconjugants. Plates were incubated at 37 ˚C overnight. The transfer efficiency was determined by dividing the transconjugant CFU/mL by donor CFU/mL. To confirm that the transconjugants were *E. coli*, PCR was used to screen the *uidA* gene, a traditional marker of *E. coli* lineages.[32] For the standard PCR reaction: 2.5 µL *Taq* ThermoPol buffer (New England Biolabs, Ipswich, MA), 0.5 µL dNTPs, 0.5 µL forward primer, 0.5 µL reverse primer, 1 µL template DNA, 0.125 µL *Taq* polymerase, and 19.9 µL nuclease-free water were used in a 25 µL reaction with primers uidA_F (5'-GCGTCTGTTGACTGGCAGGTGGTGG-3') and uidA_R (5' GTTGCCCGCTTCGAAACCAATGCCT-3').[33, 34] PCR was performed under the following cycle conditions: initial denaturation period of 95 ˚C for 30 seconds; 30 cycles of 95 ˚C for 30 seconds, 61 ˚C for 1 minute, 68 ˚C for 30 seconds; and a final extension for 5 minutes. The PCR products were separated in 1% agarose gel in TAE buffer. After staining with SYBR Safe (ThermoFisher Scientific, Waltham, MA), the gel was visualized under UV light. Cotransfer of AMRGs was assessed by plating. Selection was made on MH agar plates supplemented separately with chloramphenicol, kanamycin, ampicillin, and tetracycline. They were incubated for 24 hours at 37 ˚C.

Plasmid analysis

The predicted plasmid content of each strain was identified by analysis of its assembled genome contigs at the PlasmidFinder 2.1 webserver (*https://cge.cbs.dtu.dk/services/PlasmidFinder/*). Noting the precedent for conjugative IncHI2 plasmids in *Salmonella*,[34] and the successful transfer of tellurite resistance from PSU-3260 to *E. coli* DH5α, we chose the IncHI2 replicon in PSU-3260 for further study. The complete plasmid sequence of pSTM6-275 was downloaded from NCBI (NZ_CP019647.1) and was used as a database for local BLASTn search. All contigs of PSU-3260 were used as queries against this database, and those with significant identity to the pSTM6-275 plasmid were retained in a FASTA file. The sequences of pSTM6-275 and homologous PSU-3260 contigs were then used in the construction of a ring diagram by BRIG,[36] according to the software's standard settings.

RESULTS

Presence and prevalence of heavy metal resistance genes in Salmonella enterica and Escherichia coli

The five *S. enterica* strains were chosen from a collection of *Salmonella* isolates from wild birds, and the five *E. coli* strains were obtained from sequenced isolates deposited in the *E. coli* Reference Center (ECRC); isolates are listed in **Table 1**. Most *E. coli* strains were isolated from animals used as livestock, and most *Salmonella* strains were isolated from water birds (**Table 1**). Among the sampled *S. enterica* strains, 20 genes considered to confer heavy metal resistance were found under stress genotypes using the isolate browser from the NCBI Pathogen Detection database (*https://www.ncbi.nlm.nih.gov/pathogens*).

These heavy metal resistance genes included: for copper (*golT*, *pcoA, pcoB, pcoC, pcoD, pcoE, pco*R, *pcoS*); for silver (*silA, silB, silC, silE, silF, silP, sil*R. *silS*); for tellurite (*terD, terW, terZ);* and for arsenic (*arsD*) (**Table 1**). A total of 21 HMR genes were found among the sampled *E. coli* strains. These were: for copper (*pcoA, pcoB, pcoC, pcoD, pcoE, pco*R, *pcoS*); for silver (*silA, silB, silC, silE, silF, silP, sil*R, *silS*); for arsenic (*arsA, arsD, ars*R)*;* and for tellurite (*terD, terW, terZ*) (**Table 1**).

Genus & species	Strain	Serovar or Serotype	Isolation source	Heavy metal genes	Plasmid Inc-types	Isolate references
Salmonella enterica	PSU-3176	Typhimurium	Gut; Gallinule, Common (*Gallinula galeata*)	*golT, pcoABCDERS, silABCEFPRS*	IncFIA, IncFII, IncI1-I(Alpha)	Fu *et al.,* 2021
Salmonella enterica	PSU-3260	Typhimurium	Dowitcher, Long billed (*Limnodromus scolopaceus*)	*golT, terDWZ*	IncHI2, IncHI2A	Fu *et al.,* 2021
Salmonella enterica	PSU-3373	Montevideo	Owl, Snowy (*Bubo scandiacus*) colon	*golT, arsD*	IncC	Fu *et al.,* 2021
Salmonella enterica	PSU-3384	Schwarzengrun	Gull, Ring-billed (*Larus delawarensis*) colon	*golT, pcoABCDERS, silABCEFPRS*	Col(pHAD28)	Fu *et al.,* 2021
Salmonella enterica	PSU-3390	Saintpaul	Gull, Ring-billed (*Larus delawarensis*) colon	*golT, silABCEFPRS*	IncFIB(K), IncN	Fu *et al.,* 2021
Escherichia coli	PSU-4439	O15:H45	Chicken	*pcoABCDERS, silABCEFPRS*	IncFIA, IncFIB(AP001918), IncFII, IncFII(pHN7A8), IncI1-I(Alpha), IncX4	PDT001079836.1*****
Escherichia coli	PSU-4474	O73:H19	Pig, (Porcine)	*arsADR, pcoABCDERS, silABCEFPRS*	Col(pHAD28), IncFIA(HI1), IncHI1A, IncHI1B(R27)	PDT001079841.1*****
Escherichia coli	PSU-4512	O8:H19	Avian	/	Col(MG828), IncI1-I(Alpha)	PDT001079838.1*
Escherichia coli	PSU-4521	O9:H30	Cow, (Bovine)	*copABCDERS, silABCEFPRS*	IncFIB(AP001918), IncFIC(FII), IncY	PDT001079821.1*****
Escherichia coli	PSU-4612	O157:H7	Cow, (Bovine)	*terDWZ*	IncFIA, IncFIB(AP001918), IncFII	PDT001079829.1*

/No heavy metal resistance genes found.
*Accession number from the NCBI Pathogen Detection Isolate Browser.

Table 1. List of characteristics from isolated bacterial strains.

Most strains exhibited the simultaneous presence of resistance genes for copper and silver (50%; 5/10) (**Figure 1**). Strain PSU-4474 had resistance genes for three metals (copper, arsenic, and silver), and strain PSU-4612 carried resistance genes for one metal (tellurite), whilst only strain PSU-4512 lacked detectable HMRGs (**Table 3**). Copper resistance-conferring genes were the most widespread among both bacterial species (80%; 8/10). Meanwhile, *arsA* and *arsR* genes had the lowest prevalence (10%; 1/10), present only in *E. coli* strain PSU-4474 (**Figure 2 & Table 3**). Additionally, *arsD* and all tellurite resistance-conferring genes were observed at a low frequency of occurrence (20%; 2/10) (**Figure 2**).

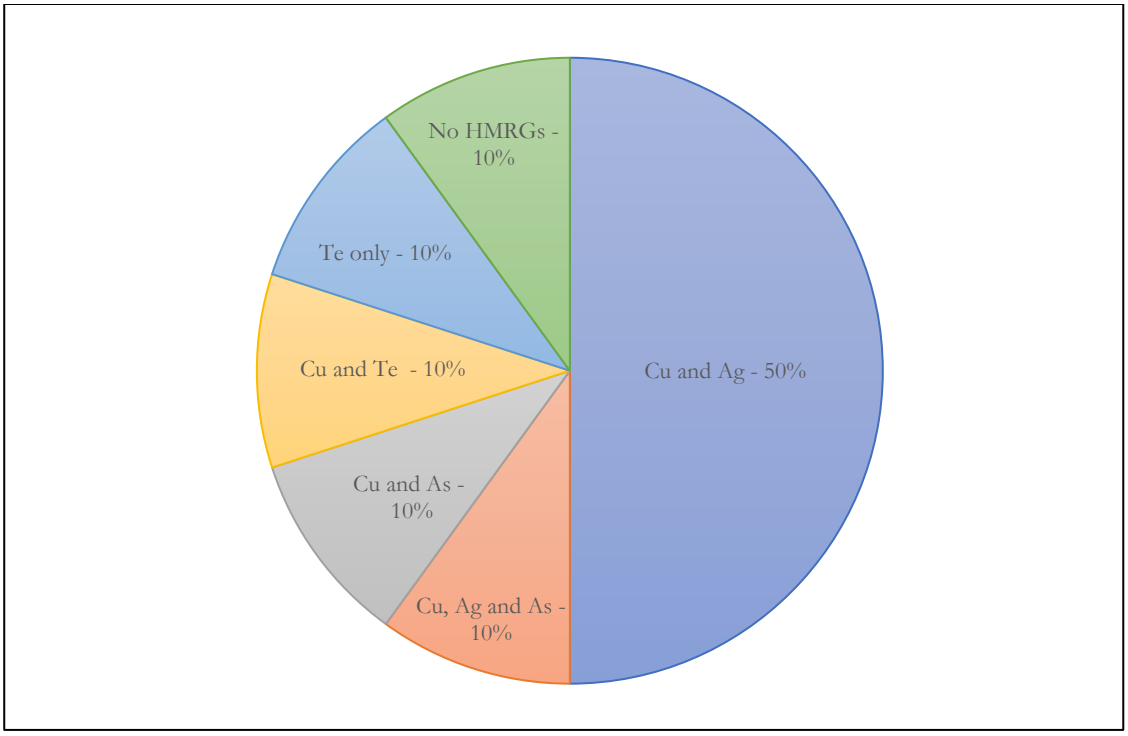

Figure 1. Proportion of heavy metal resistance genes among the sampled isolates. 80% of the samples carry resistance to multiple metals. Abbreviations: (Cu) copper; (Ag) silver, (As) arsenic, and (Te) tellurite.

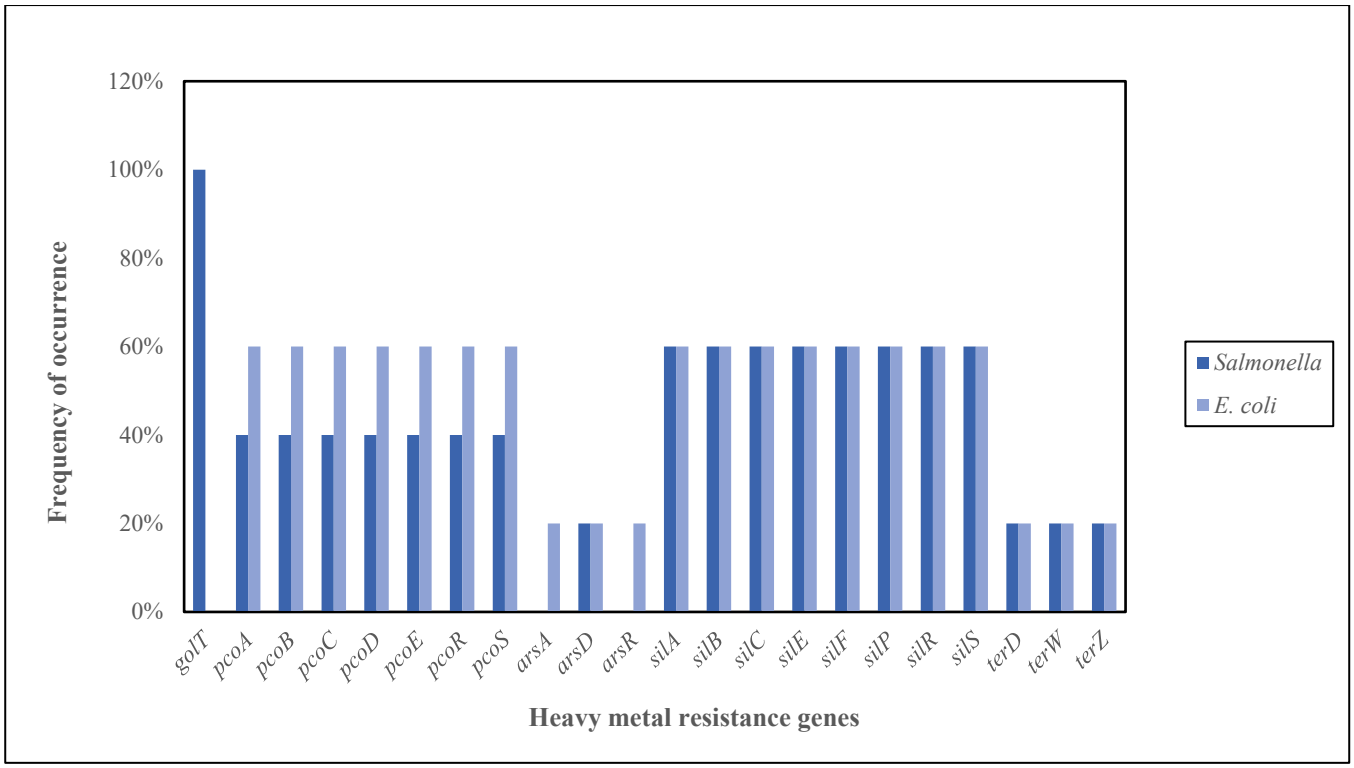

Figure 2. Prevalence of heavy metal resistance genes in *S. enterica* and *E. coli* isolates. *gol-* and *pco-* genes confer resistance to copper (Cu); *sil-* genes confer resistance to silver (Ag); *ars-* genes confer resistance to arsenic (As); and *ter-* genes confer resistance to tellurite (Te).

Minimum inhibitory concentrations of heavy metals for S. enterica and E. coli

MIC was interpreted as the minimum heavy metal concentration at which bacterial growth was not observed. Heavy metal susceptibility or resistance was established using *Salmonella* strain LT2 and *E. coli* strain DH5α as reference for their respective bacterial species. Strains with MICs greater than those of LT2 or DH5α were considered resistant. MIC assays were first performed without adjusting the pH of metal-supplemented broth. In subsequent trials, metal-supplemented media were neutralized before inoculation to account for possible pH effects on bacterial growth (**Table 2**).

	Copper (mM)		**Arsenic (mM)**		**Silver (mM)**		**Tellurite (mM)**	
Strain	No pH adjustment	pH adjustment	No pH adjustment	pH adjustment	No pH adjustment	pH adjustment	No pH adjustment	pH adjustment
LT2	32	32	8	0.125	0.063	0.125	0.25	0.016
PSU-3176	32	32	8	0.063	0.125	0.5	0.016	0.016
PSU-3260	32	32	8	0.063	0.063	0.25	0.125	0.016
PSU-3373	32	32	>8	0.5	0.031	0.25	1	0.016
PSU-3384	32	32	8	0.5	0.031	0.25	0.016	0.016
PSU-3390	32	32	0.031	0.063	0.063	0.25	0.016	0.016
DH5α	*	16	*	1	*	0.125	*	0.016
PSU-4439	32	32	8	4	0.063	0.25	0.031	0.016
PSU-4474	32	32	8	8	0.063	0.125	0.031	0.016
PSU-4512	32	32	8	8	0.031	0.25	0.016	0.016
PSU-4521	32	32	8	8	0.125	0.25	0.016	0.016
PSU-4612	32	32	>8	4	0.125	0.25	0.016	0.016
DH5α (pPSU-3260) transconjugant	*	16	*	1	*	0.125	*	1

**Not determined*

> growth started in first well

Table 2. Comparison between minimal inhibitory concentrations (MIC) with and without pH adjustments.

Copper MICs were identical (32 mM) among most *Salmonella* and *E. coli* strains, including LT2, demonstrating a comparable tolerance to the metal with one of the reference strains (**Table 3**); the only exception to MIC=32 mM was DH5α (16 mM). Notably, strains PSU-4512 and PSU-4612 (*E. coli*) were tolerant to copper despite lacking any copper-specific HMRGs. For arsenic, seven of the strains sampled had a higher MIC value than their respective reference strains, even though no apparent arsenic-specific HMRGs were present for most strains. These were *Salmonella* strains PSU-3384, and *E. coli* strains PSU-4439, PSU-4512, PSU-4521, and PSU-4612; strains PSU-3373 (*Salmonella*) and PSU-4474 (*E. coli*) were the only strains to present arsenic-specific resistance genes (**Table 3**). In the silver MICs, eight out of 10 strains had a value of 0.25 mM. Two exceptions were strains PSU-3176 for *Salmonella* and PSU-4474 for *E. coli* (**Table 3**); all strains were resistant to silver aside from *E. coli* strain PSU-4474. Four strains (PSU-3260, -3373, -4512, and -4612) had a higher MIC value than their respective reference strains (0.125 mM) while lacking silver-specific HMRGs. Additionally, *E. coli* strain PSU-4474 had the same value as the reference strain while presenting eight silver HMRGs. For tellurite, all strains had the same MIC as the reference strains (0.016 mM). This was the lowest dilution for the minimum inhibitory concentration. Yet, two of them (PSU-3260 and PSU-4612) had three tellurite-specific HMRGs. Moreover, the tested isolates showed resistance to copper (5/10; 50%), arsenic (7/10; 70%) and silver (9/10; 90%) (**Figure 3**). Among the 10 strains sampled, the accordance between geno- and phenotypic heavy metal resistance was fair for copper (kappa = 0.4), none to slight for arsenic (kappa = 0.19) and tellurite (kappa = 0), and no agreement for silver (kappa = -0.19) (**Table 4**). For tellurite, the value of kappa indicates that the agreement is the same as would be expected by chance, meanwhile, for silver, the agreement is less than random chance.

Copper			Genes								Arsenic	Genes			Silver	Genes							Tellurite	Genes		
Genus and species	Strain	MIC (mM)	*golT*	*pcoA*	*pcoB*	*pcoC*	*pcoD*	*pcoE*	*pcoR*	*pcoS*	MIC (mM)	*arsA*	*arsD*	*arsR*	MIC (mM)	*silA*	*silB*	*silC*	*silE*	*silF*	*silP*	*silR*	*silS*	MIC (mM)	*terD*	*terW*	*terZ*
S. enterica	LT2	32	+	-	-	-	-	-	-	-	0.125	-	-	-	0.125	-	-	-	-	-	-	-	-	0.016	-	-	-
S. enterica	PSU-3176	32	+	+	+	+	+	+	+	+	0.063	-	-	-	0.5	+	+	+	+	+	+	+	+	0.016	-	-	-
S. enterica	PSU-3260	32	+	-	-	-	-	-	-	-	0.063	-	-	-	0.25	-	-	-	-	-	-	-	-	0.016	+	+	+
S. enterica	PSU-3373	32	+	-	-	-	-	-	-	-	0.5	-	+	-	0.25	-	-	-	-	-	-	-	-	0.016	-	-	-
S. enterica	PSU-3384	32	+	+	+	+	+	+	+	+	0.5	-	-	-	0.25	+	+	+	+	+	+	+	+	0.016	-	-	-
S. enterica	PSU-3390	32	+	-	-	-	-	-	-	-	0.063	-	-	-	0.25	+	+	+	+	+	+	+	+	0.016	-	-	-
E. coli	DH5α	16	-	-	-	-	-	-	-	-	1	-	-	-	0.125	-	-	-	-	-	-	-	-	0.016	-	-	-
E. coli	PSU-4439	32	-	+	+	+	+	+	+	+	4	-	-	-	0.25	+	+	+	+	+	+	+	+	0.016	-	-	-
E. coli	PSU-4474	32	-	+	+	+	+	+	+	+	8	+	+	+	0.125	+	+	+	+	+	+	+	+	0.016	-	-	-
E. coli	PSU-4512	32	-	-	-	-	-	-	-	-	8	-	-	-	0.25	-	-	-	-	-	-	-	-	0.016	-	-	-
E. coli	PSU-4521	32	-	+	+	+	+	+	+	+	8	-	-	-	0.25	+	+	+	+	+	+	+	+	0.016	-	-	-
E. coli	PSU-4612	32	-	-	-	-	-	-	-	-	4	-	-	-	0.25	-	-	-	-	-	-	-	-	0.016	+	+	+
E. coli	DH5α (pPSU-3260) transconjugant	16									1				0.125									1			

Grey boxes indicate resistance in comparison to the respective reference strains.
Dark grey boxes indicate inaccurate genotypic prediction in regard to MIC values.
MIC values were determined using the adjusted pH values.
Presence of golT was excluded from the statistical analysis.

Table 3. Heavy metal minimum inhibitory concentrations and resistance genes.

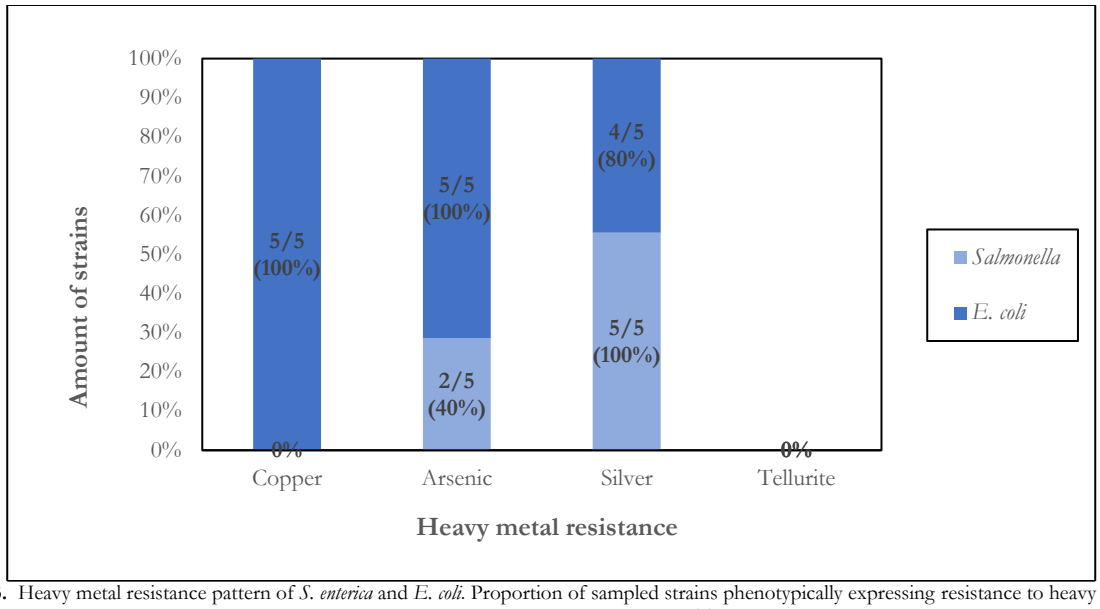

Figure 3. Heavy metal resistance pattern of *S. enterica* and *E. coli*. Proportion of sampled strains phenotypically expressing resistance to heavy metals in comparison to their respective reference strains, LT2 and DH5α.

	Susceptible Phenotype		Resistant Phenotype				
Heavy metal	**Resistant genotype**	**Susceptible genotype**	**Resistant genotype**	**Susceptible genotype**	**Agreement**	**Kappa Coefficiency**	**p-value**
Copper	2	3	3	2	60.00%	0.4	0.0311
Arsenic	0	3	2	5	50.00%	0.19	0.0716
Silver	1	0	5	4	50.00%	-0.19	0.8882
Tellurite	2	8	0	0	80.00%	0	/

/No value available

Table 4. Genotypic and phenotypic comparison for heavy metal resistance.

Transfer of heavy metal and AMR determinants

All five *Salmonella* strains were tested as plasmid donors with the recipient strain *E. coli* DH5α. Isolation of transconjugants was performed by selecting for the nalidixic acid-resistant phenotype of the recipient and the heavy metal-resistant phenotype of the given donor. Transconjugants were obtained only from the genotypically tellurite-resistant strain PSU-3260, which yielded a transfer frequency of 10^{-3} transconjugants per donor. The tellurite-resistant *E. coli* transconjugant was also resistant to kanamycin, ampicillin and tetracycline. In strain PSU-3260, the tellurite-resistant genes reside on an IncHI2-type plasmid that shares homology with known HMRG-disseminating *Salmonella* plasmids (**Figure 4**). Interestingly, the reference plasmid harbors *sil/pco* genes, yet these were not found in the PSU-3260 plasmid (**Table 1 & Figure 4**).

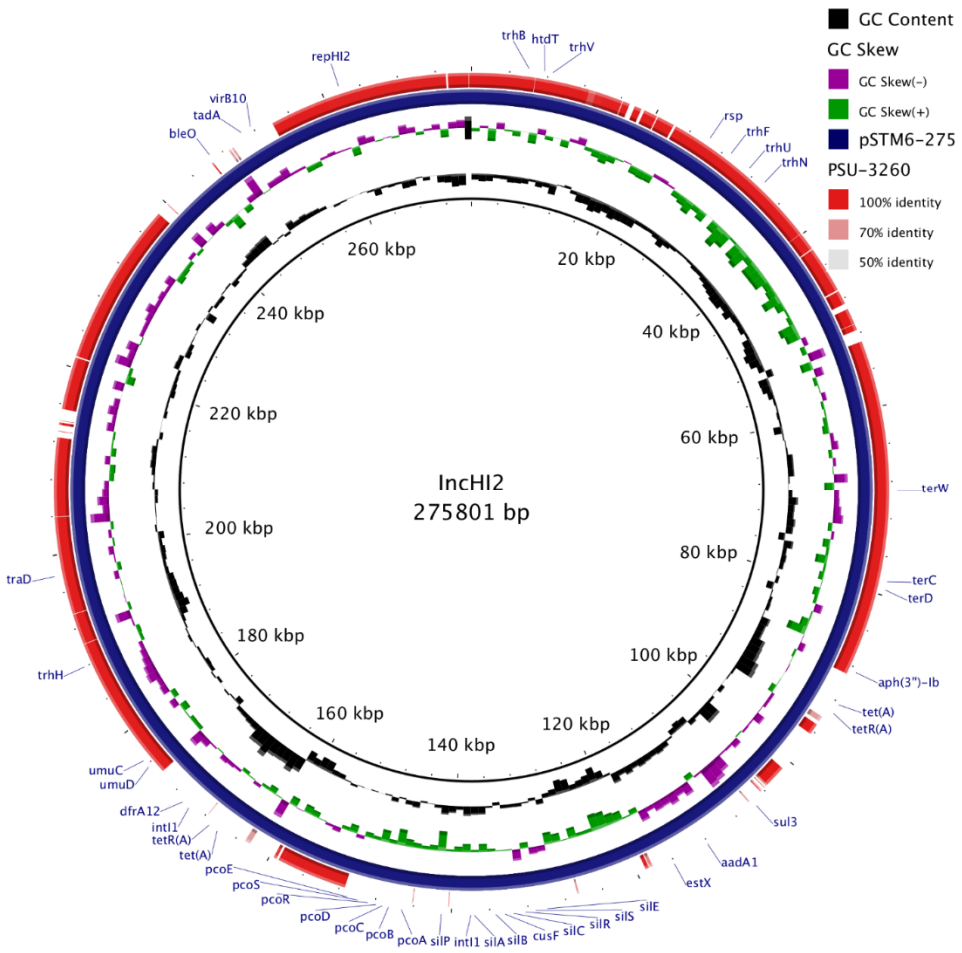

Figure 4. PSU-3260 carries a conjugative IncHI2 plasmid. Tellurite resistance genes (*ter*) were transferred from *S.* Typhimurium donor PSU-3260 to *E. coli* recipient DH5a by plasmid conjugation. Transconjugants selected on tellurite were also resistant to kanamycin, ampicillin, and tetracycline. Contigs from the genome assembly of PSU-3260 were compared to the closed IncHI2 plasmid of *S.* 1,4,5,12:i:- strain TW-Stm6,[34] and the figure was constructed using BRIG.[36]

DISCUSSION

In bacterial cells, resistance to antimicrobials can be observed by blockage or reduced entry of the antimicrobial into the cell, effluxion of such,[24, 37] modification of the antimicrobial or its target, destruction of the antimicrobial, or bypass of its effect.[38] Reduced antimicrobial susceptibility may be innate, developed via mutations, or by acquiring genetic elements.[24] Multiple genes predicted to confer heavy metal resistance were found in this study.

Often, pH adjustment changed the MIC values (**Table 2**). These adjusted values, used to evaluate heavy metal susceptibility or resistance, seemed to portray more accurate results in terms of correlation than those with no adjustment (**Tables 2 & 3**). Copper had the highest MIC values in comparison to the other metals evaluated. Copper is a common environmental pollutant from agricultural activities[17, 39] and is involved in host defense against bacterial pathogens.[40] Additionally, copper is beneficial in bacterial metabolism though it is still toxic in high concentrations.[17] Therefore, mechanisms to maintain copper homeostasis have evolved to protect bacterial cells from its increasing availability and cytotoxicity.[41] Consequently, this could be the reason for such high MIC values, in addition to the ability of certain silver resistance genes to confer resistance against copper (**Table 3**). Emphasis is given towards copper resistance mechanisms because of its high MIC values and metabolic role in the sampled enterobacteria.

The results indicated no considerable correlation between the genotype and phenotype of the bacterial species (**Table 4**). Cases were observed where HMRG presence did not correlate with phenotypic resistance. Likewise, HMRG absence did not assure heavy metal susceptibility nor eliminate the possibility of resistance or tolerance to the administered heavy metals. For instance, most isolates tested showed resistance to arsenic (7/10; 70%) (**Figure 3**), yet genes for arsenic resistance had the lowest prevalence (10-20%; 1/10; 2/10) (**Figure 2**). Among the 10 strains sampled, nine had inconsistencies regarding geno- and

phenotypic heavy metal resistance (**Table 3**). Though in the case of tellurite there was an 80% agreement between the harboring of HMR genes with phenotypic expression of resistance to said metal, for the remaining three metals (arsenic, silver and copper) an accuracy of 50, 50 and 60% was observed respectively.

Previous studies have established a genotypic and phenotypic correlation regarding ARGs. Antibiotic susceptibility/resistance phenotypes have been predicted, and geno- & phenotypic correlation has been achieved with an accuracy ranging from 96-99% in *Salmonella*, *E. coli* and *Klebsiella pneumoniae* isolates.[42—45] Yet, unlike with antibiotics, there are no established MIC breakpoints for heavy metals; thus, leading to the use of reference strains to compare MIC results. There is a need to standardize clinical breakpoints and protocols regarding heavy metals. There are significant problems that complicate the comparison of studies regarding heavy metal resistance. When it comes to testing heavy metal susceptibility/resistance, the following are advised: (1) use of standardized media (*e.g.*, MH) as choice (the concentration of metal available can be compromised with the use of other complex media since some of their components can sequester free metal ions); (2) pH should be adjusted after supplementing with metal (metal addition can alter the final pH of the media) to guarantee that bacteria grow favorably and accurate results are obtained; and (3) the reference strain and test isolates should be the same bacterial species.[41] MH was used mainly throughout the experiments in this study, except for the samples supplemented with silver. After initially supplementing MH broth with said metal, the precipitation of silver was observed. Therefore, MH was replaced with LB without salt to prevent the salt and silvers' interaction, hence averting precipitation.

Moreover, there are multiple genetic possibilities for which no considerable correlation was observed between the genotype and phenotype of the bacterial species, contrary to antibiotics. First, the conditions for gene expression may vary from those used in the experiment. For example, in the case of those strains with HMRGs that did not display resistance to the corresponding metals, the genes may need to be under stress conditions to be expressed. In culture-based antimicrobial susceptibility testing, the variance of expression of a phenotype is not necessarily reflected by the controlled setting in which resistance is measured.[46] Perhaps the same event could be observed with culture-based heavy metal susceptibility testing. Also, there are possibly some heavy metal resistance-conferring genes/mechanisms that are still unknown, or have not yet been included in database libraries, hence the tolerance/resistance of a particular strain to a specific metal even though there are no apparent HMRGs present. A possible helpful approach could be the application of microbial genome-wide association studies (GWAS) to heavy metal resistance; GWAS have been used for AMR to identify unknown resistance determinants and to assess single-nucleotide polymorphisms (SNPs) or genes' effects on resistance in bacterial species.[47]

Co-occurrence of HMRGs and ARGs validates that heavy metal and antibiotic resistance could be correlated.[21, 48] One of five *Salmonella* strains (PSU-3260) carried a plasmid that could be conjugated to DH5α. Following selection on tellurite-supplemented plates, the transconjugant also grew on plates supplemented with kanamycin, ampicillin, and tetracycline; thus, demonstrating that heavy metal resistance is transferable between bacteria. Regarding the other strains, it could be possible that they needed to be under changing physiological conditions to achieve a conjugative transfer, as seen in a previous study.[34]

CONCLUSION

Our results indicated no considerable correlation between the genotype and phenotype of heavy metal resistance in the sampled *S. enterica* and *E. coli*. These results are preliminary, and though the sample size of this study was not sufficient to establish a pattern due to the limitation of time, this data can contribute to the scarce literature in heavy metal resistance. Although multiple reasons are proposed to explain the disparity, they were not thoroughly investigated in this research. Thus, further studies are required to establish a pattern, and more examinations are needed to verify these results. The fact that heavy metal resistance was observed without HMRGs could be of concern to the industry of commercial agriculture, and the One Health perspective, which interconnects humans, animals, plants, and their environment.[49] The lack of standardized protocols and MIC clinical breakpoints for heavy metals prove the necessity of research in this area. Finally, said deficiencies or the possible presence of unknown genes/mechanisms that provide HMR might be the main reasons there was no clear correlation between the possession of HMRGs and actual resistance among all sampled strains.

ACKNOWLEDGEMENTS

This work was supported by the U.S. Department of Agriculture: Bugs in my Food: Research and Professional Development in Food Safety for Undergraduates from Non-Land Grant Institutions. Grant No. 2017-67032-26022. Thank you to the U.S. Geological Survey (USGS) for providing the strains, Yezhi Fu for sequencing such, and José N. Díaz-Caraballo for aiding with the statistical analysis.

REFERENCES

1. Mueller, M., and Tainter, C. (2020) Escherichia Coli, in *StatPearls*. StatPearls Publishing.
2. Terajima, J., Izumiya, H., Hara-Kudo, Y., and Ohnishi, M. (2017) Shiga toxin (verotoxin)-producing *Escherichia coli* and foodborne disease: A Review, *J Food Saf* 5, 35–53. *https://doi.org/10.14252/foodsafetyfscj.2016029*
3. Lee, K.-S., Jeong, Y.-J., and Lee, M. S. (2021) *Escherichia coli* shiga toxins and gut microbiota interactions, *Toxins* 13, 416. *https://doi.org/10.3390/toxins13060416*
4. Centers for Disease Control and Prevention. *Escherichia coli* (*E. coli*), *https://www.cdc.gov/ecoli/pdfs/CDC-E.-coli-Factsheet.pdf* (accessed Sep 2021)
5. Coburn, B., Grassl, G., and Finlay, B. B. (2007) *Salmonella*, the host and disease: a brief review, *Immunol Cell Biol* 85, 112–118. *https://doi.org/10.1038/sj.icb.7100007*
6. Aljahdali, N., Sanad, Y., Han, J., and Foley, S. (2020) Current knowledge and perspectives of potential impacts of *Salmonella enterica* on the profile of the gut microbiota, *BMC Microbiol* 20, 353. *https://doi.org/10.1186/s12866-020-02008-x*
7. Scallan, E., Hoekstra, R. M., Angulo, F. J., Tauxe, R. V., Widdowson, M., Roy, S.L., Jones, J. L., and Griffin, P. M. (2011) Foodborne Illness Acquired in the United States—Major Pathogens, *Emerg Infect Dis* 17, 7–15. *https://doi.org/10.3201/eid1701.p11101*
8. McMillan, E., Jackson, C., and Frye, J. (2020). Transferable Plasmids of *Salmonella enterica* Associated With Antibiotic Resistance Genes, *Front Microbiol* 11, 562181. *https://doi.org/10.3389/fmicb.2020.562181*
9. Centers for Disease Control and Prevention. Outbreak of *E. coli* infections linked to ground beef, *https://www.cdc.gov/ecoli/2019/o103-04-19/index.html* (accessed Feb 2022)
10. Centers for Disease Control and Prevention. *Salmonella* outbreaks linked to Backyard Poultry, *https://www.cdc.gov/salmonella/backyardpoultry-05-21/index.html* (accessed Feb 2022)
11. Hejna, M., Gottardo, D., Baldi, A., Dell'Orto, V., Cheli, F., Zaninelli, M., and Rossi L. (2018) Review: Nutritional ecology of heavy metals, *Animal* 12, 2156–2170. *https://doi.org/10.1017/s175173111700355x*
12. Figueiredo, R., Card, R. M., Nunez-Garcia, J., Mendonça, N., da Silva, G. J., and Anjum, M. F. (2019) Multidrug-Resistant *Salmonella enterica* Isolated from Food Animal and Foodstuff May Also Be Less Susceptible to Heavy Metals, *Foodborne Pathog Dis* 16, 166–172. *https://doi.org/10.1089/fpd.2017.2418*
13. Seiler, C., and Berendonk, T. U. (2012) Heavy metal driven co-selection of antibiotic resistance in soil and water bodies impacted by agriculture and aquaculture, *Front Microbiol* 3, 399. *https://doi.org/10.3389/fmicb.2012.00399*
14. Yu, Z., Gunn, L., Wall, P., and Fanning, S. (2017) Antimicrobial resistance and its association with tolerance to heavy metals in agriculture production, *Food Microbiol* 64, 23–32. *https://doi.org/10.1016/j.fm.2016.12.009*
15. López-Alonso, M. (2012) Animal feed contamination by toxic metals, in *Animal Feed Contamination* (Fink-Gremmels, J., Ed.) 183–204, Woodhead Publishing.
16. Hernández-Ramírez, K., Reyes-Gallegos, R. I., Chávez-Jacobo, V. M., Díaz-Magaña, A., Meza-Carmen, V., and Ramírez-Díaz, M. I. (2018) A plasmid-encoded mobile genetic element from Pseudomonas aeruginosa that confers heavy metal resistance and virulence, *Plasmid* 98, 15–21. *https://doi.org/10.1016/j.plasmid.2018.07.003*
17. Argudín, M.A., Hoefer, A., and Butaye, P. (2019) Heavy metal resistance in bacteria from animals, *Vet Sci Res J* 122, 132–147. *https://doi.org/10.1016/j.rvsc.2018.11.007*
18. Baker-Austin, C., Wright, M. S., Stepanauskas, R., and McArthur, J. V. (2006) Co-selection of antibiotic and metal resistance, *Trends Microbiol* 14, 176–182. *https://doi.org/10.1016/j.tim.2006.02.006*
19. Zhao, Y., Su, J. Q., An, X. L., Huang, F. Y., Rensing, C., Brandt, K. K., and Zhu, Y. G. (2018) Feed additives shift gut microbiota and enrich antibiotic resistance in swine gut, *Sci Total Environ* 621, 1224–1232. *https://doi.org/10.1016/j.scitotenv.2017.10.106*
20. Mustafa, G., Zhao, K., He, X., Chen, S., Liu, S., Mustafa, A., He, L., Yang, y., Yu, X., Penttinen, P., Ao, X., Liu, A., Shabbir, M., Xu, X., and Zou, L. (2021) Heavy Metal Resistance in *Salmonella Typhimurium* and Its Association With Disinfectant and Antibiotic Resistance, *Front Microbiol* 12, 702725. *https://doi.org/10.3389/fmicb.2021.702725*
21. Yang, S., Deng, W., Liu, S., Yu, X., Mustafa, G., Chen, S., He, L., Ao, X., Yang, Y., Zhou, K., Li, B., Han, X., Xu, X., and Zou, L. (2020) Presence of heavy metal resistance genes in *Escherichia coli* and *Salmonella* isolates and analysis of resistance gene structure in *E. coli* E308, *J Glob Antimicrob Resist* 21, 420–426. *http://dx.doi.org/10.1016/j.jgar.2020.01.009*
22. Imran, M., Das, K. R., and Naik, M. M. (2019) Co-selection of multi-antibiotic resistance in bacterial pathogens in metal and microplastic contaminated environments: An emerging health threat, *Chemosphere* 215, 846–857. *https://doi.org/10.1016/j.chemosphere.2018.10.114*
23. Pal, C., Asiani, K., Arya, S., Rensing, C., Stekel, D. J., Larsson, D. G. J., and Hobman, J. L. (2017) Metal resistance and its association with antibiotic resistance, *Adv Microb Physiol* 70, 261–313. *https://doi.org/10.1016/bs.ampbs.2017.02.001*

24. Cheng, G., Ning, J., Ahmed, S., Huang, J., Ullah, R., An, B., Hao, H., Dai, M., Huang, L., Wang, X., and Yuan, Z. (2019) Selection and dissemination of antimicrobial resistance in Agri-food production, *Antimicrob Resist Infect Control* 8, 158. *https://doi.org/10.1186/s13756-019-0623-2*

25. Wales, A. D., and Davies, R. H. (2015) Co-Selection of Resistance to Antibiotics, Biocides and Heavy Metals, and Its Relevance to Foodborne Pathogens, *Antibiotics* 4, 567–604. *https://doi.org/10.3390/antibiotics4040567*

26. Van Alen, S., Kaspar, U., Idelevich, E. A., Köck, R., and Becker, K. (2018) Increase of zinc resistance in German human derived livestock-associated MRSA between 2000 and 2014, *Vet Microbiol* 214, 7–12. *https://doi.org/10.1016/j.vetmic.2017.11.032*

27. Fu, Y., M'ikanatha, N. M., Whitehouse, C. A., Tate, H., Ottesen, A., Lorch, J. M., Blehert, D. S., Berlowski-Zier, B., and Dudley, E. G. (2021) Low occurrence of multi-antimicrobial and heavy metal resistance in *Salmonella enterica* from wild birds in the United States, *Environ Microbiol* 24, 1380–1394. *https://doi.org/10.1111/1462-2920.15865*

28. Feldgarden, M., Brover, V., Gonzalez-Escalona, N., Frye, J. G., Haendiges, J., Haft, D. H., Hoffmann, M., Pettengill, J. B., Prasad, A. B., Tillman, G. E., Tyson, G. H., and Klimke, W. (2021) AMRFinderPlus and the reference gene catalog facilitate examination of the genomic links among antimicrobial resistance, stress response, and virulence, *Sci Rep* 11, 12728. *https://doi.org/10.1038/s41598-021-91456-0*

29. Clinical and Laboratory Standards Institute. (2021) Performance Standards for Antimicrobial Susceptibility Testing in *CLSI supplement M100* 31st ed., Clinical and Laboratory Standards Institute, USA.

30. Tuan, V. P., Narith, D., Tshibangu-Kabamba, E., Dung, H. D., Viet, P. T., Sokomoth, S., Binh, T. T., Sokhem, S., Tri, T. D., Ngov, S., Tung, P. H., Thuan, N. P., Truc, T. C., Phuc, B. H., Matsumoto, T., Fauzia, K. A., Akada, J., Trang, T. T., and Yamaoka, Y. (2019) A next-generation sequencing-based approach to identify genetic determinants of antibiotic resistance in Cambodian helicobacter pylori clinical isolates, *J Clin Med* 8, 858. *https://doi.org/10.3390/jcm8060858*

31. McHugh, M. L. (2012) Interrater reliability: the kappa statistic, *Biochem Med* 22, 276–282.

32. Cleuziat, P., and Robert-Baudouy, J. (1990) Specific detection of *Escherichia coli* and *Shigella* species using fragments of genes coding for β-glucuronidase, *FEMS Microbiol Lett* 72, 315–322. *https://doi.org/10.1016/0378-1097(90)90324-j*

33. Walk, S. T., Alm, E. W., Gordon, D. M., Ram, J. L., Toranzos, G. A., Tiedje, J. M., and Whittam, T. S. (2009) Cryptic lineages of the genus *Escherichia*, *Appl Environ Microbiol* 75, 6534–6544. *https://doi.org/10.1128/aem.01262-09*

34. Johnson, J. R., Johnston, B. D., and Gordon, D. M. (2017) Rapid and specific detection of the *Escherichia coli* sequence type 648 complex within Phylogroup F, *J Clin Microbiol* 55, 1116–1121. *https://doi.org/10.1128/jcm.01949-16*

35. Billman-Jacobe, H., Liu, Y., Haites, R., Weaver, T., Robinson, L., Marenda, M., and Dyall-Smith, M. (2018) PSTM6-275, a conjugative IncHI2 plasmid of *Salmonella enterica* that confers antibiotic and heavy-metal resistance under changing physiological conditions, *Antimicrob Agents Chemother* 62, e02357-17. *https://doi.org/10.1128/aac.02357-17*

36. Alikhan, N. F., Petty, N. K., Ben Zakour, N. L., and Beatson, S. A. (2011) BLAST ring image generator (BRIG): Simple prokaryote genome comparisons, *BMC Genom* 12, 402. *https://doi.org/10.1186/1471-2164-12-402*

37. Lekshmi, M., Ammini, P., Kumar, S., and Varela, M. F. (2017) The food production environment and the development of antimicrobial resistance in human pathogens of animal origin, *Microorganisms* 5, 11. *https://doi.org/10.3390/microorganisms5010011*

38. Centers for Disease Control and Prevention. How antibiotic resistance happens, *https://www.cdc.gov/drugresistance/about/how-resistance-happens.html* (accessed Feb 2022)

39. Poole, K. (2017) At the nexus of antibiotics and metals: The impact of Cu and Zn on antibiotic activity and resistance, *Trends Microbiol* 25, 820–832. *https://doi.org/10.1016/j.tim.2017.04.010*

40. Djoko, K. Y., Ong, C. Y., Walker, M. J., and McEwan, A. G. (2015) The role of copper and zinc toxicity in innate immune defense against bacterial pathogens, *J Biol Chem* 290, 18954–18961. *https://doi.org/10.1074/jbc.r115.647099*

41. Rensing, C., Moodley, A., Cavaco, L. M., and McDevitt, S. F. (2018) Resistance to Metals Used in Agricultural Production, *Microbiol Spectr* 6. *https://doi.org/10.1128/microbiolspec.ARBA-0025-2017*

42. Stoesser, N., Batty, E. M., Eyre, D. W., Morgan, M., Wyllie, D. H., Del Ojo Elias, C., Johnson, J. R., Walker, A. S., Peto, T. E., and Crook, D. W. (2013) Predicting antimicrobial susceptibilities for *Escherichia coli* and *Klebsiella pneumoniae* isolates using whole genomic sequence data, *J Antimicrob Chemother* 68, 2234–2244. *https://doi.org/10.1093/jac/dkt180*

43. McDermott, P. F., Tyson, G. H., Kabera, C., Chen, Y., Li, C., Folster, J. P., Ayers, S. L., Lam, C., Tate, H. P., and Zhao, S. (2016) Whole-genome sequencing for detecting antimicrobial resistance in nontyphoidal *Salmonella*, Antimicrob Agents Chemother 60, 5515–5520. *https://doi.org/10.1128/aac.01030-16*

44. Neuert, S., Nair, S., Day, M. R., Doumith, M., Ashton, P. M., Mellor, K. C., Jenkins, C., Hopkins, K. L., Woodford, N., de Pinna, E., Godbole, G., and Dallman, T. J. (2018) Prediction of phenotypic antimicrobial resistance profiles from whole genome sequences of non-typhoidal *Salmonella enterica*, *Front Microbiol* 9, 592. *https://doi.org/10.3389/fmicb.2018.00592*

45. Wilson, A., Fox, E. M., Fegan, N., and Kurtböke, D. Í. (2019) Comparative genomics and phenotypic investigations into antibiotic, heavy metal, and disinfectant susceptibilities of *Salmonella enterica* strains isolated in Australia, *Front Microbiol* 10, *1620. https://doi.org/10.3389/fmicb.2019.01620*

46. Su, M., Satola, S. W., and Read, T. D. (2019) Genome-based prediction of bacterial antibiotic resistance, *J Clin Microbiol* 57, e01405-18. *https://doi.org/10.1128/jcm.01405-18*
47. Lo, S. W., Kumar, N., and Wheeler, N. E. (2018) Breaking the code of antibiotic resistance, *Nat Rev Microbiol* 16, 262. *https://doi.org/10.1038/nrmicro.2018.33*
48. Di Cesare, A., Eckert, E. M., D'Urso, S., Bertoni, R., Gillan, D. C., Wattiez, R., and Corno, G. (2016) Co-occurrence of Integrase 1, antibiotic and heavy metal resistance genes in municipal wastewater treatment plants, *Water Res* 94, 208–214. *https://doi.org/10.1016/j.watres.2016.02.049*
49. McEwen, S. A., and Collignon, P. J. (2018) Antimicrobial resistance: A one health perspective, *Microbiol Spectr* 6. *https://doi.org/10.1128/microbiolspec.arba-0009-2017*

ABOUT STUDENT AUTHORS

Jeevan Rivera-Díaz and Haley Phillippi graduated in May 2022 from the University of Puerto Rico in Aguadilla, PR, and Mount Aloysius College, Cresson, PA. Jeevan earned a Bachelor's of Science with a major in Biology, an emphasis in Genetics, and a minor in Biomedical Sciences, and is aiming to enter medical school. Haley earned a Bachelor's of Science in Biology with a concentration in Molecular & Cellular Biology and is planning to earn a Master's degree in Genetics. Nyduta Mbogo is completing her Master's degree with a thesis regarding *E. coli* and *Salmonella* in wastewater. Her future directions are focused on working in the industry.

PRESS SUMMARY

Contamination in the food supply chain is an area of concern. Animal feed may be supplemented with heavy metals. Yet, excessive exposure to undesirable levels of such damages the health of food-producing animals, and its accumulation could subsequently threaten consumers' health. Bacteria have acquired many metal resistance genes to adapt to exposure to metals. *Salmonella enterica* and *Escherichia coli* are two bacteria of worldwide importance that can infect the gastrointestinal tract. A better understanding of the association between genes and their expression will allow for better characterization of bacterial virulence factors. Additionally, the spread of resistance could be monitored by evaluating the transfer of these genes. In this study, our objectives were to assess in a small sample of bacteria the association between resistance genes and their expression to certain heavy metals and the ability of said bacteria to transfer antimicrobial resistance genes and heavy metal resistance genes. Our results indicated no significant association between the harboring of resistance genes and actual resistance towards heavy metals in the sampled bacteria and demonstrated that heavy metal resistance is transferable between bacteria.

Preventing the Activation of a Stress Gene Response in *Escherichia coli* Using Acetate, Butyrate, and Propionate

Kaylee M. Weigel, Kathleen M Ruff-Schmidt*, Birgit M. Prüß, & Danielle L J Condry**

Department of Microbiological Sciences, North Dakota State University, Fargo, ND

https://doi.org/10.33697/ajur.2022.065

Student email: kaylee.weigel@ndsu.edu, kathleen.schmidt@ndsu.edu
*Mentor email: birgit.pruess@ndsu.edu, danielle.condry@ndsu.edu**

**Authors contributed equally*

ABSTRACT
Regulation of microbial symbiosis in the human intestinal tract is imperative to maintain overall human health and prevent dysbiosis-related diseases, such as inflammatory bowel disease and obesity. Short-chain fatty acids (SCFA) in the intestine are produced by bacterial fermentation and aid in inflammation reduction, dietary fiber digestion, and metabolizing nutrients for the colon. SCFA, notably acetate, butyrate, and propionate, are starting to be used in clinical interventions for GI diseases. While acetate has been shown to mitigate a stress response in the proteome of *Escherichia coli* cells, little is known about the effects of butyrate and propionate on the same cells. This study aims to evaluate the effects that butyrate and propionate have on the activation of stress promoters in *E. coli* when induced with a known stressor. Three different strains of *E. coli* containing the pUCD615 plasmid were used, each with a different promoter fused to the structural genes of the *lac* operon on the plasmid. Each promoter detected a unique stress response: *grpE'::lux* fusion (heat shock), *recA'::lux* fusion (SOS response), and *katG'::lux* fusion (oxidative damage). Activation of these stress promoters by treatment groups resulted in the emission of bioluminescence which was quantified and compared across treatment groups. All three SCFAs at 25 mM added to cultures prior to stressing the bacteria caused significantly lower bioluminescence levels when compared to the stressed culture without prior addition of SCFA. This indicates that these SCFAs may reduce the stress response in *E. coli*.

KEYWORDS
Short-chain fatty acids; acetate; butyrate; propionate; *Escherichia coli;* stress response; *Vibrio fischeri luxCDABE; grpE; katG; recA*

INTRODUCTION

Metabolic syndromes, including obesity and type 2 diabetes, are 21st-century epidemics, and their etiologies have been linked to the gut microbiota.[1] The gastrointestinal tract harbors approximately 40 trillion bacteria that metabolize short-chain fatty acids (SCFA) from the fermentation of indigestible foods— particularly the metabolic breakdown of complex sugars.[2] The chemical structures of SCFAs are organic compounds with carboxylic acid functional groups attached. SCFAs have been shown to have many beneficial effects on the host: being used as fuel for epithelial cells in the colon, protection against metabolic control deterioration and inflammation, increasing colonic and hepatic portal venous blood flow, and maintenance of mucosal integrity.[3–5]

SCFAs are important to human digestive health and maintenance, produced as fermentation byproducts by bacteria of the gut microbiota.[6] They are critical in overall metabolic integrity and are large energy producers for intestinal epithelial cells (IECs); their energy supplement ranking being butyrate > propionate > acetate.[1,7] SCFAs that escape from colon cells enter the portal vein of the liver and can be converted into acetyl coenzyme A, which serves a key role in cellular metabolism and is a fundamental indicator of cellular metabolic state.[8] This class of nutrients is sensed by unique gut receptors FFA2, FFA3, GPR109a, and Olfr78– the role of these receptors is regulation of intestinal motility and maintenance of both the epithelial barrier and immune cell function.[9] While there are seven common SCFAs present in the gastrointestinal tract (GIT), the three most common occur in ratios between 40:20:20 to 75:15:10 as acetate, propionate, and butyrate, respectively.[9,10] Acetate, propionate, and butyrate are closely related in structure, only differing in the number of carbons. **Figure 1** depicts these structural differences. SCFAs butyrate and propionate activate a neural circuit between the gut and the brain, which induces intestinal gluconeogenesis—a metabolic process that has several metabolic benefits.[11] A significant role of these acids is their assets as an energy source and their ability to induce positive metabolic outcomes, such as insulin sensitivity.[1,11] Specifically, propionate acts as a glucose precursor in the gut, which activates a portal glucose sensor, which leads to improved glucose tolerance and insulin sensitivity.[10,11]

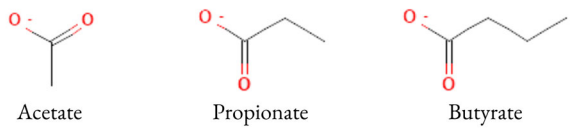

Figure 1. Chemical structure of acetate,[12] propionate,[13] and butyrate,[14] respectively.

Although naturally produced SCFAs have positive effects on the microbiome, there is evidence to suggest that acetate, when externally added in the acidic form, induced a stress response in *Escherichia coli*.[15] Kirkpatrick et al found that acetic acid at 50 mM induced multiple members of the RpoS regulon; Dps (a DNA-binding protein) was the most strongly induced, while seventeen proteins were repressed.[15] RpoS is a sigma factor responsible for the general stress response and regulating stationary phase in bacterial cells.[16] Kirkpatrick et al also found that formic acid prompted a stress response in *E. coli* like that of acetic acid. The addition of acetic acid after the stress response mitigated the activation of those proteins.[15] Further studies have shown that sodium acetate enhanced the resistance of *E. coli* to oxidative stress and heat killing, and all three SCFAs (acetate, butyrate, and propionate) at neutral pH increased the acid survival of *E. coli*.[6] Although there is substantive research exploring the effects of acetate on stress response in *E. coli*, there is a current gap in understanding the same effects of butyrate and propionate.

Although *E. coli* represents less than 1% of intestinal microbiota, it is the predominant facultative aerobic species in the gut.[17] As a commensal organism, *E. coli* promotes normal gut homeostasis.[17] In this study, *E. coli* is the model organism for the human microbiota to demonstrate the absence or presence of an oxidative stress response, a DNA damage response, and the heat shock response when the bacteria are exposed to acetate, butyrate, and propionate.

E. coli harbors many proteins that are essential for cell survival and adaptation to stressors. RecA is a protein of *E. coli* induced in response to DNA damage, in addition to homologous recombination.[18] In the SOS response, the RecA protein is converted into a specific and active protease and cleaves the LexA repressor.[19] GrpE is one of three proteins that constitute the *E. coli* DnaK chaperone machine, belonging to the heat shock protein family.[20] The expression of this protein is transiently induced under stress conditions, specifically regarding heat or ethanol treatment.[21] GrpE, along with DnaK and DnaJ, is responsible for reactivating damaged proteins under stress, proteolysis, and autoregulation of the heat shock response.[21] The *katG* gene is a catalase gene in *E. coli* that encodes for hyperperoxidase I (HPI) synthesis in the presence of H_2O_2 and is regulated by OxyR.[22,23] KatG participates in antioxidant defense mechanisms regarding oxidative damage and hydrogen peroxide-induced stress.[24]

For this study, promoter fusions to the *luxCDABE* operon from *Vibrio fischeri* were used in *E. coli* W3110. These fusions had been constructed and used previously to detect stress.[25,26] The plasmid used for testing was pUCD615 which is a broad-host-range plasmid containing promoterless *luxCDABE*.[25,26] Stress promoters are added to the 5' end of the *luxCDABE* operon to detect the stress response with bioluminescence output. The heat shock response is determined by the *grpE'::lux* fusion, the *katG'::lux* fusion shows the oxidative damage response, and the SOS response is tested using the *recA'::lux* fusion.[25,27] Activation of these stress promoters is determined and quantified via the emission of bioluminescence.[28] Kanamycin resistance was used as a selective marker, and the map of the plasmid used is shown in **Figure 2**.

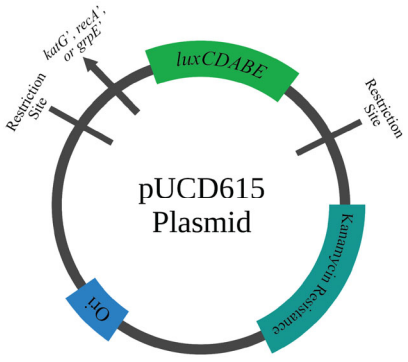

Figure 2. Map of the pUCD615 plasmid. Ori is the origin of replication. Each fusion plasmid contains one of the promoters of the indicated genes: *katG', recA',* or *grpE'*. The *luxCDABE* operon is from *V. fischeri*.

Based on previous research that established a protective effect of SCFAs on the intestinal microbiota,[5,29,30] we hypothesize that the addition of acetate, butyrate, and propionate would prevent the activation of the stress genes in *E. coli* in the presence of the respective known stressor.

MATERIALS AND METHODS

Short Chain Fatty Acid Compounds

All SCFAs used were analytical grade (> 98% purity) and were in their sodium salt form (sodium propionate, sodium butyrate, and sodium acetate). Sodium propionate and sodium butyrate were purchased from Tokyo Chemical Industry (TCI) Co Chemicals: sodium propionate CAS RN: 137-40-6, > 98% purity; sodium butyrate CAS RN: 156-54-7, > 98% purity. Sodium acetate was purchased from BeanTown Chemical, CAS number 127-09-3, > 99.995% trace metal basis. All SCFA were used at three concentrations: 12.5 mM, 25 mM, and 50 mM. The concentration of 25 mM was selected based on similar concentrations of SCFAs (specifically butyrate and propionate) found naturally in the human gut.[31,32] The concentration of 50 mM was chosen based on previous research regarding acetic acid at 50 mM inducing the RpoS regulon in *E. coli*.[15] The pH of the LB media containing SCFA at these three concentrations was nearly identical to the pH of the LB media alone.

Bacterial Strain and Plasmids

All *E. coli* strains and plasmids were kindly provided by Dr. Amy Vollmer (Swathmore College, PA). **Table 1** summarizes strains used containing all *lux* fusion plasmids and all detailed descriptions are cited in the references provided.

Strains/Plasmid	Description	Reference(s)
Strains		
W3110	F-, λ-, IN(*rrnD-rrnE*)1, *rph*-1	33
DPD2511	pKatGLux2/RFM443	27
TV1061	pGrpELux5/RFM443	34
DPD2794	pRecALux3/RFM443	26
Plasmids		
pUCD615	Amp^r Kan^r multiple cloning site upstream of *luxCDABE*	35
pKatGLux2	Same as pUCD615, but *katG'::luxCDABE*	27
pGrpELux5	Same as pUCD615, but *grpE'::luxCDABE*	34
pRecALux3	Same as pUCD615, but *recA'::luxCDABE*	26

Table 1. *E. coli* strains and plasmids.

Growth of the Bacteria

All *E. coli* strains were grown on Luria-Bertani (LB) agar plates containing 50 μg/mL kanamycin sulfate and were incubated at 37 °C. Experimental cultures were inoculated into 5 mL tubes containing LB and 25 μg/mL kanamycin sulfate overnight prior to each experiment. The overnight cultures were diluted into 5mL tubes containing fresh LB at an OD_{600} of 0.05 and incubated at 37 °C for four hours prior to being added into the plate. These *E. coli* subcultures were added to the 96 well plates with LB media and incubated at 37 °C for an additional two hours prior to adding treatments. **Figure 3** depicts a timeline of the complete process.

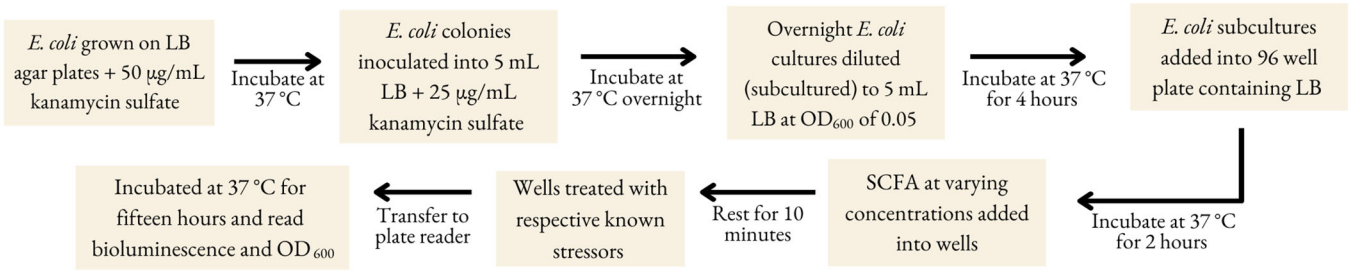

Figure 3. Timeline of experiments. For combinations of SCFAs and stressors, see Table 2.

SCFA Treatment of the Bacteria

This experiment had two treatment groups in addition to positive and negative controls for the *E. coli* strains: a baseline SCFA treatment and stress reduction treatment. The baseline SCFA treatment group involved each strain treated with one SCFA at concentrations of 12.5 mM, 25 mM, or 50 mM. The stress reduction group involved each strain treated with each SCFA at all three concentrations and adding the known stressor ten minutes after SCFA addition. **Table 2** shows the treatment groups used.

Treatment Group	Well Composition
Negative Control	*E. coli* strain + LB media
Positive Control	*E. coli* strain + LB media + known stressor
Baseline SCFA	*E. coli* strain + LB media + each SCFA
Reduced Stress Expression	*E. coli* strain + LB media + each SCFA + known stressor

Table 2. Treatment Group Descriptions.

Known Stressors of Bacterial Genes

All strains of *E. coli* were exposed to known stressors in the 96 well plate to induce the respective stress genes and serve as a baseline to compare our treatment groups to. The *recA'* wells were exposed to UV light (MODEL UVL-56 BLAK-RAY LAMP, UVP Inc. San Gabriel, CA) three inches above the plate for fifteen seconds to positively test for the SOS response mechanism. All *grpE'* wells were treated with 40% EtOH to positively test for the heat shock response, and *katG'* was treated with 0.04% H_2O_2 as a positive control to test for oxidative damage.[25,26] All stressors were added to wells that already contained bacteria. Both EtOH and H_2O_2 solutions were wrapped in aluminum foil and stored at -18 °C. Each plasmid containing a promoter had the ability to emit bioluminescence when evoking a stress response, and bioluminescence was measured in relative light units (RLU) every twenty minutes for fifteen hours. Biomass was measured simultaneously with OD_{600}.

96-well Plate Design

A 96-well plate was used to perform the experiment. Total amounts in each well were 200 µl. The volume of LB was adjusted to accommodate for the additional volume of SCFAs and stressors. Plate stickers were used to prevent evaporation over the 15-hour period. All experiments were performed in three technical replicates on one plate. One representative plate was used for analysis. In addition, five biological (different overnight cultures) replicates were done to verify trends in the data. Bioluminescence and biomass were read by a BioTek Synergy H1 Reader (Agilent, Santa Clara, CA).

Data Analysis

Bioluminescence data obtained as RLU was divided by the biomass data obtained as OD_{600} to obtain values that were normalized to the biomass. This value served as the mean of the replicates of the respective combinations of promoter fusion, stress, and SCFA. The average and standard deviations were determined across the three replicates from a representative plate and expressed as RLU/OD_{600}. Statistical analysis was done using the Graphpad Prism8 software. A one-way ANOVA with a post-Dunnett's multiple comparison test was performed to compare the ratios of biomass and bioluminescence to the positive control at the 20-minute time point. All statistics were analyzed with a 95% confidence interval (p-value <0.05) as a cut-off for statistical significance between the groups.

RESULTS

Biomass was not affected by the addition of SCFA

The biomass (OD_{600}) and bioluminescence (RLU) curves of *E. coli* DPD2511, TV1061, DPD2794, and W3110 containing the plasmids with the *recA'::lux*, *katG'::lux*, and *grpE'::lux* and promoterless *luxCDAB*E operon can be seen in **Figure 4**. Three different SCFAs – acetate, butyrate, and propionate – were used for testing. **Figure 4** depicts the *E. coli* response to propionate; the two remaining SCFAs followed significantly similar trends (data not shown). All *E. coli,* regardless of the promoter fusion, showed stagnant biomass over a 15-hour period. The biomass was independent of the treatments and controls for each strain, and differences were not statistically significant (p-value >0.05) between any of the strains.

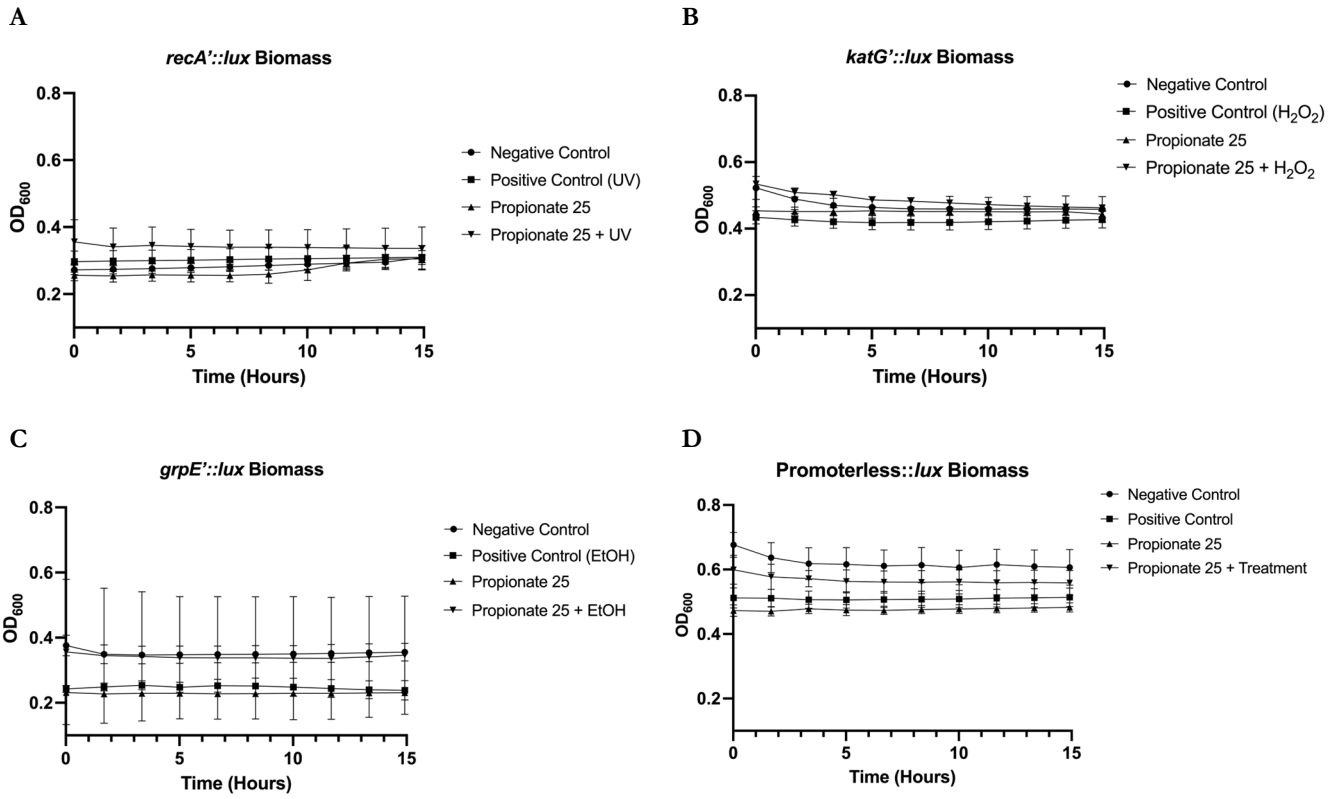

Figure 4. *E. coli* biomass for all four treatments. A) Shows the biomass of DPD2794 (*recA'*). B) Shows the biomass of DPD2511 (*katG'*). C) Shows the biomass of TV1061 *(grpE')*. D) Shows the biomass of W3110 with promoterless plasmid. Treatment groups consisted of negative control (•), positive control (▪) (known stressors UV light, H_2O_2, and EtOH, respectively), SCFA at 25 mM concentration (▲), and an SCFA at 25 mM in addition to a known stressor (▼).

Bioluminescence response to SCFAs

The stress response for the first three hours in *E. coli* strains DPD2794 *(recA')*, DPD2511 (*katG')*, TV1061 (*grpE')*, and W3110 (promoterless) can be seen in **Figure 5**. Propionate data can be seen in **Figure 5** as a representative; acetate and butyrate followed similar patterns (data not shown).

The stress caused an almost immediate bioluminescence response, measured in relative light units (RLU) in the positive control treatments, which lasted for about two hours, then dramatically decreased. The *recA'::lux* fusion (**Figure 5A**) was stressed with UV as a positive control and exhibited peak bioluminescence at 20 minutes. All other treatment groups were significantly different (p-value <0.0001) from the positive control (UV). The *katG'::lux* (**Figure 5B**), which was stressed with H_2O_2, and the *grpE'::lux* (**Figure 5C**) which was stressed with EtOH followed the same pattern, and both exhibited peak bioluminescence at 20 minutes. The promoterless plasmid (**Figure 5D**) showed no bioluminescence throughout the entire 15-hour period and was used to demonstrate that the responses measured were not specific to the *lux* operon reporter genes.

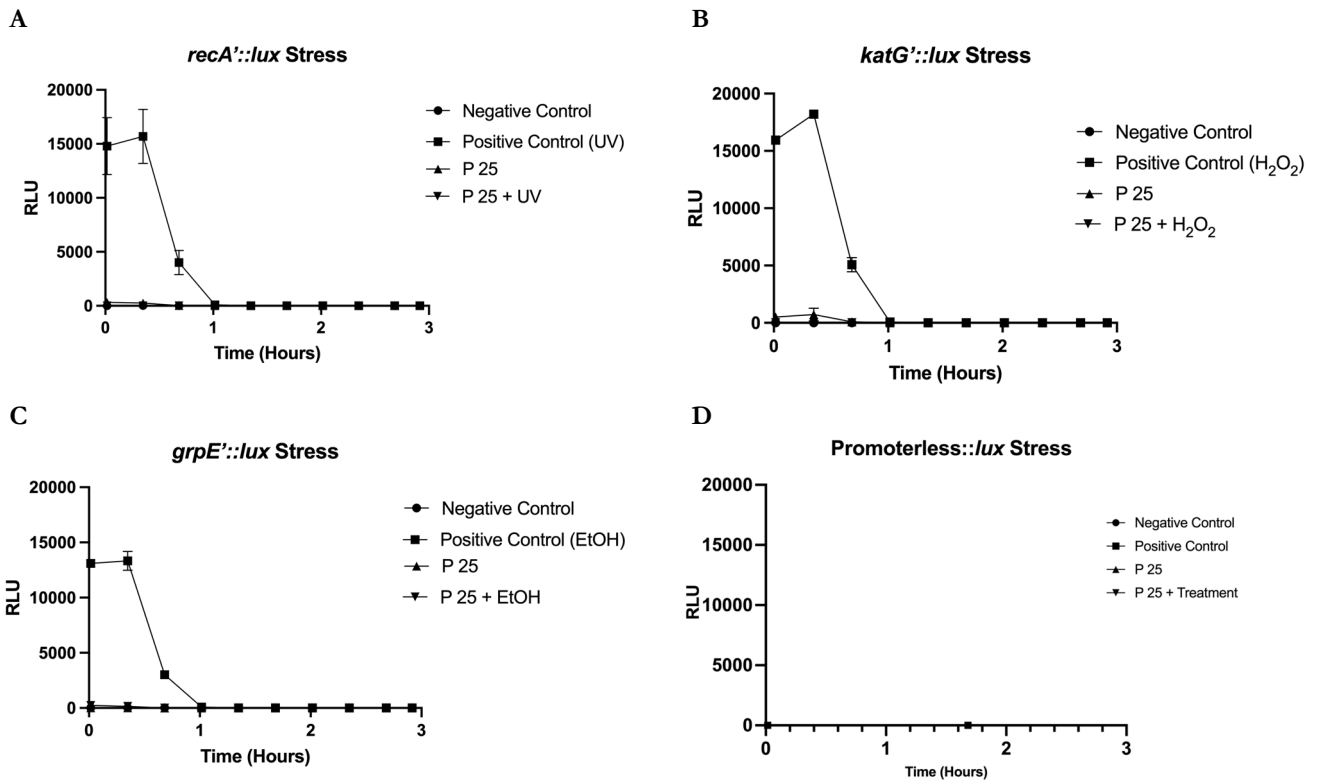

Figure 5. *E. coli* bioluminescence for all four treatments. A) Shows the bioluminescence of DPD2794 *(recA').* B) Shows the bioluminescence of DPD2511 (*katG').* C) Shows the bioluminescence of TV1061 *(grpE').* D) Shows the bioluminescence of W3110 with promoterless plasmid. Treatment groups consisted of negative control (•), positive control (▪) (known stressors UV light, H_2O_2, and EtOH, respectively), SCFA at 25 mM concentration (▲), and an SCFA at 25 mM in addition to a known stressor (▼).

SCFAs mitigate activation of stress promoters in the presence of known stressors

Figure 6 shows the normalized data from the 20-minute time points in **Figure 4** and **5**, when bioluminescence data in RLU were divided by the OD_{600} values for each of the treatments and promoter fusions. The negative control was statistically significant from the positive control *(p*-value <0.0001), but not statistically significant from the SCFA treatment groups at all concentrations. This trend was observed for all three promoters (data not shown).

Normalized bioluminescence was compared to the positive control in the *recA'* promoter across treatment groups for acetate, butyrate, and propionate at 25 mM and 25 mM + a known stressor (UV) (**Figure 6A**). The positive control (UV) was significantly different *(p*-value <0.0001) from the negative control and all other treatments as shown by a one-way ANOVA with a Dunnett's post-hoc test.

The SCFAs acetate, butyrate, and propionate at 25mM concentration and with the addition of a known stressor in cells containing the *katG'* promoter followed a similar trend to the *recA'* data as shown in **Figure 6B** at 20 minutes. All SCFA treatments, in addition to the negative control, displayed a statistically significant difference *(p*-value <0.0001) from the positive control (H_2O_2).

Different treatment groups of SCFAs with the same concentrations as described in **Figure 6A** and **6B** were utilized to test *grpE'* as shown in **Figure 6C.** Similar to the other promoters, all SCFA treatments, in addition to the negative control, displayed a statistically significant difference *(p*-value <0.0001) from the positive control (EtOH).

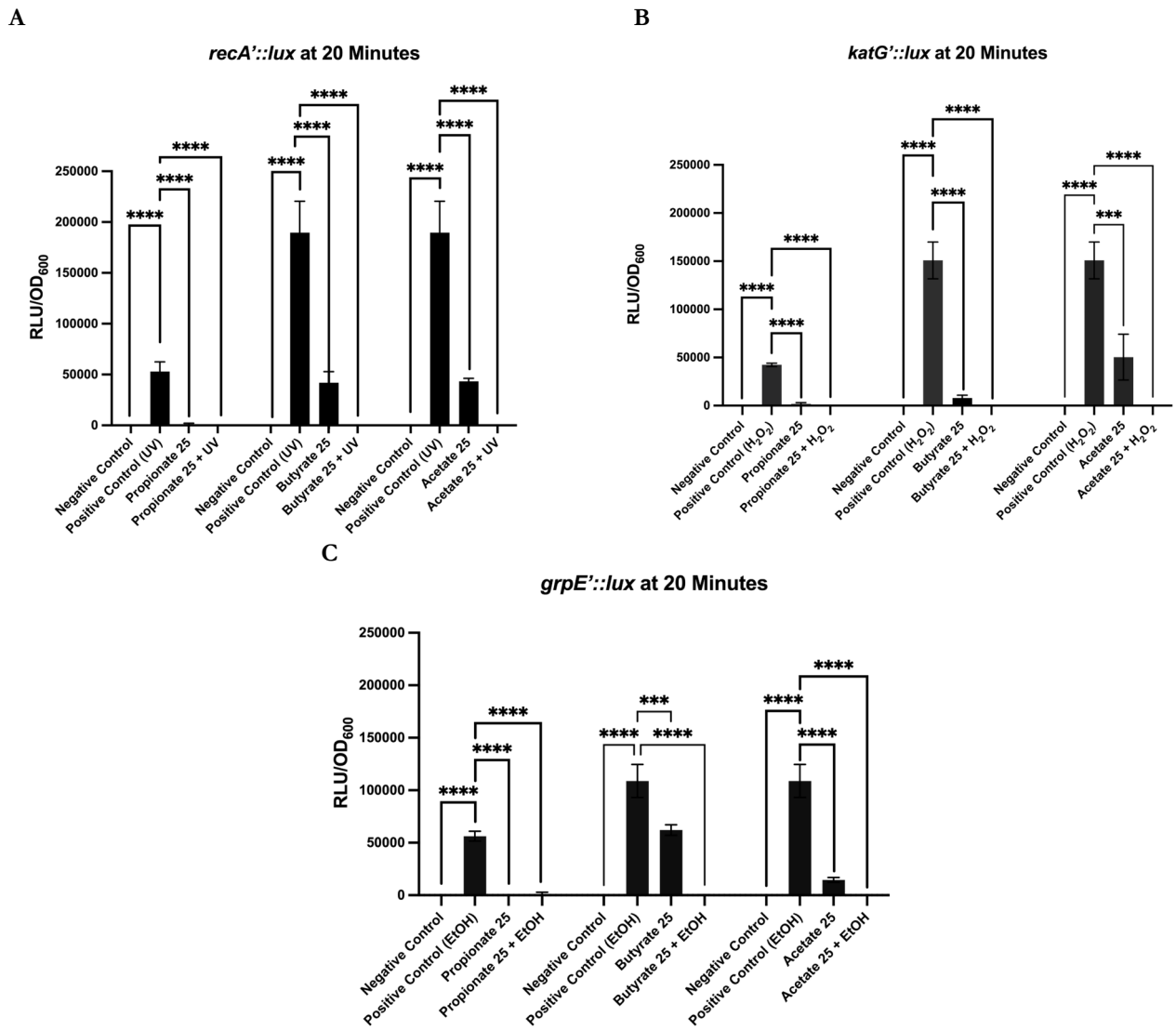

Figure 6. Maximum bioluminescence/OD_{600} at the 20-minute time point. A) DPD2794 (*recA'*). B) DPD2511 (*katG'*). C) TV1061 *(grpE').* **** indicates a statistically significant difference (p<0.0001*)* from the positive control as determined by a one-way ANOVA and a Dunnett's *post hoc* test.

DISCUSSION

The goal of this study was to test the hypothesis that SCFAs acetate, butyrate, and propionate would prevent the activation of stress promoters in the presence of their respective known stressors. The results demonstrate that acetate, butyrate, and propionate at a concentration of 25 mM does not appear to activate stress promotors in *E. coli* as shown in the DPD2794 *recA'::lux,* DPD2511 *katG'::lux,* and TV1061 *grpE'::lux.* Additionally, acetate, butyrate, and propionate at 25 mM prevented the activation of stress promoters even in the presence of known stressors. This may indicate that the presence of these SCFAs protected the bacteria from activating a respective stress response.

In addition to bioluminescence, biomass was measured every 20 minutes for 15 hours. Biomass in all the strains used for testing – DPD2794 *recA'::lux,* DPD2511 *katG'::lux,* TV1061 *grpE'::lux,* and the W3110 promoterless::*lux* – was consistent over the entire 15 hours with no statistically significant differences between treatments. The positive controls and concentrations were chosen due to their ability to cause stress, but not kill the bacteria. Biomass of *E. coli* did not produce a standard growth curve throughout experimentation, possibly due to high OD readings at the point of inoculation. This was intended to show that the induced stress did not impact growth. The stationary phase biomass levels also helped maintain a steady state of ATP that is required to maximize bioluminescence from the *luxCDABE* operon.[36] In the *lux* operon, especially the *lux* C, D, and E genes, fatty-acid reductase is used for light emission due to the aldehyde-independent genes that flank luciferase genes.[36]

Normalized stress gene expression, measured as RLU/OD_{600} over a 15-hour period, peaked at 20 minutes for the positive control treatments. The positive control was the only treatment option that showed a significant difference from the negative control. There was no statistically significant difference between the negative control and the SCFA treatment groups, which indicates that the SCFAs in their sodium form do not cause any of the three tested stresses in *E. coli* at the mM levels used in this study. The SCFAs at 25 mM in addition to a known stressor also did not elicit a stress response in the gene, a response that was observed in the known stressors alone, which shows a lack of activation of the *lux* operon from the respective stress promoter. This could be indicative of a protective effect of SCFAs on the *E. coli* stress response, preventing the activation of a stress response gene in the presence of stressors.

Prior to this study, there was limited knowledge on how SCFAs acetate, butyrate, and propionate in their sodium forms affect the *E. coli* stress response. One study was done by Kirkpatrick to determine how acetate in its acidic form causes stress to *E. coli* when combined with formic acid.[15] Kirkpatrick *et al.* determined that acetic acid at 50 mM induced the RpoS regulon. They also found that acetic acid induced metabolic enzymes GatY and YfiD, which are part of stress response to acid (low pH), indicating that the stress activation response may be due to the acidic nature of acetic acid and not based on the SCFA itself.[15,37] Further, formic acid was found to induce a stress response in a similar fashion to acetic acid, but *E. coli* stress responses were reduced when formic acid was added in addition to acetic acid.[15] However, in our study, the starting pH of the culture did not change due to the presence of the SCFAs. This could explain the contradiction between the above studies and ours. SCFAs used for the purpose of this study were in their sodium form to limit the effect that pH changes had on the bacteria. Another study showed that pretreatment with sodium acetate exhibited a protective effect against oxidative stress and increased acidic survival in *E. coli* O157:H7.[6] However, there was a lack of research on whether SCFAs butyrate and propionate have the same effects on *E. coli,* which our study addressed. The mechanism of action for how these SCFAs prevent the activation of stress promoters in *E. coli* is unknown. It has been hypothesized that their effect is dependent on oxygen availability and environment pH.[32]

Future directions for this experiment would seek to test whether the SCFAs butyrate and propionate in their sodium form specifically caused a protective effect in *E. coli.* Due to the results of previous research on acetate and based on the patterns observed in **Figure 6**, there is the possibility that the SCFAs are protective against stress. To further examine this effect, it would need to be determined that SCFAs at 25 mM directly increase the survival rate of *E. coli.* Additionally, a broader effect of SCFA stress in the gut microbiome could be investigated by performing similar experiments in other bacterial species, such as *Listeria monocytogenes*.[38] Further research could explore other stress genes, such as the *lexA'::lux* to determine if SCFAs have a protective effect against low pH.[39]

Currently, medical treatments are being explored by artificially using SCFAs – specifically butyrate—to rescue the gut microbiota and restore normal functions in those who experience metabolic syndromes that correlate with the depletion of normal levels of these fatty acids.[40,41] Various ailments and conditions such as ulcerative colitis, type 1 and type 2 diabetes, obesity, and other forms of gut dysbiosis are improved by dietary supplementation of SCFAs, which restore homeostasis in the gut microbiome.[1,9,40,41] Understanding the relationship between SCFAs and survival rates of *E. coli* could allow for a better understanding of how acetate, butyrate, and propionate affect the gut microbiome and host homeostasis, with the ultimate goal of using them as a mitigation technique for gut dysbiosis.

ACKNOWLEDGEMENTS

The authors thank Dr. Amy Vollmer for providing the strains used in this study, Dr. Glenn Dorsam for providing acetate, butyrate, and propionate, Dr. Barney Geddes for helpful insight and discussions, and the Department of Microbiological Sciences at North Dakota State University for their financial support.

REFERENCES

1. Tan J, McKenzie C, Potamitis M, Thorburn AN, Mackay CR, Macia L. (2014) The Role of Short-Chain Fatty Acids in Health and Disease. *Adv Immunol* 91-119. *doi:10.1016/B978-0-12-800100-4.00003-9*
2. Sender R, Fuchs S, Milo R. (2016) Revised Estimates for the Number of Human and Bacteria Cells in the Body. *PLOS Biology* 1-14. *doi:10.1371/journal.pbio.1002533*
3. Topping DL. (1996) Short-chain fatty acids produced by intestinal bacteria. *Asia Pacific Journal of Clinical Nutrition* 15-19.
4. Cook SI, Sellin JH. (1998) Review article: Short chain fatty acids in health and disease. *Alimentary Pharmacology and Therapeutics* 499-507. *doi:10.1046/j.1365-2036.1998.00337*
5. Morrison DJ, Preston T. (2016) Formation of short chain fatty acids by the gut microbiota and their impact on human metabolism. *Gut microbes* 189-200. *doi:10.1080/19490976.2015.1134082*
6. Arnold CN, McElhanon J, Lee A, Leonhart R, Siegele DA. (2001) Global Analysis of *Escherichia coli* Gene Expression during the Acetate-Induced Acid Tolerance Response. *Journal of Bacteriology* 2178-2186. *doi:10.1128/JB.183.7.2178-2186.2001*

7. Lin Y, Fang ZF, Che LQ, Xu SY, Wu D, Wu CM, Wu XQ. (2014) Use of Sodium Butyrate as an Alternative to Dietary Fiber: Effects on the Embryonic Development and Anti-Oxidative Capacity of Rats. *PLOS One. doi:10.1371/journal.pone.0097838*
8. Shi L, Tu BP. (2015) Acetyl-CoA and the regulation of metabolism: Mechanisms and consequences. *Current Opinion in Cell Biology* 125-131. *doi:10.1016/j.ceb.2015.02.003*
9. Priyadarshini M, Kotlo KU, Dudeja PK, Layden BT. (2018) Role of Short Chain Fatty Acid Receptors in Intestinal Physiology and Pathophysiology. *Comprehensive Physiology* 1091-1115. *doi:10.1002/cphy.c170050*
10. Wong JMW, de Souza R, Kendall CWC, Emam A, Jenkins DJA. (2006) Colonic Health: Fermentation and Short Chain Fatty Acids. *Journal of Clinical Gasterenterology* 235-243. *doi:10.1097/00004836-200603000-00015*
11. De Vadder F, Kovatcheva-Datchary P, Zitoun C, Duchampt A, Bäckhed F, Mithieux G. (2016) Microbiota-Produced Succinate Improves Glucose Homeostasis via Intestinal Gluconeogenesis. *Cell Metabolism* 151-157. *doi:10.1016/j.cmet.2016.06.013*
12. National Center for Biotechnology Information. PubChem Compound Summary for CID 175, Acetate, *https://pubchem.ncbi.nlm.nih.gov/compound/Acetate*
13. National Center for Biotechnology Information. PubChem Compound Summary for CID 104745, Propionate, *https://pubchem.ncbi.nlm.nih.gov/compound/Propionate*
14. National Center for Biotechnology Information. PubChem Compound Summary for CID 104775, Butyrate, *https://pubchem.ncbi.nlm.nih.gov/compound/Butyrate*
15. Kirkpatrick C, Maurer LM, Oyelakin NE, Yoncheva YN, Maurer R, Slonczewski JL. (2001) Acetate and Formate Stress: Opposite Responses in the Proteome of *Escherichia Coli. Journal of Bacteriology* 6466-6477. *doi:10.1128/JB.183.21.6466-6477.2001*
16. Battesti A, Majdalani N, Gottesman S. (2011) The RpoS-Mediated General Stress Response in *Escherichia coli. Annual Review of Microbiology* 189-213. *doi:10.1146/annurev-micro-090110-10294*
17. Delmas J, Dalmasso G, Bonnet R. (2015) *Escherichia coli*: The Good, the Bad and the Ugly. *Clinical Microbiology. doi:10.4172/2327-5073.1000195*
18. Kowalczykowski SC. (1991) Biochemical and biological function of *Escherichia coli* RecA protein: behavior of mutant RecA proteins. *Biochimie* 289-304. *doi:10.1016/0300-9084(91)90216-N*
19. Huisman O, D'Ari R, Gottesman S. (1984) Cell-division control in *Escherichia coli*: specific induction of the SOS function SfiA protein is sufficient to block septation. *Proceedings of the National Academy of Sciences* 4490-4494. *doi:10.1073/pnas.81.14.4490*
20. Ang D, Chandrasekhar GN, Zylicz M, Georgopoulos C. (1986) *Escherichia coli* grpE gene codes for heat shock protein B25.3, essential for both lambda DNA replication at all temperatures and host growth at high temperature. *Journal of Bacteriology* 25-29. *doi:10.1128/jb.167.1.25-29.1986*
21. Wu B, Ang D, Snavely M, Georgopoulos C. (1994) Isolation and characterization of point mutations in the *Escherichia coli* grpE heat shock gene. *Journal of Bacteriology* 6965-6973. *Doi:10.1128/jb.176.22.6965-6973.1994*
22. Zhang L, Alfano JR, Becker DF. (2015) Proline Metabolism Increases *katG* Expression and Oxidative Stress Resistance in *Escherichia coli. Journal of Bacteriology* 431-440. *doi:10.1128/JB.02282-14*
23. Panek HR, O'Brian MR. (2004) KatG Is the Primary Detoxifier of Hydrogen Peroxide Produced by Aerobic Metabolism in *Bradyrhizobium japonicum. Journal of Bacteriology* 7874-7880. *doi:10.1128/JB.186.23.7874-7880.2004*
24. Doukyu N, Taguchi K. (2021) Involvement of catalase and superoxide dismutase in hydrophobic organic solvent tolerance of *Escherichia coli. AMB Express* 97. *doi:10.1186/s13568-021-01258-w*
25. Vollmer AC, Kwakye S, Halpern M, Everbach EC. (1998) Bacterial Stress Responses to 1-Megahertz Pulsed Ultrasound in the Presence of Microbubbles. *Applied and Environmental Microbiology* 3927-3931. *doi:10.1128/aem.64.10.3927-3931.1998*
26. Vollmer AC, Belkin S, Smulski DR, van Dyk TK, Larossa RA. (1997) Detection of DNA Damage by Use of *Escherichia Coli* Carrying RecA::Lux, UvrA::Lux, or AlkA::Lux Reporter Plasmids. *Applied and Environmental Microbiology* 2566-2571. *doi: 10.1128/aem.63.7.2566-2571.1997*
27. Belkin S, Smulski DR, Vollmer AC, van Dyk TK, Larossa RA. (1996) Oxidative Stress Detection with *Escherichia Coli* Harboring a KatG::Lux Fusion. *Applied and Environmental Microbiology* 2252-2256. *doi: 10.1128/aem.62.7.2252-2256.1996*
28. van Dyk TK, Majarian WR, Konstantinov KB, Young RM, Dhurjati PS, LaRossa RA. (1994) Rapid and sensitive pollutant detection by induction of heat shock gene-bioluminescence gene fusions. *Applied and Environmental Microbiology* 1414-1420. *doi:10.1128/aem.60.5.1414-1420.1994*
29. Chambers ES, Preston T, Frost G, Morrison DJ. (2018) Role of Gut Microbiota-Generated Short-Chain Fatty Acids in Metabolic and Cardiovascular Health. *Current Nutrition Reports* 198-206. *doi:10.1007/s13668-018-0248-8*
30. Silva YP, Bernardi A, Frozza RL. (2020) The Role of Short-Chain Fatty Acids From Gut Microbiota in Gut-Brain Communication. *Frontiers in Endocrinology. doi:10.3389/fendo.2020.00025*
31. Lin J, Smith MP, Chapin KC, Baik HS, Bennett GN, Foster JW. (1996) Mechanisms of acid resistance in enterohemorrhagic *Escherichia coli. Applied and Environmental Microbiology* 3094-3100. *doi:10.1128/aem.62.9.3094-3100.1996*

32. Bushell F, Herbert JMJ, Sannasiddappa TH, Warren D, Turner AK, Falciani F, Lund PA. (2021) Mapping the transcriptional and fitness landscapes of a pathogenic *E. coli* strain: The effects of organic acid stress under aerobic and anaerobic conditions. *Genes* 1-25. *doi:10.3390/genes12010053*

33. Ernsting BR, Atkinson MR, Ninfa AJ, Matthews RG. (1992) Characterization of the regulon controlled by the leucine-responsive regulatory protein in *Escherichia coli*. *Journal of Bacteriology* 1109-1118. *doi:10.1128/jb.174.4.1109-1118.1992*

34. van Dyk TK, Smulski DR, Reed TR, Belkin S, Vollmer AC, LaRossa RA. (1995) Responses to toxicants of an *Escherichia coli* strain carrying a uspA'::lux genetic fusion and an *E. coli* strain carrying a grpE'::lux fusion are similar. *Applied and Environmental Microbiology* 4124-4127. *doi:10.1128/aem.61.11.4124-4127.1995*

35. Rogowsky PM, Close TJ, Chimera JA, Shaw JJ, Kado CI. (1987) Regulation of the vir genes of *Agrobacterium tumefaciens* plasmid pTiC58. *Journal of Bacteriology* 5101-5112. *doi:10.1128/jb.169.11.5101-5112.1987*

36. Meighen EA. (1988) Enzymes and Genes from the lux Operons of Bioluminescent Bacteria. *Annual Review of Microbiology* 151-176. *doi:10.1146/annurev.mi.42.100188.001055*

37. Blankenhorn D, Phillips J, Slonczewski JL. (1999) Acid- and Base-Induced Proteins during Aerobic and Anaerobic Growth of *Escherichia coli* Revealed by Two-Dimensional Gel Electrophoresis. *Journal of Bacteriology* 2209-2216. *doi:10.1128/JB.181.7.2209-2216.1999*

38. Quereda JJ, Dussurget O, Nahori MA, Ghozlane A, Volant S, Dillies MA, Regnault B, Kennedy S, Mondot S, Villoing B, Cossart P, Pizarro-Cerda J. (2016) Bacteriocin from epidemic *Listeria* strains alters the host intestinal microbiota to favor infection. *Proceedings of the National Academy of Sciences* 5706-5711. *doi:10.1073/pnas.1523899113*

39. Dri AM, Moreau PL. (1994) Control of the LexA regulon by pH: evidence for a reversible inactivation of the LexA repressor during the growth cycle of *Escherichia coli*. *Molecular Microbiology* 621-629. *doi:10.1111/j.1365-2958.1994.tb01049.x*

40. Chapman MAS, Grahn MF, Hutton M, Williams NS. (2005) Butyrate metabolism in the terminal ileal mucosa of patients with ulcerative colitis. *British Journal of Surgery* 36-38. *doi:10.1002/bjs.1800820115*

41. Scheppach W, Sommer H, Kirchner T, Paganelli GM, Bartram P, Christl S, Richter F, Dusel G, Kasper H. (1992) Effect of butyrate enemas on the colonic mucosa in distal ulcerative colitis. *Gastroenterology* 51-56. *doi:10.1016/0016-5085(92)91094-K*

ABOUT STUDENT AUTHORS

Kathleen Ruff-Schmidt graduated from North Dakota State University with a B.S. in Microbiology in May of 2022. She is currently attending medical at the University of North Dakota and plans to obtain her MD. Kaylee Weigel will graduate from North Dakota State University in May of 2023 with a B.S. in Microbiology and in May of 2024 with an M.S. in Microbiology. She plans to attend medical school to obtain both an MD and a Ph.D.

PRESS SUMMARY

Regulation of microbes in the human intestinal tract maintains overall human health and prevents diseases, such as inflammatory bowel disease and obesity. Short-chain fatty acids (SCFAs) in the intestine are produced by bacterial fermentation and aid in inflammation reduction, dietary fiber digestion, and metabolizing nutrients for the colon. SCFAs are starting to be used in clinical interventions for inflammatory diseases. This study aims to evaluate the effects of SCFA on the activation of the stress response in *E. coli,* which is a representative bacterium of the intestine. Three different SCFAs were added to cultures prior to stressing the bacteria causing a lower level of stress activation when compared to bacteria that were stressed in the absence of SCFAs. Our data is consistent with the idea that SCFAs reduce stress in bacteria and consequently the inflammatory response that contributes to disease.

Quantification of Microfibers from Marine Sediments from Three Locations in Southern California: An Exposed Beach (Ventura County), a Watershed (Los Angeles County), and an Enclosed Harbor (Orange County)

Adrianna Ebrahim[a] & Mia LeClerc*[b]*

[a]*Department of Biological Sciences, California Lutheran University, Thousand Oaks, CA*
[b]*Department of Earth and Environmental Science, California Lutheran University, Thousand Oaks, CA*

https://doi.org/10.33697/ajur.2022.066

Students: aebrahim@callutheran.edu, mleclerc@callutheran.edu**
Mentor: huvard@callutheran.edu

ABSTRACT
Microfibers are small (<5 mm) fibers made of synthetic materials that are ubiquitous in the environment. The purpose of this observational study was to quantify the number of microfibers in marine sediments and determine which locations have the highest risk for this type of pollution. Sediment samples were taken from three locations in Southern California (Sycamore Watershed, Ventura State Beach Jetty, and Newport Beach Harbor) to determine which had the highest number of microfibers. It was hypothesized that microfibers would be found at each sample site and that the most microfibers would be found at Sycamore Watershed due to its proximity to a wastewater discharge point. The microfibers were separated from the sediment through a process of stratification and filtration and analyzed by a one-way ANOVA and Tukey s test. Per sample, there was an average of 111.5 (±99.3, n=14) microfibers found per sample at Sycamore Watershed, 59 (±17.4, n=18) at Newport Beach Harbor, and 53 (±14.4, n=18) at Ventura State Beach Jetty. A total of 3,590 microfibers were found from all three sample sites. Analysis revealed that Sycamore Watershed had significantly more microfibers than any other site ($p<.05$). It is likely that Sycamore Watershed had the most microfibers because of its proximity to a sewage-sludge disposal site that contains the polluted water from our washing machines. In conclusion, microfibers are polluting the sediments in harbors, open coastlines, and watersheds in California, negatively affecting the ecosystems in these areas.

KEYWORDS
Microfiber; Microplastic; Macroplastic; Marine Pollution; Synthetic Materials; Wastewater Treatment Plants; Sediments; Watershed; Harbor; Jetty

INTRODUCTION

Ocean pollution is a pressing issue that impacts all depths of the oceans, their coastliness, and the organisms that rely on the seas for food. Much of this pollution comes from plastic waste of varying sizes. As the plastic is broken into smaller pieces over time, it can become considered microplastic. Though microplastics are less than 5 mm across and smaller than macroplastics, they are still a growing and concerning type of pollution.[1, 2] Microplastic debris accumulate in natural habitats worldwide, from the North to the South poles and the bottom of the seafloor to urban beaches.[3, 4] While most microplastics come from larger pieces that have been weathered, some microplastics enter the ocean in their original state. For instance, microbeads in exfoliating scrubs are made of plastic, and once rinsed off and flushed down the drainage system, can sometimes avoid or pass through the filters in wastewater treatment facilities and end up accumulating in the environment. More than eight trillion microbeads are dumped into the water systems in the United States every day.[5, 6] The more these plastics accumulate in the ocean, the more scientists are beginning to see how they are harming the ecosystems at many levels of the trophic pyramid.

Microfibers are the most abundant category of microplastics. They are categorized as a synthetic plastic most commonly made out of polyester, acrylic, or nylon that has been shaped into a fiber used to form different styles of clothing, textiles, or non-woven textiles.[1, 2, 7-9] Today, synthetic fibers make up 14.5% of plastics produced by mass and account for almost 2/3 of fibers produced worldwide. [9] The majority of these fibers make their way into the ocean from washing machines that discharge their untreated

wastewater or from wastewater treatment plants (WWTPs), where the greywater has not been properly treated, leading to the microfibers being released into the ecosystem.[2, 8-11] Browne *et al.*, (2011)[10] found that a single piece of clothing can produce over 1900 microfibers from one wash cycle. In a study by Peller *et al.* (2019)[12], it was estimated that as many as eight trillion microfibers are emitted daily from WWTPs operating in the United States. Microfibers have been found worldwide but are present in higher quantities in areas with high populations of humans and runoff. [1, 10, 13]

Natural fabrics are made from natural materials like silk, cotton, wool, and linen. As technology has advanced, new synthetic fabrics have been created to improve upon the durability of natural fabrics and lower the manufacturing cost. These synthetic fabrics have garnered global usage for their inexpensive, versatile, and durable nature, but are also negatively impacting our marine environment. Synthetic textiles are a danger due to the same factors that make them marketable: they are resistant, lightweight, and long lasting. Their durability means that the synthetic threads that make up the clothing are not biodegradable and will persist in an environment for decades. The thread's lightweight nature allows them to be carried hundreds if not thousands of miles from their point of origin and their diversity in shapes makes them available to be ingested by numerous aquatic organisms.[5, 10, 11, 14, 15] Ingestion of these items is a growing concern for organisms at all levels of the food chain. If ingested, the plastic thread can lead to starvation by blocking or damaging the stomach and lessening feeding. Organisms that ingest plastic have also been found to have lower energy reserves, decreased ability to remove bacteria, and are more susceptible to oxidative stress.[15] This also becomes a problem where trophic-transfer occurs, as when small organisms such as zooplankton ingest synthetic threads, the pollutants are transferred up the food chain, and if enough are accumulated, it could harm a predator higher on the trophic pyramid. [6, 11, 16] Synthetic materials are not only dangerous for these factors, but also for the fact that they can leach many chemicals into the surrounding environment. For instance, flame retardants such as triphenyl phosphate (TPhP), AZO dyes, PFCs (Perfluorocarbon), and formaldehydes can be added to clothing to make them stain and wrinkle resistant as well as waterproof. These additives have been found to be cancerous and in some cases linked to hormone disruption in humans.[17] Chemical additives play a great role in modifying physical or chemical properties of plastic materials.[18] Plastic additives include plasticizers such as dibutyl phthalate (DBP), benzyl butyl phthalate (BBP), diisobutyl phthalate (DiBP), bis (2-ethylhexyl) phthalate (DEHP), and other phthalates to promote the plasticity and flexibility of the material.[19] These same chemicals leach into marine ecosystems following a machine wash cycle and, along with the fibers, can threaten the health of marine organisms.

These increased quantities of microfibers are a danger to all marine organisms, especially to filter feeders and other organisms at the bottom of the food chain. Due to their long, thin shape, they have a higher probability of becoming entangled in an animal's digestive tract, and if the digestive system is blocked long enough, the fiber can leach chemicals into the animal, causing disruptions in its endocrine system and hormone regulation.[5, 6] It has been noted that in zooplankton, ingestion of microplastics and fibers has had negative repercussions for the organism's growth, sexual development, and mortality.[6] Over 200 marine and aquatic species, from filter feeders to crabs and fish, have been documented to have ingested microplastics.[16] Microfibers are extremely widespread, having been found in a study by Browne *et al.* (2011)[10] on six continents and 18 sites worldwide. Microfibers have been documented in beach sediments and throughout the water column from the shallows to the deep sea, 5000 m below the surface.[20] This type of pollution is an issue especially in the deep sea because the organisms rely on detritus from the euphotic zone in the form of 'marine snow 'for the majority of their nutrients. These microfibers are the same size as much of that detritus and are being readily ingested by those organisms despite the fact that the point of origin of the plastic was thousands of meters above them . [15] In Cape Town, South Africa, Ryan *et al.* (2020)[14] found microfibers in 26 of their 30 total sediment cores sampled from a public beach. They also noted that microfibers were in the overwhelming majority of particulate pollutants that were found, accounting for 99.7% of microplastics on the study beach.

The purpose of this observational study is to quantify microfibers found at different locations to determine which has the most and discuss possible reasons why some locations may be more polluted than others. The locations sampled in Southern California are Sycamore Watershed, Ventura State Beach Jetty, and Newport Harbor. These three locations were selected because they experience different degrees of wave action and polluted runoff due to their geographical location and environment makeup. Sycamore Watershed in Los Angeles County receives wastewater runoff from WWTPs in Southern Ventura County. Ventura State Beach Jetty in Ventura County is located at an exposed coastline that receives high amounts of wave action and water circulation. Newport Harbor in Orange County is the largest small-boat harbor on the west coast and is a stagnant location with little wave action.

This study will help to fill a local knowledge gap about levels of microfiber pollution in Southern California and to compare sediment microfiber quantities from very different marine environments to understand if there are differences in microfiber abundance between sediments from an exposed beach, a watershed and an enclosed urban harbor. If the results are significant, it could be worth looking into the local WWTPs or runoff sewers to determine if there is a large amount of pollution caused by dumping or improper water treatment. It is expected that there will be microfibers found at all three locations. It is also expected

that Sycamore Watershed will have the highest number of microfibers, as it directly receives wastewater contaminated with microfibers from inland wastewater treatment plants.

METHODS AND PROCEDURES

Sample collection

Sand samples were collected from Sycamore Watershed, Ventura State Beach Jetty, and Newport Harbor at the hightide water line. 14 samples were taken from Sycamore Watershed, 18 from Ventura State Beach Jetty, and 18 from Newport Harbor. Samples were collected from Sycamore Watershed in summer 2021 and from Ventura Jetty and Newport Harbor in summer 2020. There were 14 samples taken from Sycamore Watershed due to time restraints. The sediment from Ventura Jetty and Newport Harbor was collected on the same day and as such, the same number of samples were taken. All of the sediment samples were collected by hand every few feet along the hightide water line and placed into new, previously unopened 1-gallon Ziploc bags that were immediately closed and remained closed until the samples were processed in the lab.

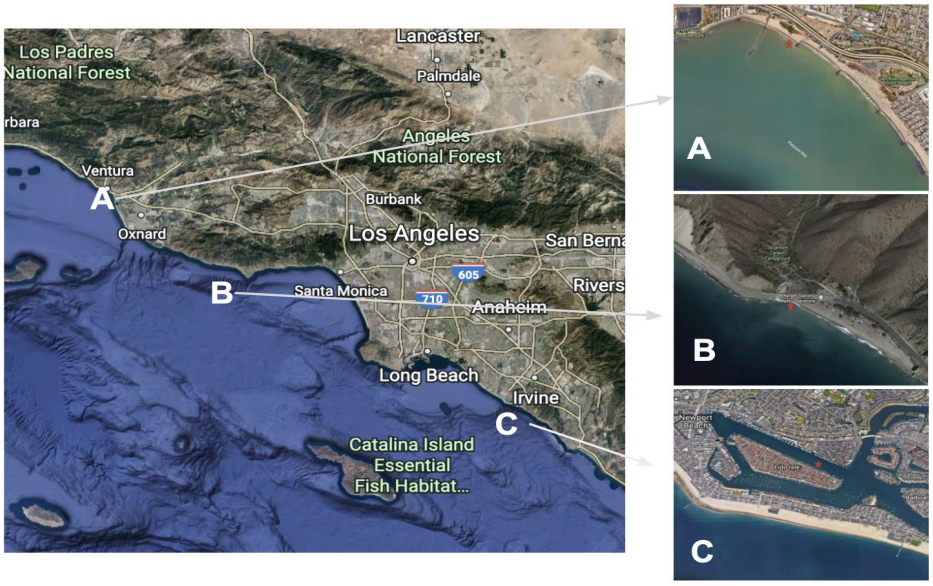

Source: Aerial Image" Southern California Coast." 34.31338°N -118.92202°W. Google Earth.

Figure 1. Location of samples taken from southern California (A: Ventura State Beach Jetty, B: Sycamore Watershed, C: Newport Harbor).

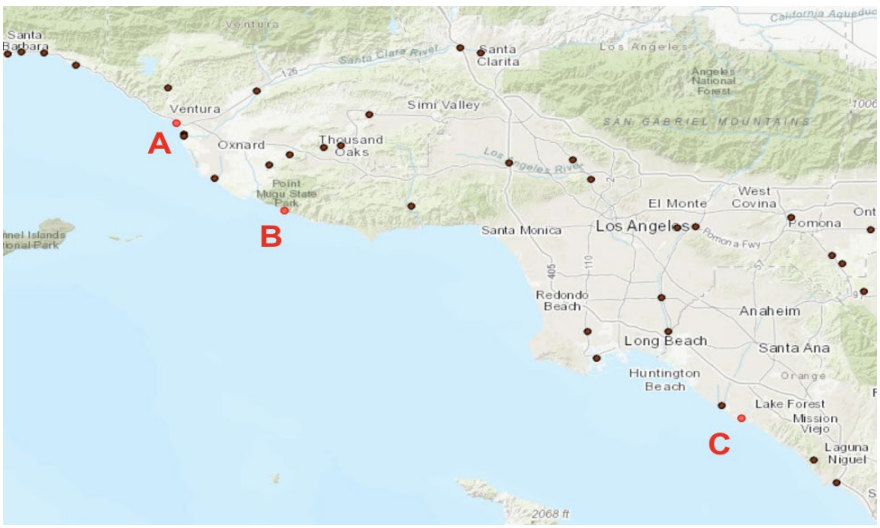

Source: Data Basin WasteWater Treatment Plants, California, *USA"* Conservation Biology Institute.

Figure 2. Map of the Wastewater Treatment Plants in Southern California with Sample Sites Labeled (A: Ventura State Beach Jetty, B: Sycamore Watershed, C: Newport Harbor).

Sample preparation

Instant seawater was made and kept in a closed system in the lab to avoid being contaminated by microfibers and maintained at a salinity of 35 ppm. 100 mL of dry sand was mixed with 200 mL instant seawater in a beaker. The mixture was stirred, suspending the microfibers in the seawater mixture, and allowed to settle so the denser sediment would fall to the bottom. During the stratification process, the mixture was covered with saran wrap to ensure no microfibers fell into the beaker from the air. To avoid potential contamination, cotton lab coats were worn, the mixtures were covered to avoid microfiber fallout from the air, and the samples were only uncovered for brief periods when they were being actively filtered or observed.

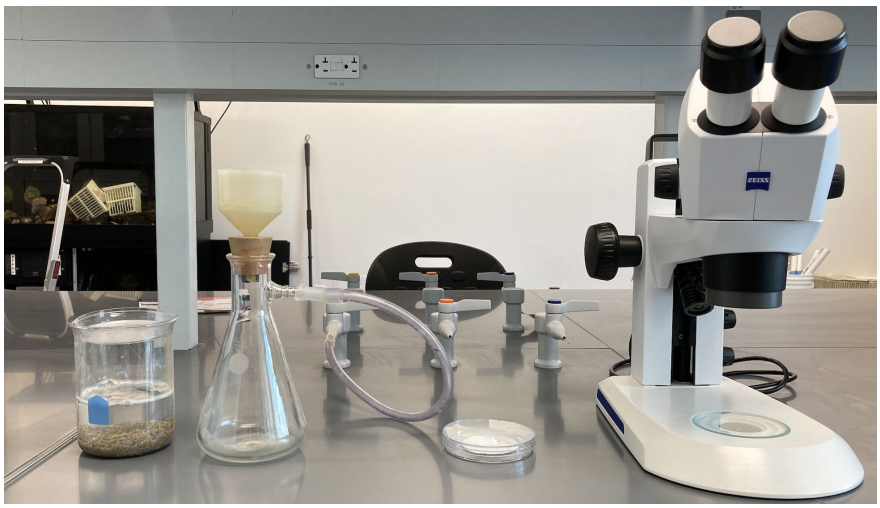

Figure 3. The process by which microfibers were stratified out from sediment, filtered, and observed.

Filtration

Once the sediment in each sample settled, the seawater solution above the sediment layer was poured off and filtered through a Buchner Funnel filtration system that used a 5 µm cellulose nitrate filter paper to catch the microfibers from the mixture. The process was completed a total of six times for samples from Sycamore Watershed and five times for samples from Ventura Jetty and Newport Harbor. The samples from Sycamore Watershed still had microfibers present after five washes had been done, unlike most of the samples from Ventura and Newport, and thus a sixth wash was performed to obtain a more accurate count of the microfibers in each sample. Following the sixth wash, there were zero microfibers observed in the majority of samples, and it was decided that a seventh wash was not needed.

Observation and validation of microfibers

The filter paper was released from the filtration system and placed into a petri dish for examination. The filter paper remained covered in a petri dish to reduce contamination until it was placed under a dissecting microscope. The filter papers were analyzed under a Nikon Stereo dissecting microscope, and the number and color of the microfibers present were noted. Microfibers were counted based on their overall shape and texture, which was consistent with microfibers observed by the lab in previous years. The microfibers generally were smooth, one solid color, and had twisted shapes. Lab blanks were used as a control to determine approximately how much microfiber contamination was in the lab. 20 samples were processed without sediment using the prior methodology. 200 mL of instant seawater was stirred, allowed to settle, and passed through a filter paper. One microfiber was found in one sample, and as such, it is likely that there was very little airborne microfiber contamination in the sediment samples that were processed.

Data analysis

The data were analyzed using Microsoft Excel. The program was used to determine the sums and averages of microfibers found at all three locations based on the number of microfibers per sample. Excel was also used to conduct a one-way analysis of variance (ANOVA) to determine if a difference existed in the means of all three locations sampled. Due to the significance of the

data, a post-hoc Tukey's test was conducted using the website Astatsa to determine which specific locations had a significantly different number of microfibers from each other. Results were significant at $p<.05$.

RESULTS

There were microfibers present in sediment samples from each of the three locations (Sycamore Watershed, Ventura State Beach Jetty, and Newport Harbor). Black, red, green, and other colors, such as purple or blue microfibers **(Figure 4)** were all analyzed under a dissecting microscope. A total of 3,590 microfibers were found. 1,561 of those microfibers were found in Sycamore Watershed, accounting for 43.5% of all microfibers observed. There were 1,062 microfibers found in Newport Harbor and 967 fibers in Ventura State Beach Jetty **(Figure 5).**

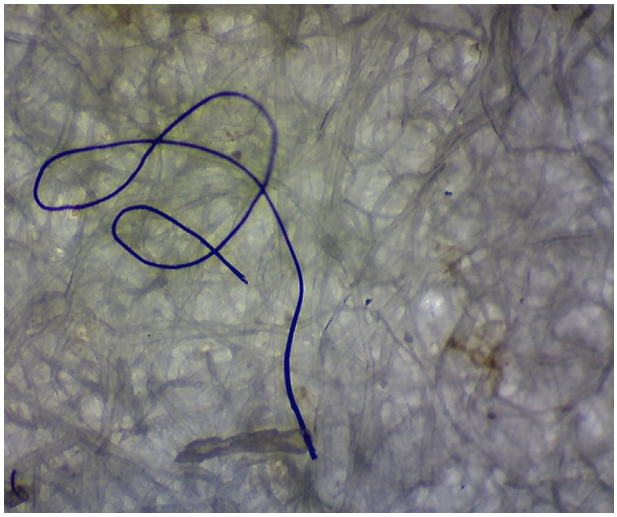

Figure 4. A blue microfiber under a dissecting microscope.

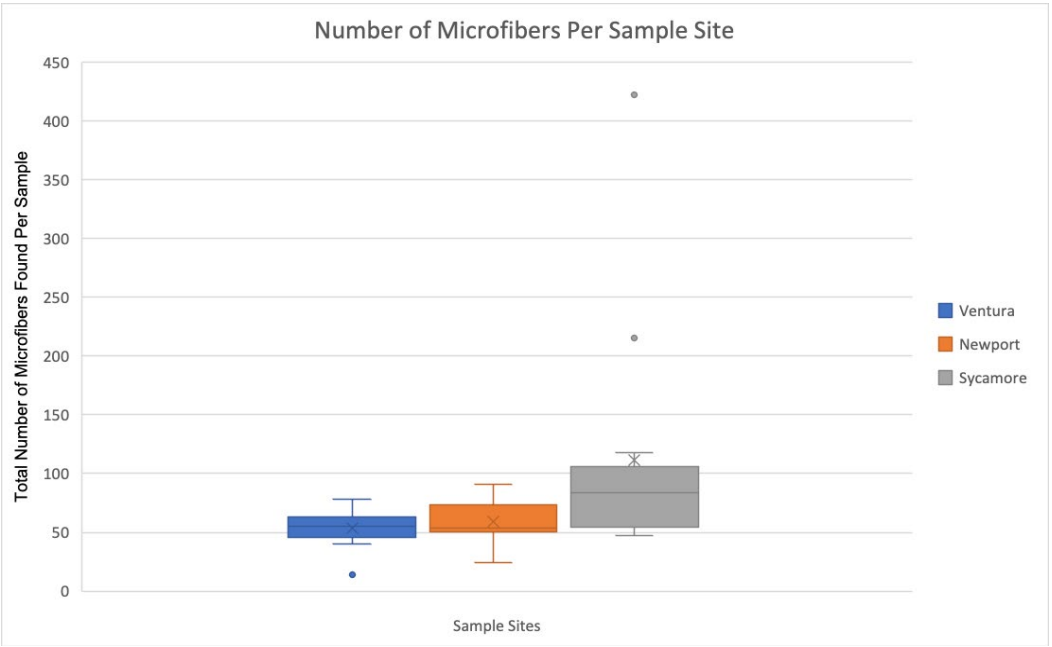

Figure 5. Box and whisker plot displaying the distribution of microfibers found from all three sample sites (n=18, n=18, n=14).

Sycamore Watershed had the highest average number of microfibers per sample, with 111.5 fibers per sample. Newport Harbor had the second-highest average number of microfibers per sample with 59 fibers per sample. Ventura State Beach Jetty had an average of 53.7 microfibers per sample.

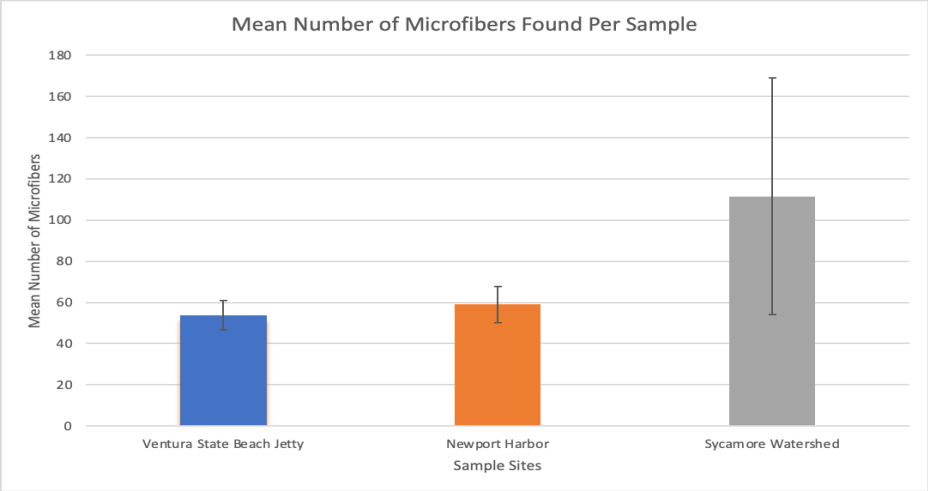

Figure 5. Bar graph depicting the mean number of microfibers found per sample at the Ventura State Beach Jetty (53.7 ±14.4, n=18), Newport Harbor (59 ± 17.4, n=18), and Sycamore Watershed (111.5 ±99.3, n=14) sample sites. (Error bars represent 95% confidence interval).

A one-way ANOVA revealed that there was a significant difference in the mean number of microfibers found in at least two sample sites (DF (2, 47) = 5.3099, p=0.0083) **(Table 1)**. A Tukey's post-hoc test was done to determine which locations differed from each other and found that Sycamore Watershed had significantly more microfibers than the other locations (p<.05) **(Table 2)**. Ventura State Beach Jetty and Newport Harbor were not different from each other.

Data Summary				
Groups	**N**	**Mean**	**Std. Dev.**	**Std. Error**
Group 1	18	53.7222	14.3519	3.3828
Group 2	18	59	17.4356	4.1096
Group 3	14	111.5	99.2555	26.5271

ANOVA Summary					
Source	**Degrees of Freedom DF**	**Sum of Squares SS**	**Mean Square MS**	**F-Stat**	**P-Value**
Between Groups	2	30896.9034	15448.4517	5.3099	0.0083
Within Groups	47	136741.1177	2909.3855		
Total:	49	167638.0211			

Table 1. A one-way ANOVA was performed to determine if sample means differed between groups (Group 1: Ventura State Beach Jetty, Group 2: Newport Harbor, Group 3: Sycamore Watershed).

Treatments Pair	Tukey HSD Q Statistic	Tukey HSD p-value
Sycamore vs Ventura	4.2511	.011
Sycamore vs Newport	3.8628	.024
Ventura vs Newport	.4151	.90

Table 2. Results of the Tukey's post-hoc test done following the ANOVA to determine differences in means between all three sample sites.

DISCUSSION

Microfibers were abundant at all three sample sites, with Sycamore Watershed having significantly more microfibers than the other locations. Field investigations have shown that microplastic abundance in sediments is correlated to the amount of human activity in the surrounding environment.[21] There are multiple factors that influence microfiber contamination levels, such as proximity to sources of effluent discharge, nearby human activity, and geography, which must all be taken into account when looking at the global problem that is plastic pollution.[1, 10] It is likely that Sycamore Watershed had the most microfibers due to the fact that wastewater from washing machines runs through this sediment, which traps microfibers that have detached from clothing. Newport Harbor had the second greatest amount of microfibers, possibly because the stagnant water allows microfibers from pollution in the harbor to settle to the sediment. Ventura State Beach Jetty has the highest amount of wave action of the three locations, as it is an exposed beach and is subject to constant water circulation which could carry the microfibers out to sea, beyond the high tide line where samples were taken. Microfibers are present in multiple locations bordered by the Pacific Ocean, further supporting the hypothesis that microfibers are ubiquitous.

Sediment samples were also collected from Oahu, HI (n=24), as well as Bundegi Exmouth (n=3) and Turquoise Bay (n=2) in Western Australia by Dr. Huvard s previous research students and shipped to our lab. The samples were processed the same way in summer 2021, but since the collection methods were different, it was decided that they could not be directly compared to the Southern California samples. Even so, the data collected supports the idea that microfibers are ubiquitous in the marine environment, as fibers were found in Hawaii at an average of 16.4 (±10.2) per sample. Bundegi Exmouth had an average of 20.7 (±1.5) and Turquoise Bay an average of 34.5 (±2.1) microfibers per sample. Hawaii could have had a smaller average number of microfibers per sample than all three locations in Southern California due to having a less dense population compared to the sample sites in California, where over 20 million people live along the southern coastline.

As the global demand for plastic increases, the number of all living organisms ingesting microplastics will too. Microfibers detrimentally affect marine ecosystems and could do the same for human health. Although in current literature there is limited data on the toxicity of microplastics in humans, it is likely that microplastics absorb monomers, additives, and persistent organic pollutants (POPs), which have been linked to a disruption in humans 'gut biomes.[22] With microfibers prevailing in many environments from the Arctic to terrestrial environments and the deep seafloor, microfiber pollution is truly a global issue.[23, 24] A standardized methodology for determining the number or concentration of microfibers in a given sample location would lead to results that could be shared with labs worldwide and in turn aid in determining the toxicological risk microplastics pose to filter feeders, humans, and other organisms. Long-term studies looking at seasonal variability in microfiber concentrations would also be useful to determine the impact that tides and wave action have on microfiber deposition on beaches. It is important to study the levels of microfiber pollution so that mitigation strategies and cleanup efforts can be implemented to help curb microfiber pollution, especially in the most heavily impacted areas.

Solutions include improving globally based pollution prevention, introducing microorganisms to degrade polymers and additives, and reducing plastic use. Recent work indicates that certain microorganisms may be capable of degrading petroleum-based synthetic polymers. For example, Halle *et al.* (2020)[20] observed that the gut bacteria of mealworms can slowly break down polystyrene, and although residues remain, this could be a way to reduce the amount of plastic in our environment. Yoshida *et al.* (2015)[25] reported that bacteria exposed to polyethylene terephthalate at a recycling site produced enzymes that could degrade it to its basic monomers. This reveals that steps can be taken within the scientific community to help decrease the impact of plastic pollution.

The differences in techniques of isolating and identifying microfibers make it difficult to compare the levels of pollution between studies. The creation of a more uniform and effective method should be developed in the future to ensure consistency. While our process was simpler than that completed by other studies, it was unique in that it gave us an easily reportable and exact number of microfibers found at each location. Many studies, like the one performed by Claessens *et al.* (2011)[26] reported microfiber pollution as concentration instead of number. They used a dry sand density of 1.6 g/cm^3 to find the concentration of microfibers at a given location and compared those values to determine how polluted a location was. The number of microfibers recorded in our study might be slightly overestimated due to airborne fibers in the laboratory, water supplies, and materials that could have contaminated the samples. We measured approximately 100 mL of sediment per sample, but as it was not precise, we did not feel comfortable converting our data to concentrations and chose to report our data as averages so as to not over or underestimate the true number of microfibers found. As our data were collected on individual days, they represent a snapshot of microfiber pollution at these locations on these given days. Further studies should look at long-term microfiber pollution and how it could be influenced by seasonal or tidal changes. Despite the limitations of this study, microfibers were observed in large numbers in every sample taken from all three locations, indicating widespread microfiber pollution at these sites. Our data also still indicate that Sycamore Watershed was significantly more polluted than the other locations, with both the highest average number of fibers and the highest total microfiber count of the three sites.

CONCLUSIONS

The results of this observational study of microfiber quantities in sand sediments from three different locations support both of our hypotheses. There were microfibers found at all three sites and by using an ANOVA and Tukey's post-hoc test, it was determined that Sycamore Watershed had the highest average number of microfibers per sample. To our knowledge, this is the first observational study documenting microfiber pollution in sediment from Sycamore Watershed, Ventura State Beach Jetty, and Newport Harbor. This study shows that microfiber pollution is a pressing issue for land masses bordered by the Pacific Ocean and that better pollution prevention methods are needed.

ACKNOWLEDGMENTS

We thank our research mentor, Dr. Andrea Huvard for her guidance and knowledge throughout this project. We thank Dr. Bryan Swig for assisting us with analyzing the statistics of our data. We thank Elijah Hill for collecting sediment samples in the summer of 2020. We thank ALLIES in STEM and the Swenson family through their Swenson Summer Fellowship for funding our research and California Lutheran University for allowing us to conduct this research in the new Swenson Science building.

REFERENCES

1. Mathalon, A., Hill, P. (2014) Microplastic fibers in the intertidal ecosystem surrounding Halifax Harbor, Nova Scotia, *Marine Pollution Bulletin,* 81: 69–79. *https://doi.org/10.1016/j.marpolbul.2014.02.018*
2. Hope, J., Coco, G., Thrush, S. (2020) Effects of Polyester Microfibers on Microphytobenthos and Sediment-Dwelling Infauna, *Environmental Science and Technology* 54: 7970–7982. *https://doi.org/10.1021/acs.est.0c00514*
3. Barnes, D., Galgani, F., Thompson, R., Barlaz, M. (2009) Accumulation and fragmentation of plastic debris in global environments, *Philosophical Transactions Of The Royal Society B: Biological Sciences* 364: 1985-1998. *https://doi.org/10.1098/rstb.2008.0205*
4. Moore, CJ. (2008) Synthetic Polymers In The Marine Environment: A Rapidly Increasing, Long-Term Threat, *Environmental Research* 108 (2): 131-139. *Elsevier BV https://doi.org/10.1021/es2031505*
5. Galloway, T., Lewis, C. (2016) Marine microplastics spell big problems for future generations, *Proceedings of the National Academy of Sciences of the United States of America*, 113 (9): 2331–2333. *https://doi.org/10.1073/pnas.1600715113*
6. Cole, M., Lindeque, P., Fileman, E., Halsband, C., Goodhead, R., Moger, J., Galloway, T. (2013) Microplastic ingestion by zooplankton, *Environmental Science and Technology* 47 (12): 6646–6655. *https://doi.org/10.1021/es400663f*
7. Sussarellu, R., Suquet, M., Thomas, Y., Lambert, C., Fabioux, C., Pernet, M., Le Goïc, N., Quillien, V., Mingant, C., Epelboin, Y., Corporeau, C., Guyomarch, J., Robbens, J., Paul-Pont, I., Soudant, P., Huvet, A. (2016) Oyster reproduction is affected by exposure to polystyrene microplastics, *Proceedings of the National Academy of Sciences of the United States of America* 113 (9): 2430–2435. *DOI: 10.1073/pnas.1519019113*
8. Hartline, N., Bruce, N., Karba, S., Ruff, E., Sonar, S., Holden, P. (2016) Microfiber Masses Recovered From Conventional Washing Machine Washing of New or Aged Garments, *Environmental Science and Technology* 50 (21): 11532–11538. *https://doi.org/10.1021/acs.est.6b03045*
9. Suaria, G., Achtypi, A., Perold, V., Lee, J., Pierucci, A., Bornman, T., Aliana, S., Ryan, P. (2020) Microfibers in oceanic surface waters: A global characterization, *Science Advances* 6 (23): 1–8. *DOI: 10.1126/sciadv.aay8493*
10. Browne, M., Crump, P., Niven, S., Teuten E., Tonkin, A., Galloway, T., Thompson, R. (2011) Accumulation of microplastic on shorelines worldwide: sources and sinks, *Environmental Science and Technology* 45 (21): 9175–9179. *DOI: 10.1021/es201811s*
11. Murphy, F., Ewins, C., Carbonnier, F., Quinn, B. (2016) Wastewater Treatment Works (WwTW) as a Source of Microplastics in the Aquatic Environment, *Environmental Science and Technology* 50 (11): 5800-5808. *https://doi.org/10.1021/acs.est.5b05416*
12. Peller, J., Eberhardt, L., Clark, R., Nelson, C., Kostelnik, E., Iceman, C. (2019) Tracking the distribution of microfiber pollution in a southern Lake Michigan watershed through the analysis of water, sediment, and air, *Environmental Science: Processes & Impacts* 21 (9): 1549–1559. *DOI: 10.1039/c9em00193j*
13. Mizraji, R., Ahrendt, A., Perez-Venegas, D., Vargas, J., Pulgar, J., Aldana, M., Ojeda, F., Duarte, C., Galbán-Malagón, C. (2017) Is The Feeding Type Related With The Content Of Microplastics In Intertidal Fish Gut? *Marine Pollution Bulletin* 116 (1-2): 498-500. *https://doi.org/10.1016/j.marpolbul.2017.01.008*.
14. Ryan, P., Weideman, E., Perold, V., Moloney, C. (2020) Toward Balancing the Budget: Surface Macro-Plastics Dominate the Mass of Particulate Pollution Stranded on Beaches, *Frontiers in Marine Science* 7: 1–14. *https://doi.org/10.5194/os-2021-83*
15. Taylor, M., Gwinnett, C., Robinson, L., Woodall, L. (2016) Plastic microfibre ingestion by deep-sea organisms, *Nature: Scientific Reports* 6 (article 33997). *DOI: 10.1038/srep33997*
16. Watts, A., Urbina, M., Goodhead, R., Moger, J., Lewis, C., Galloway, T. (2016) Effect of microplastic on the gills of the Shore Crab *Carcinus maenas, Environmental Science and Technology* 50 (10): 5364–5369. *DOI: 10.1021/acs.est.6b01187*
17. Meeker, J., Sathyanarayana, S., & Swan, S. (2009). Phthalates and other additives in plastics: human exposure and associated health outcomes, *Philosophical Transactions Of The Royal Society B: Biological Sciences* 364(1526), 2097-2113. *DOI: 10.1098/rstb.2008.0268*

18. Wagner, S., Schlummer, M. (2020) Legacy additives in a circular economy of plastics: Current dilemma, policy analysis, and emerging countermeasures, *Resources, Conservation, and Recycling* 158: 104800. *DOI:https://doi.org/10.1016/j.resconrec.2020.104800*

19. Nurlatifah, Yamauchi, T., Nakajima, R., Tsuchiya, M., Yabuki, A., Kitahashi, T., Nagano, Y., Isobe, N., Nakata, H. (2021) Plastic additives in deep-sea debris collected from the western North Pacific and estimation for their environmental loads, *Science of The Total Environment* 768: 144537. *DOI: 10.1016/j.scitotenv.2020.144537*

20. Halle, A., Ladirat, L., Gendre, X., Goudounèche, D., Pusineri, C., Routaboul, C., Tenailleau, C., Duployer, B., Perez, E. (2016) Understanding the Fragmentation Pattern of Marine Plastic Debris, *Environmental Science and Technology* 50 (11): 5668–5675. *https://doi.org/10.1021/acs.est.6b00594*

21. Jiang, C., Yin, L., Wen, X., Du, C., Wu, L., Long, Y., Liu, Y., Ma, Y., Yin, Q., Zhou, Z., Pan, H. (2018) Microplastics in Sediment and Surface Water of Western Dongting Lake and South Dongting Lake: Abundance, Source and Composition, *International Journal of Environmental Research and Public Health.* 15 (10): 2164. *DOI: 10.3390/ijerph15102164*

22. Fournier, E. Etienne-Mesmin, L., Grootaert, C., Jelsbak, L., Syberg, K., Blanquet-Doit, S., Mercier-Bonin, M. (2021) Microplastics in the human digestive environment: A focus on the potential and challenges facing in vitro gut model development, *Journal of Hazardous Materials.* 415: 125632. *DOI: 10.1016/j.jhazmat.2021.125632*

23. Bergmann, M., Mützel, S., Primpke, S., Tekman, M. B., Trachsel, J., & Gerdts, G. (2019). White and wonderful? Microplastics prevail in snow from the Alps to the Arctic, *Science Advances 5*(8), ax1157. *DOI: 10.1126/sciadv.aax1157*

24. Bomgardner, M. M. (2017). The great lint migration, *C&EN Global Enterprise* 95(2), 16–17. *DOI: 10.1021/cen-09502-bus1*

25. Yoshida, S., Hiraga, K., Takehana, T., Taniguchi, I., Yamaji, H., Maeda, Y., Toyohara, K., Miyamoto, K., Kimura, Y., & Oda, K. (2016) A bacterium that degrades and assimilates poly (ethylene terephthalate), *Science* 351(6278), 1196–1199. *DOI: 10.1126/science.aad6359*

26. Claessens, M., De Meester, S., Van Landuyt, L., De Clerck, K., Janssen, C. (2011) Occurrence and distribution of microplastics in marine sediments along the Belgian coast, *Marine Pollution Bulletin* 62: 2199–2204. *https://doi.org/10.1016/j.marpolbul.2011.06.030*

ABOUT STUDENT AUTHORS

Adrianna Ebrahim and Mia LeClerc graduated in May 2022 from California Lutheran University with Departmental Honors. Adrianna graduated with a BS in Biology and is working as a salt marsh pollution mitigation researcher at UCSB. Mia graduated with a BS in Environmental Science and has started her career as an Environmental Scientist with EEC Environmental.

PRESS SUMMARY

Microfibers are a prevalent pollutant in our oceans and are disrupting aquatic organisms and human health worldwide. These microscopic pieces of plastic, typically defined as less than 5 mm in length, are a type of debris that originate from synthetic clothing and textiles, such as polyester and nylon. Often through the process of machine washing, fiber fragments are expelled into the wastewater and can travel long distances before eventually being deposited into the environment. It is important to figure out which locations are heavily impacted by microfiber pollution so that remediation strategies can be developed and implemented. In this study, we quantified the number of microfibers in marine sediments from a harbor, jetty, and watershed in Southern California. We discovered microfibers at all of the sample sites examined, indicating widespread microfiber pollution in these locations.

Stabilization of Cisplatin *via* Coordination of Ethylenediamine

Samantha L. Rea, Alexia Smith, Brooke Hornberger, Grace Fillmore, Jeremy Burkett, & Timothy Dwyer*

Department of Chemistry, Stevenson University, Owings Mills, MD

https://doi.org/10.33697/ajur.2022.067

Students: samantharea23@gmail.com, smith.l.alexia@gmail.com, brookehornberger14@gmail.com, fillmore456@gmail.com*
Mentors: jburkett2@stevenson.edu, tdwyer@stevenson.edu*

ABSTRACT
While the chemotherapeutic cisplatin is used to treat a variety of cancers, metal toxicity and cisplatin resistance *via* genetic and epigenetic changes limits its use and calls for alternative therapies. To combat the observed toxicities and create a more stable compound, which avoids isomerization into a *trans* configuration, three cisplatin analogues including cispalladium, dichloro-(ethylenediamine)-platinum(II), and dichloro-(ethylenediamine)-palladium(II) were synthesized as potential cisplatin alternatives. Each compound was evaluated for cytotoxicity on SK-OV-3 cells against cisplatin. Synthesis of dichloro-(ethylenediamine)-platinum(II) yielded 20.5% of the theoretical yield, while dichloro-(ethylenediamine)-palladium(II) yielded 49.1%. Results from the cytotoxicity trial revealed that cispalladium was not effective against SK-OV-3 cells, and dichloro-(ethylenediamine)-palladium had minimal effects. The dichloro-(ethylenediamine)-platinum(II) was the most efficacious with an IC_{50} value of 0.77 μg/ml compared to the IC_{50} of 0.61 μg/ml for cisplatin. With a similar IC_{50} to cisplatin, these results suggest that dichloro-(ethylenediamine)-platinum(II) has the potential to serve as a cisplatin alternative for cancer patients who develop resistance following their clinical course of cisplatin. Future studies on the cytotoxicity of dichloro-(ethylenediamine)-platinum(II) to induce cell death on cisplatin-resistance cell lines are necessary to determine the ability of the compound to be utilized as a cisplatin alternative.

KEYWORDS
Cisplatin; Ovarian Cancer; SK-OV-3; Drug Resistance; Stability; Palladium; Ethylenediamine; Cispalladium; Dichloro-(ethylenediamine)-platinum(II); Dichloro-(ethylenediamine)-palladium(II)

INTRODUCTION

Cisplatin, a current chemotherapeutic used to treat lung and other cancers including bladder, head and neck, ovarian, and testicular cancers, prevents cell replication by crosslinking DNA nucleotides along the same strand forming DNA-platinum adducts, subsequently inducing apoptosis.[1] Though widely used, formation of *trans* isomers, metal toxicity and cisplatin resistance via genetic and epigenetic changes limits its use and calls for alternative therapies.[2]

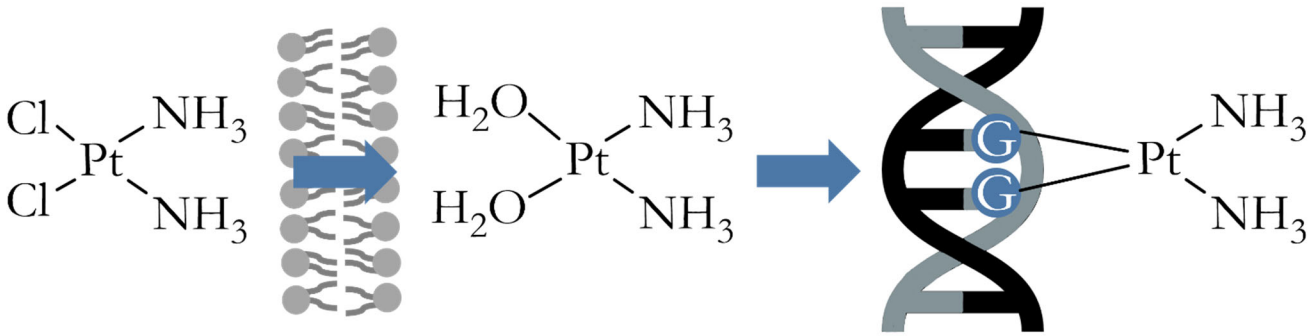

Figure 1. Once cisplatin passes through a cell membrane, it become aquated through ligand exchange, during which each chlorine atom is replaced with a water molecule.

One of the most common mechanisms of cisplatin resistance has been attributed to an observed decrease in accumulation of platinum compounds during cisplatin-resistant cell culture studies.[3] Many methods may contribute to this observation including active efflux, impaired influx, antioxidants, increases in DNA damage repair, DNA-methylation or de-methylation, membrane protein trafficking alterations via the cytoskeleton, overexpression of chaperones, inactivation of the apoptosis pathway, along with activation of the EMT and many other pathways.[3]

Severe nephrotoxicity induced by platinum compounds, is partly due to the transporter-mediated uptake in cells.[4] For cisplatin, the copper transporter 1 appears to play a role in its tumor cellular uptake, while its side effects may be due to the organic cation transporter (OCT) 2 based upon its placement and distribution among affected organs.[4] One proposed mechanism for cisplatin induced nephrotoxicity (CIN) is due to the platinum-glutathionine (GSH) conjugates formed within the kidneys.[5] Compared to metabolic intermediates, the platinum-GSH is highly unstable leading to damage in the proximal tubules.[5]

To combat the observed nephrotoxicity, secondary treatments such as amifostine, which binds to free radicals, have been approved by the FDA.[6] Previous work by these students[7] involved replacing the amine groups on cisplatin with the amine groups on amifostine, to form a singular, less toxic treatment, as seen in **Figure 2A,** which would retain the ability of cisplatin to bind to DNA, and the ability of amifostine to bind to free radicals. Though ultimately a bulky analogue with an unfavorable coordination to the platinum center was formed, as shown in **Figure 2B**, the intention was to form a less toxic compound that was stabilized through a formed ring structure. Additional methods to combat CIN include replacing the platinum center, which is the cause of the toxic side effects. While there are many other studies that have investigated cisplatin analogs as well as platinum substitutes,[8] this work will focus on the comparison of ring-stabilized analogs to their more traditional counterparts (**Figure 3**).

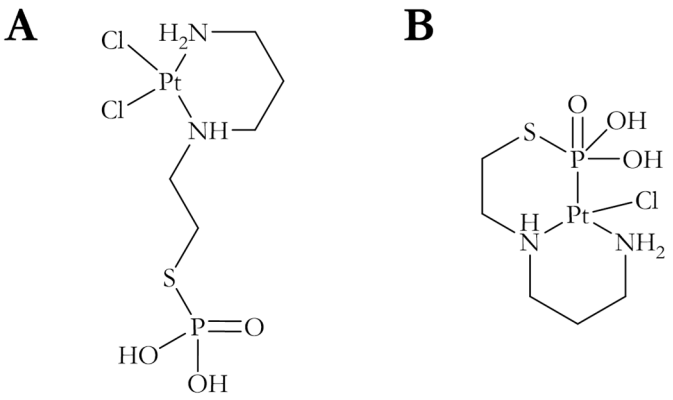

Figure 2. (A) The intended amifostine-incorporated cisplatin analogue, and (B) the analogue that was likely formed instead.

Combining the previous two strategies to combat toxicity and resistance, three cisplatin analogues shown in **Figure 3** were synthesized and analyzed for cytotoxicity in a SK-OV-3 cell line. Should resistance occur in patients receiving cisplatin treatment, these analogues have the potential to serve as cisplatin alternatives. To minimize the toxicity of the platinum component, palladium was used as a replacement metallic center to form cispalladium in hopes of minimizing toxic glutathione metabolites produced in the kidneys from cisplatin. Additionally, ethylenediamine was used to replace the amine groups in cisplatin, forming dichloro-(ethylenediamine)-platinum(II), with a stable five-membered cyclic group which may evade some of the observed mechanisms of cisplatin resistance while preventing formation of *trans* compounds. The amine groups of ethylenediamine also replaced the amine groups on cispalladium to create dichloro-(ethylenediamine)-palladium(II), a compound that utilizes both techniques. Through synthesis and cytotoxicity analyses of three cisplatin analogues, which replace the toxic platinum center and stabilize the compound through cyclic arrangements, alternative cisplatin treatments may be considered.

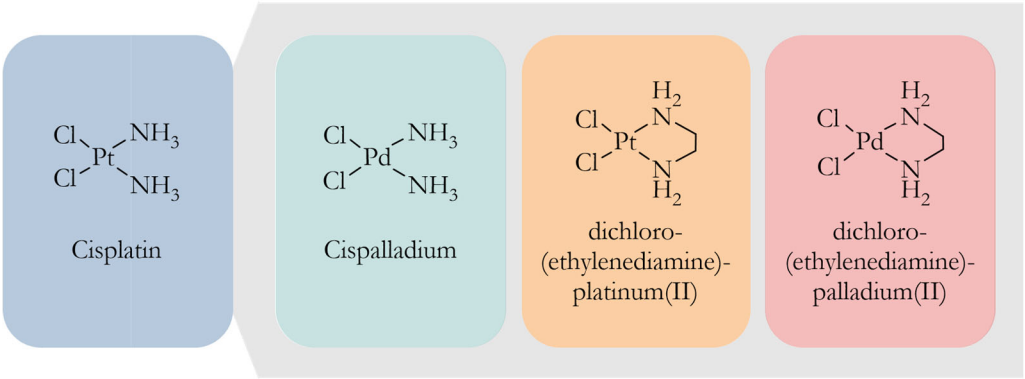

Figure 3. The chemical structures of cisplatin and the cisplatin analogues synthesized.

METHODS AND PROCEDURES

Materials

All reagents used to synthesize the cisplatin analogues were retrieved from Sigma Aldrich. Equipment utilized during analogue synthesis included the CEM Discover System Microwave (Matthews, NC) to synthesize cispalladium and a PerkinElmer Spectrum 100 FT-IR Spectrometer to obtain Infrared (IR) spectra (ATR) for each compound. For the cytotoxicity assay, SK-OV-3 ovarian cancer cells were retrieved September 2021 from Stevenson University after being frozen in 2016. Throughout the experiments, the cells were passaged a total of 12 times in 70% DMEM (20% FBS, 10% DMSO) media, retrieved from Sigma Aldrich. The absorbance of the cytotoxicity assays was measured on a Tecan Microplate Reader.

Cispalladium Synthesis

Cispalladium was synthesized using tetrachloropalladium (K_2PdCl_4) and potassium chloride (KCl) as shown in **Scheme 1** using procedures adapted from Pertruzzella *et al.*[9] Following the microwave and an ice bath, the precipitate and solute were separated through centrifugation, which was completed at 13.6 x 10^3 g for 10 minutes. After drying, the structure of the product was confirmed by IR (ATR).

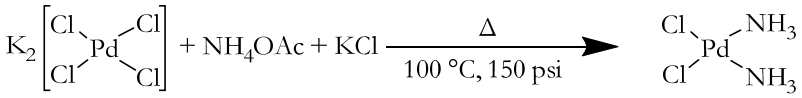

Scheme 1. Synthesis of cispalladium using a microwave[9]

Dichloro-(ethylenediamine)-platinum (II) Synthesis

The cisplatin analogue was synthesized as shown in **Scheme 2**. Potassium tetrachloroplatinate (0.244 mol) and ethylenediamine (0.244 mol) were dissolved in a 1:1 mole ratio in deionized water so that each reagent had a final concentration of 0.11 M, while stirring at room temperature (~20 °C) for approximately 20 minutes. Following centrifugation (13.6 x 10^3 g, 10 mins.), the supernatant was discarded. After drying, the structure of the product was confirmed by IR (ATR) and produced a 20.5% yield.

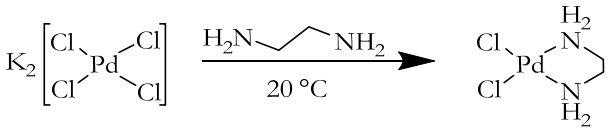

Scheme 2. Synthesis of dichloro-(ethylenediamine)-platinum(II)

Dichloro-(ethylenediamine)-palladium (II) Synthesis

The cisplatin analogue was synthesized as shown in **Scheme 3**. Potassium tetrachloropalladate (0.244 mol) and ethylene diamine (0.244 mol) were dissolved in a 1:1 mole ratio in deionized water so that each reagent had a final concentration of 0.11 M, while stirring at room temperature (~20 °C) for approximately 20 minutes. Following centrifugation (13.6 x 10^3 g, 10 mins.), the supernatant was discarded. After drying the structure of the product was confirmed by IR (ATR) and produced a 49.1% yield.

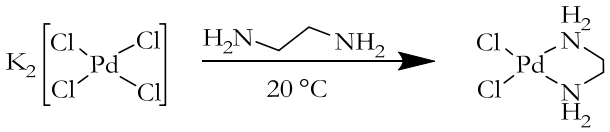

Scheme 3. Synthesis of dichloro-(ethylenediamine)-palladium(II)

Cell Culture and Cytotoxicity Assay

Each of the cisplatin analogues was tested for cytotoxicity as shown in **Figure 4**. During the first trial, SK-OV-3 cells were plated in a 96-well round-bottom plate at 1000 cells/well. Following a 24-hour incubation (5% CO_2, 37 °C), four different treatments including cisplatin, cispalldium, dichloro-(ethylenediamine)-platinum(II), and dichloro-(ethylenediamine)-palladium(II) dissolved in 0.9% sodium chloride (NaCl) solution were separately administered in quadruplicates with five half-serial dilutions in concentrations ranging from 100 μg/ml to 6 μg/ml. The control wells received a 0.9% NaCl solution *in lieu* of a treatment.

Following a 72-hour incubation period, cells were washed with PBS (100 μl/well) and then incubated at 20 °C in 10% glutaraldehyde solution (100 μl/well). After another PBS (100 μl/well) wash, the cells were stained using 1X crystal violet solution (50 μl/well) and incubated at 37 °C. The wells were washed twice with PBS (100 μl/well) and any remaining crystal violet was solubilized with 33% acetic acid (100 μl/well). The wells were then shaken to dissolve the crystal violet and scanned on an absorbance plate reader at 580 nm with reference at 650 nm using cvsinglescan and cvsinglescancontrol. Cytotoxicity was

calculated by averaging the absorbances of each quadruplicate and then dividing the average treatment absorbance (A_{drug}) by the average absorbance of the control ($A_{control}$).

The procedures were repeated in a second trial using three treatments including cisplatin, dichloro-(ethylenediamine)-platinum(II), dichloro-(ethylenediamine)-palladium(II) in quadruplicates with seven half-serial dilutions ranging from 5 μg/ml to 0.08 μg/ml. The control wells received additional DMEM media *in lieu* of a treatment. The IC_{50} scores for cisplatin and dichloro-(ethylenediamine)-platinum(II) were determined using linear regression equations for doses between 0.16 and 1.3 μg/ml. The y-variable in each subsequent equation was substituted with 0.5 and solved for the x-variable.

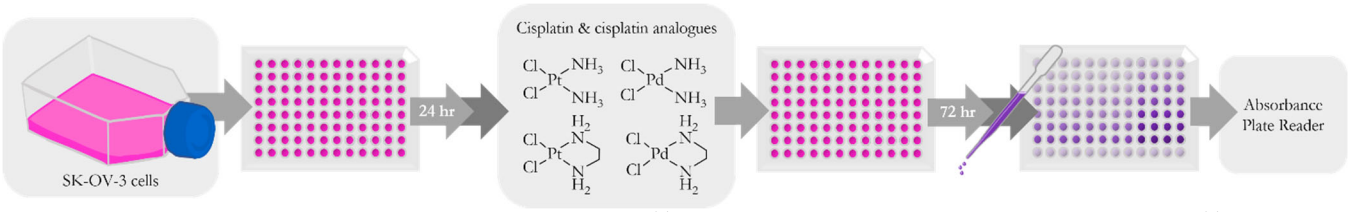

Figure 4. Cytotoxicity assay procedures were completed using SK-OV-3 cells. The cells were incubated and allowed to adhere on a 96 well plate. The following day, each drug was administered to the cells as separate treatments and allowed to incubate for 3 days. The remaining viable cells were stained with a crystal violet solution, and the absorbance was measured.

RESULTS

Analogue Synthesis

The synthesized dichloro-(ethylenediamine)-platinum(II) yielded 20.5% of the theoretical, and the dichloro-(ethylenediamine)-palladium(II) yielded 49.1%. Following synthesis of cispalladium, dichloro-(ethylenediamine)-platinum (II), and dichloro-(ethylenediamine)-palladium (II) IR spectra were obtained for each and plotted against cisplatin and ethylenediamine as shown in **Figure 5** (**(A)** cispalladium**, (B)** dichloro-(ethylenediamine)-platinum (II), **(C)** dichloro-(ethylenediamine)-palladium (II)). Peaks located at 3200 and 1560 nm^{-1} in cisplatin and each of the analogues confirmed the presence of the *cis* amine groups in each of the analogues. Additional peaks at 2800 nm^{-1} in the ethylenediamine, dichloro-(ethylenediamine)-platinum(II), and dichloro-(ethylenediamine)-palladium(II) confirm the presence of alkane groups, which are not existent in the cisplatin IR.

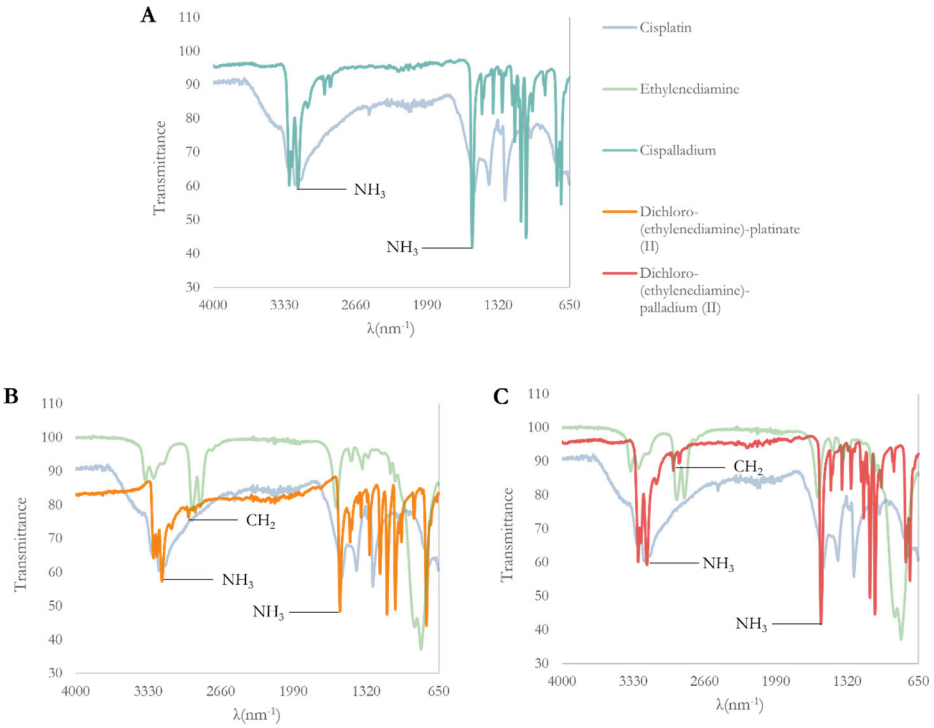

Figure 5. IRs (ATR) of each cisplatin analogue compared to the IR of **(A)** cisplatin. The IRs for **(B)** dichloro-(ethylenediamine)-platinum(II) and **(C)** dichloro-(ethylenediamine)-palladium(II) are also plotted against the IR of ethylenediamine. The peaks indicative of amines and alkanes on each analogue, which are shared with cisplatin or ethylenediamine, are labeled.

Cytotoxicity Trial 1

During the first cytotoxicity trial, cisplatin and each of the three proposed analogues were incubated with SK-OV-3 cells, which were then stained and measured for absorbance to indicate the proportion of remaining viable cells. The cytotoxicity scores of each compound at consecutive concentrations indicated in **Figure 6** reveals that the cytotoxicity scores for cispalladium at every concentration tested were greater than a value of one ($A_{cispalladium}/A_{control}$ >1). Of the three the other three treatments, dichloro-(ethylenediamine)-palladium(II) had the highest cytotoxicity scores beginning at 0.976 at the lowest concentration (100 µg/ml) and progressively decreasing to 0.610 at its highest concentration (100 µg/ml). The cisplatin had the second lowest cytotoxicity score of 0.218 at a concentration of 12.5 µg/ml, and the cytotoxicity scores progressively increased to 0.924 as concentration of the treatment increased to its maximum dose (100 µg/ml). The dichloro-(ethylenediamine)-platinum(II) treatment yielded the lowest cytotoxicity scores of 0.186 at a concentration of 25 µg/ml, and had a maximum cytotoxicity of 0.336 at the lowest administered dose (6.3 µg/ml).

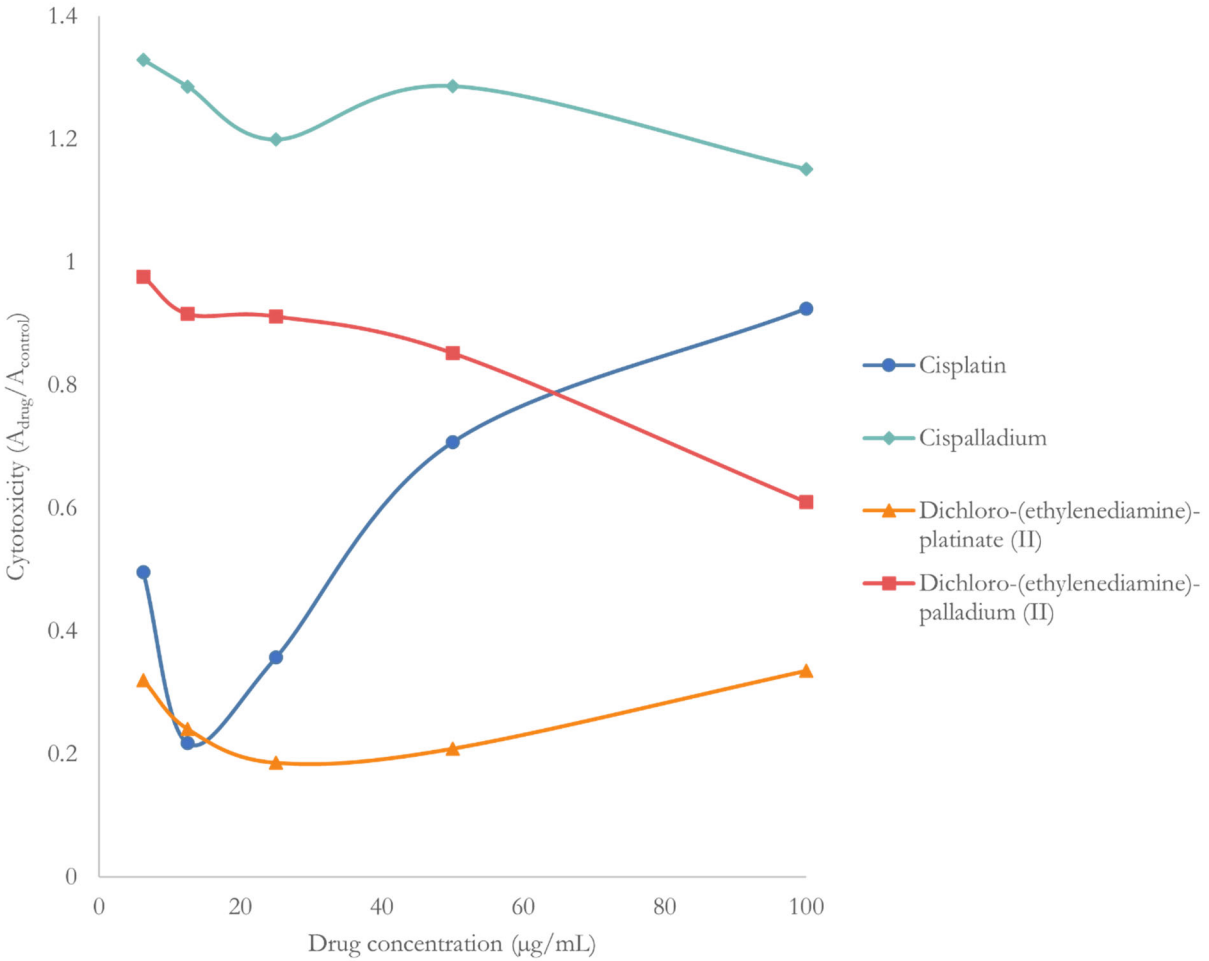

Figure 6. Cytotoxicity of cisplatin;(●), cispalladium (♦), dichloro-(ethylenediamine)-platinum (II) (▲), dichloro-(ethylenediamine)-palladium(II) (■) at five concentrations (100 µg/ml, 50 µg/ml, 25 µg/ml, 12.5 µg/ml, and 6.25 µg/ml).

Cytotoxicity Trial 2

The second trial included cisplatin, dichloro-(ethylenediamine)-platinum(II), and dichloro-(ethylenediamine)-palladium (II). The results shown in **Figure 7** indicate that dichloro-(ethylenediamine)-palladium was the least efficacious with the highest cytotoxicity scores between 0.830 and 1.098. The cytotoxicity scores for cisplatin and dichloro-(ethylenediamine)-platinum(II) followed a similar trend to each other. The IC_{50} scores of the two compounds were determined using linear regression equations

as shown in **Figure 8**. Substituting 0.5 for the y-variable and solving for the concentration indicated by the x-variable yielded an IC_{50} equal to 0.61 µg/ml for cisplatin and an IC_{50} equal to 0.77 µg/ml for dichloro-(ethylenediamine)-platinum(II).

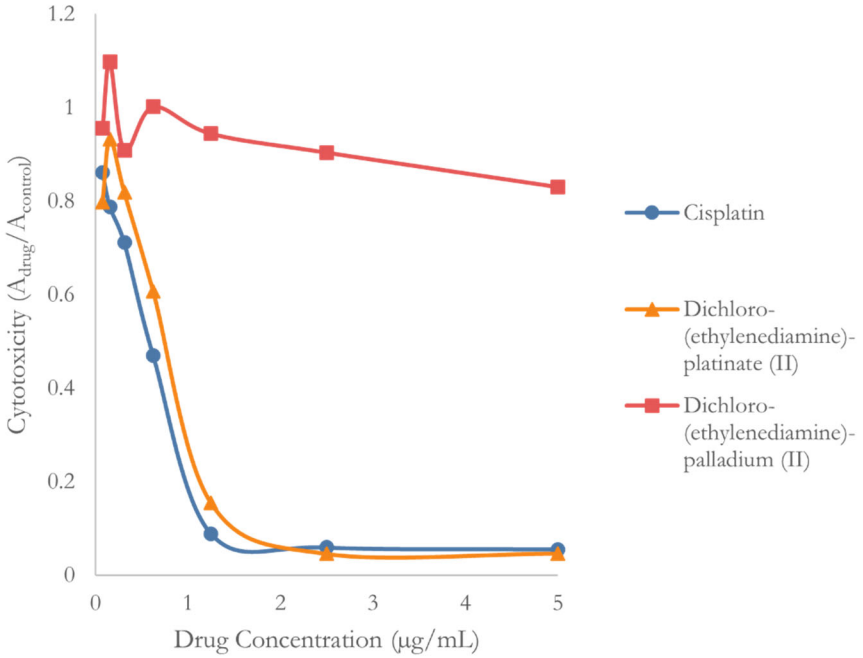

Figure 7. Cytotoxicity of cisplatin (●), dichloro-(ethylenediamine)-platinum(II) (▲), and dichloro-(ethylenediamine)-palladium(II) (■) in the second trial at seven concentrations (5 µg/ml, 2.5 µg/ml, 1.3 µg/ml, 0.63 µg/ml, 0.31 µg/ml, 0.16 µg/ml, 0.08 µ/ml).

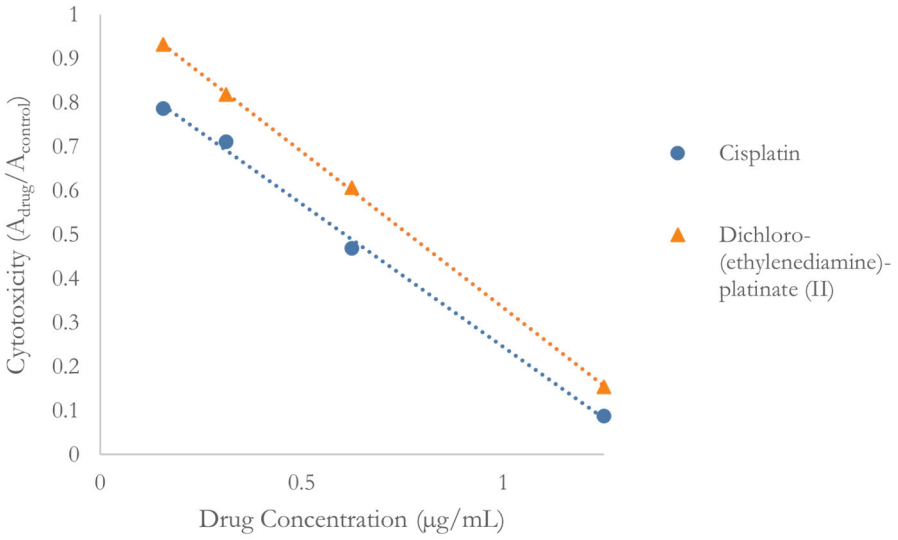

Figure 8. Linear regressions for the cytotoxicity of cisplatin and dichloro-(ethylenediamine)-platinum(II) between 0.16 and 1.3 µg/ml. The IC_{50} for each treatment was calculated using the linear regression equation associated with cisplatin (● $y = -0.6494x + 0.8944$; $R^2 = 0.9973$) or dichloro-(ethylenediamine)-platinum (▲ $y = -0.7095x + 1.0433$; $R^2 = 0.9998$) and found to be 0.61 µg/ml and 0.77 µg/ml, respectively.

DISCUSSION

Synthesis of the proposed analogues was completed to create a ring-stabilized alternative treatment to cisplatin, which may exhibit less toxicity than cisplatin or serve as a treatment once cisplatin resistance develops. The identity of each analogue was confirmed using IR spectra. The existence of amine groups is suggested by the similar peaks in the cisplatin and analogue IRs at 3200 and 1560 nm^{-1} as shown in **Figure 5**. Additionally, the existence of alkane groups at similar peaks in ethylenediamine and two of the analogue IRs, dichloro-(ethylenediamine)-platinum(II) and dichloro-(ethylenediamine)-palladium(II), suggests the presence of alkane groups which are not present in the cisplatin IR. Therefore, the similarities and differences in the IR of cisplatin, ethylenediamine, and the analogues confirm the identities of each of the analogues.

From the first cytotoxicity trial, it was determined that cispalladium was not efficacious as none of the cytotoxicity scores dipped below a value of 1.00 as shown in **Figure 6**. Since the cytotoxicity scores represent what ratio of SK-OV-3 cells were killed compared to the control which received no treatment based on absorbance readings ($A_{cispalladium}/A_{control}$), the results suggest that cispalladium did not cause any detectable cell death, and thus was not efficacious. Of the three treatments which did induce cell death ($A_{cispalladium}/A_{control}<1$), dichloro-(ethylenediamine)-palladium was the least efficacious, with a minimum cytotoxicity score of 0.610. The minimum cytotoxicity score for cisplatin was the second lowest at 0.218, while the dichloro-(ethylenediamine)-platinum(II) yielded the lowest cytotoxicity score of 0.186, providing initial evidence that the analogue may be more cytotoxic than cisplatin. The second trial, however, contradicted these results. Upon further inspection of the cytotoxicity scores in **Figure 6**, one can appreciate the increase in cytotoxicity of cisplatin as the dosage was increased. These results suggest that cisplatin solution had reached supersaturation, causing some of the drug to come out of solution. As a result, the cisplatin would have been unable to be taken up by the plated cells to induce damage to the DNA. Additionally, each of the compounds was dissolved in a 0.9% NaCl solution and applied to the cells rather than DMEM media which may have affected cell growth. The control for this group also received a volume of 0.9% NaCl equivalent to the DMEM media previously administered.

Given the results and limitations from the first cytotoxicity experiment, the experiment was rerun using three treatment groups: cisplatin, dichloro-(ethylenediamine)-platinum(II), and dichloro-(ethylenediamine)-palladium(II). Each drug was dissolved in the appropriate media, and the control cells received the same cell media to mitigate the potential limitations from the first experiment. Additionally. the concentrations at which the compounds were administered to the treatment groups was lowered to prevent supersaturation. As shown in **Figure 7**, dichloro-(ethylenediamine)-palladium(II) was the least efficacious and failing to reach a cytotoxicity score below 0.830 within the examined dosages, which is consistent with the previous results. On the contrary, the results suggest that cisplatin and dichloro-(ethylenediamine)-platinum(II) have similar efficacy, as their cytotoxicity scores followed a similar trend. This conclusion is further supported by the calculated IC_{50} values using linear regression equations for cisplatin and dichloro-(ethylenediamine)-platinum(II) which were 0.61 μg/ml for cisplatin and 0.77 μg/ml for dichloro-(ethylenediamine)-platinum(II). The calculated IC_{50} value in this work is also consistent with previously published IC_{50} concentrations for cisplatin.[10] One potential limitation to this cytotoxicity assay is the inconsistent cell incubation conditions. Throughout the incubation stages of the assay and prior passaging of the SK-OV-3 cells, the CO_2 concentration dipped below 5% multiple times, disrupting the ideal growth conditions.

Overall, the results suggest that dichloro-(ethylenediamine)-platinum(II) may serve as a cisplatin alternative due to its comparable IC_{50} value to that of cisplatin, while cispalladium and dichloro-(ethylenediamine)-palladium(II) are not effective. Should individuals receiving cisplatin, develop resistance to the drug, dichloro-(ethylenediamine)-platinum(II) may serve as a similarly efficacious alternative, which is stabilized in the *cis* confirmation by a ring structure. Since the arrangement of cisplatin is significant to its mechanism, the ring formed by ethylenediamine in this analogue may prevent formation of a *trans* isomer that would typically disrupt its mechanism of action.

Overall, the conflicting cytotoxicity levels between the cisplatin and dichloro-(ethylenediamine)-platinum(II) versus cispalladium and dichloro-(ethylenediamine)-palladium(II) are most likely due to the differences in the metallic center of the compounds. Palladium and platinum clearly have different binding affinities to both the temporary water ligands as well as the eventual guanine bases, which likely leads to the palladium-containing compounds binding less effectively to DNA, which is significant to the mechanism of cisplatin.

Furthermore, to confirm that dichloro-(ethylenediamine)-platinum(II) may serve as cisplatin alternative following the development of cisplatin resistance, future cytotoxicity studies on the compound in cisplatin-resistant cell lines should be

conducted. Additionally, the cytotoxicity of the compound should be tested at lower concentrations to confirm the calculated IC_{50} concentration, as previous work has cited the IC50 concentration of cisplatin have varied between 0.022 μg/ml and 0.56 μg/ml.

While, dichloro-(ethylenediamine)-platinum(II) may offer a favorable alternative treatment to cisplatin also due to its simplistic synthetic requirements, the procedures proposed in this work resulted in a minimal yield (20.5%). Therefore, other synthetic methods or adjustments to these procedures may be required to provide an appropriate yield for mass production of the compound. While the reagents tetrachloroplatinate and ethylenediamine for the synthesis of dichloro-(ethylenediamine)-platinum(II) are required to coordinate in a one to one (1:1) ratio, the formation of the analogue may be pushed to a greater yield by keeping tetrachlroplatinate as the limiting reagent and supplementing a greater equivalent of ethylenediamine as opposed to the 1:1 equivalents utilized in this work.

Based on the results from the IR spectra, and cytotoxicity assay, it can be concluded that all three cisplatin analogues were successfully synthesized, but only dichloro-(ethylenediamine)-platinum(II) provided an efficacious potential alternative to cisplatin.

CONCLUSIONS

While all three cisplatin analogues were successfully synthesized, only dichloro-(ethylenediamine)-platinum(II) was efficacious with an IC_{50} value of 0.77 μg/ml. Additionally, the proposed synthesis of the analogue is simplistic, though may require adjustments to increase synthetic yield. In the future, dichloro-(ethylenediamine)-platinum(II) must be tested on cisplatin-resistant cells to confirm their potential as a cisplatin alternative for individuals who develop resistance to cisplatin.

ACKNOWLEGEMENTS

The authors thank Dr. Tracey Mason for providing the SK-OV-3 cells and cell culture equipment necessary for the described experiments, along with her guidance in conducting cell culture and cytotoxicity work.

REFERENCES

1. Dasari, S.; Bernard Tchounwou, P. (2014) Cisplatin in Cancer Therapy: Molecular Mechanisms of Action. *Eur. J. Pharmacol.* 740, 364–378. *https://doi.org/10.1016/j.ejphar.2014.07.025*.
2. Kishimoto, T.; Yoshikawa, Y.; Yoshikawa, K.; Komeda, S. (2019) Different Effects of Cisplatin and Transplatin on the Higher-Order Structure of DNA and Gene Expression. *Int. J. Mol. Sci.*, 21, 34. *https://doi.org/10.3390/ijms21010034*.
3. Shen, D.-W.; Pouliot, L. M.; Hall, M. D.; Gottesman, M. M. (2012) Cisplatin Resistance: A Cellular Self-Defense Mechanism Resulting from Multiple Epigenetic and Genetic Changes. *Pharmacol. Rev.*, 64, 706–721. *https://doi.org/10.1124/pr.111.005637*.
4. Harrach, S.; Ciarimboli, G. (2015) Role of Transporters in the Distribution of Platinum-Based Drugs. *Front. Pharmacol.*, 6, 85. *https://doi.org/10.3389/fphar.2015.00085*.
5. Hanigan, M. H.; Devarajan, P. (2003) Cisplatin Nephrotoxicity: Molecular Mechanisms. *Cancer Ther.*, 1, 47–61.
6. Hayati, F.; Hossainzadeh, M.; Shayanpour, S.; Abedi-Gheshlaghi, Z.; Beladi Mousavi, S. S. (2015) Prevention of Cisplatin Nephrotoxicity. *J. Nephropharmacology*, 5, 57–60.
7. Rea, S.; Best, J.; Fillmore, G. [Unpublished Paper] (2020) Synthesis of a Cisplatin Analog Using Amifostine to Potentially Minimize Nephrotoxicity.
8. Johnstone, T. C.; Suntharalingam, K.; Lippard, S. J. (2016) The next Generation of Platinum Drugs: Targeted Pt (II) Agents, Nanoparticle Delivery, and Pt (IV) Prodrugs. *Chem. Rev.*, 116, 3436–3486. *https://doi.org/10.1021/acs.chemrev.5b00597*
9. Petruzzella, E.; Chirosca, C. V.; Heidenga, C. S.; Hoeschele, J. D. (2015) Microwave-Assisted Synthesis of the Anticancer Drug Cisplatin, Cis-[Pt(NH $_3$) $_2$ Cl $_2$]. *Dalton Trans.*, 44, 3384–3392. *https://doi.org/10.1039/C4DT03617D*.
10. Rantanen, V.; Grénman, S.; Kulmala, J.; Grénman, R. (1994) Comparative Evaluation of Cisplatin and Carboplatin Sensitivity in Endometrial Adenocarcinoma Cell Lines. *Br. J. Cancer*, 69, 482–486. *doi: 10.1038/bjc.1994.87*

ABOUT STUDENT AUTHORS

Samantha Rea and Brooke Hornberger will graduate from Stevenson University in December 2021, while Alexia Smith and Grace Fillmore will graduate in May 2022 also from Stevenson University.

PRESS SUMMARY

A widely used cancer chemotherapy drug called cisplatin has limited use due to its toxicity from the incorporated heavy metal platinum, and the resistance patients often develop to the drug, which results in cancer reoccurrence. Additionally, two configurations of the drug exist, one of which is ineffective and may reduce the efficiency of the cancer treatment. To mitigate

these challenges, three similar compounds were synthesized to serve as potential alternatives to cisplatin should an individual develop cisplatin resistance. Each of these structures either replaced the platinum within cisplatin using a less toxic metal called palladium, added a second structure called ethylenediamine to prevent formation of the ineffective version of cisplatin, or used a combination of both methods. Each of these compounds was tested against cisplatin for its ability to kill ovarian cancer cells. While two of the new compounds were ineffective, the third compound called dichloro-(ethylenediamine)-platinum(II) was able to kill the ovarian to a similar degree as cisplatin, suggesting that this new compound may provide an alternative treatment for cancer patients.

Novel Interactors of the SH2 Domain of the Signaling Adaptors CRK and CRKL Identified in Neuro2A Cells

*Caroline M. Dumas†, Anna M. Schmoker‡, Shannon R. Bennett‡, Amara S. Chittenden‡, Chelsea B. Darwin‡, Helena K. Gaffney‡, Hannah L. Lewis‡, Eliana Moskovitz‡, Jonah T. Rehak‡, Anna A. Renzi‡, Claire E. Rothfelder‡, Adam J. Slamin‡, Megan E. Tammaro‡, Leigh M. Sweet, & Bryan A. Ballif**

Department of Biology, University of Vermont, 109 Carrigan Drive, 120A Marsh Life Sciences, Burlington, VT 05405, USA

https://doi.org/10.33697/ajur.2022.068

Students: Caroline.Dumas@uvm.edu, Shannon.Bennett@uvm.edu, Amara.Chittenden@uvm.edu, Cheslea.Darwin@uvm.edu, Helena.Gaffney@vum.edu, Hannah.Lewis@uvm.edu, Eliana.Moskovitz@uvm.edu, Jonah.Rehak@uvm.edu, Anna.Renzi@uvm.edu, Claire.Rothfelder@uvm.edu, Adam.Slamin@uvm.edu, Megan.Tammaro@uvm.edu
*Mentor: bballif@uvm.edu**

† Co-first authors, equal contribution
‡Equal contribution

ABSTRACT
CT10 regulator of kinase (CRK) and CRK-like (CRKL) form a family of signaling adaptor proteins that serve important roles in the regulation of fundamental cellular processes, including cell motility and proliferation, in a variety of cell types. The Src Homology 2 (SH2) domain of CRK and CRKL interacts with proteins containing phosphorylated tyrosine-X-X-proline (pYXXP) motifs, facilitating complex formation during signaling events. A handful of CRK/CRKL-SH2-specific interactors have been identified to date, although *in silico* analyses suggest that many additional interactors remain to be found. To identify CRK/CRKL-SH2 interactors with potential involvement in neuronal development, we conducted a mass spectrometry-based proteomics screen using a neuronal cell line (Neuro2A, or N2A). This resulted in the identification of 132 (6 known and 126 novel) YXXP-containing CRK/CRKL-SH2 interactors, of which 77 were stimulated to bind to the CRK/CRKL-SH2 domain following tyrosine phosphatase inhibition. Approximately half of the proteins identified were common interactors of both the CRK- and CRKL-SH2 domains. However, both CRK family member SH2 domains exhibited unique binding partners across experimental replicates. These findings reveal an abundance of novel neuronal CRK/CRKL-SH2 domain binding partners and suggest that CRK family SH2 domains possess undescribed docking preferences beyond the canonical pYXXP motif.

KEYWORDS
CRK; CRKL; SH2; LC-MS/MS; Proteomics; Neurodevelopment; Signal Transduction

INTRODUCTION

CT10 regulator of kinase (CRK) and CRK-Like (CRKL) form a family of signaling adaptor proteins that are conserved throughout metazoans and pre-metazoans, playing essential roles in fundamental cellular processes such as proliferation and motility. CRK and CRKL come from two distinct genes that have been shown to play overlapping roles in some signaling pathways.[1] Interestingly, CRK and CRKL have also been shown to have unique roles *in vivo*, as knockout mice for CRK show differing phenotypes than knockout mice for CRKL.[2,3] Both CRK family members possess a Src homology 2 (SH2) domain, which binds phosphorylated tyrosine residues in YXXP motifs (Y=tyrosine, P=proline, X=any amino acid), and two SH3 domains, which bind proline-rich sequences. CRK is known to express as two different isoforms, both have an SH2 domain, but one with two SH3 domains and the other with only one SH3 domain. CRKL only has one isoform containing one SH2 domain and two SH3 domains.[5] Through these modular binding domains, CRK and CRKL facilitate the formation of cellular signaling complexes required for numerous signal transduction pathways.[1,4-7]

CRK and CRKL are particularly important for the proper positioning of cortical neurons during embryonic brain development via Reelin signaling.[4] Src family kinases are activated within a migrating neuron following the binding of Reelin to the Reelin receptors VLDLR and ApoER2. Activated src family kinases then phosphorylate tyrosine residues of receptor-bound Disabled-1 (DAB1) in YXXP motifs, which leads to the translocation of CRK/CRKL and their SH3-bound guanine nucleotide exchange factors complexes to membrane-localized small GTPases, which regulate cytoskeletal dynamics.[1,4,7]

In addition to DAB1, several known CRK/CRKL-SH2 interactors have been characterized, including members of the CRK-associated substrate (CAS) and discoidin, CUB, and LCCL domain-containing protein (DCBLD) families (**Supplementary Table 1**).[8-10] Further, in a recent *in silico* proteomics screen we predicted several CRK- and CRKL-SH2 binding partners, although many of these have yet to be shown to interact experimentally.[9] To identify new neuronal CRK/CRKL-SH2 interactors we made use of a murine neuroblastoma cell line, Neuro2A (or N2A). N2A cells were treated with or without tyrosine phosphatase inhibitors and extracts were incubated with either the CRK- or the CRKL SH2 domain. Bound proteins were ultimately identified using liquid chromatography–tandem mass spectrometry (LC-MS/MS).

METHODS.

Materials.

Penicillin/Streptomycin (100X) and Dulbecco's Modified Eagle Medium (DMEM) were acquired from Mediatech (Manassas, VA, USA). Fetal bovine serum (FBS) and cosmic calf serum (CCS) were obtained from Hyclone (Logan, Utah, USA). The bovine serum albumin (BSA) standard for Bradford assays and the Bradford Reagent were purchased from Amresco Life Sciences, LLC (Cleveland, OH, USA). Enhanced chemiluminescence (ECL) reagents used for Western blot development were purchased from Pierce (Rockford, IL, USA), and x-ray film was from Denville scientific (Metuchen, NJ, USA). Nitrocellulose membranes were from GVS Life Sciences (Sanford, ME, USA). All additional reagents were purchased from Sigma (St. Louis, MO, USA) unless otherwise noted.

Plasmids and antibodies.

The bacterial expression plasmid encoding the fusion of glutathione-S-transferase (GST) with the CRKL-SH2 domain (GST-CRKL-SH2) was a gift from A. Imamoto (U. of Chicago). The bacterial expression plasmid encoding GST-CRK-SH2 was acquired from Addgene (Cambridge, MA; plasmid #46418), and was originally constructed by Bruce Mayer (U. of Connecticut).

The α-tubulin (mouse) antibody (Cell Signaling Technology; Danvers, MA, USA) and α-phosphotyrosine (pY; mouse) antibody (EMD Millipore; Burlington, MA, USA) were diluted 1:1,000 in Tris-Buffered Saline (150 mM NaCl, 40 mM Tris, pH 7.5) containing 0.05% Tween 20 (TBS-T) with 1.5% BSA and 0.005% sodium azide for Western blotting. The secondary α-mouse-HRP antibody, diluted 1:10,000 in TBS-T for Western blotting, was obtained from Jackson Immunolabs (Westgrove, PA, USA).

Cell culture, stimulation, and cell lysis.

N2A cells were grown at 37 ˚C in 5% atmospheric CO_2 in DMEM with 5% FBS, 5% CCS, 50 U/mL penicillin, and 50 μg/mL streptomycin. Cells were either treated or not treated with 8.8 mM H_2O_2 for 15 minutes prior to lysis. Cells were placed on ice, washed with cold phosphate-buffered saline (PBS), then lysed in lysis buffer (25 mM Tris pH 7.2, 137 mM NaCl, 10% glycerol, 1% Igepal, 25 mM NaF, 10 mM $Na_2H_2P_2O_7$, 1mM Na_3VO_4, 1 mM phenylmethylsulfonyl fluoride (PMSF), and 10 mg/mL each leupeptin and pepstatin-A). Lysates were centrifuged at 4 ˚C, and the supernatant was reserved at -20˚ C for pulldown assays. A Bradford assay was used to normalize protein levels in the cell extract.

GST-CRKL-SH2 pull-down assay, Western blotting, and SDS-PAGE.

Purification of GST, and the GST-CRK-SH2 and GST-CRKL-SH2 fusion proteins on glutathione resin was previously described.[10] N2A whole cell extracts (WCEs) used in pulldown assays for LC-MS/MS analysis were pre-cleared on a column packed with GST-bound glutathione resin. N2A extracts (1 mg total protein for Western blotting, 2-3 mg for LC-MS/MS analysis) were incubated with GST-CRK-SH2 or GST-CRKL-SH2 resin for 1-2 days at 4 ˚C, rocking. The resin was then washed three times with lysis buffer. Bound proteins were eluted and denatured in sample buffer (150 mm Tris pH 6.8, 2% SDS, 5% β-mercaptoethanol, 7.8% glycerol, 0.01% bromophenol blue) at 95 ˚C for 5 min. Denatured pulldowns and WCEs (15 μg per lane) were separated on a 10% acrylamide gel (30% w/v and 37.5:1 acrylamide:bis-acrylamide) with 4.2% acrylamide stacking gels. The current was kept at 20 mA per gel through the stacking layers and 30 mA through the separating gels. Gels were either transferred to nitrocellulose membranes for Western blot analysis or stained with Coomassie Brilliant Blue in preparation for mass spectrometry.

For Western blotting, total protein levels on transfers were determined by staining membranes with a reversible Ponceau stain (0.5% Ponceau and 1% acetic acid in H_2O). Membranes were then blocked with TBS-T containing 5% w/v non-fat dry milk and incubated in primary antibodies overnight at 4 ˚C. Membranes were then washed with TBS-T three times (ten minutes each wash) and incubated overnight with the HRP-conjugated secondary antibody solution at 4 ˚C. After three final washes in TBS-T, blots were developed with ECL reagents and x-ray film.

Peptide preparation and analysis by LC-MS/MS.

Pulldowns for LC-MS/MS analysis were conducted in triplicate (complete biological replicates using separate cell cultures and conducted by separate personnel) each with GST-CRK-SH2 and GST-CRKL-SH2. Each lane of a given Coomassie-stained gel

was divided into four regions by molecular weight (**Figure 2A**), and then cut into 1-mm cubes. Gel pieces were de-stained in 50 mM ammonium bicarbonate and 50% acetonitrile at 37 ˚C, and dehydrated in 100% acetonitrile. Proteins were digested with trypsin in-gel at 37 ˚C for 18 hours. Tryptic peptides were extracted with 2.5% formic acid in 50% acetonitrile and further with 100% acetonitrile. Peptides were dried under vacuum centrifugation.

Peptides were re-suspended in Solvent A (2.5% acetonitrile, 2.5% formic acid) and separated via HPLC (300 nL/min) using the Easy n-LC 1200 prior to MS/MS analysis on the Q Exactive Plus mass spectrometer fitted with a Nanospray Flex ion source and supplied with Thermo Xcalibur 4.0 software (Thermo Fisher Scientific). Chromatography columns (15 cm x 100 μm) were packed in-house with 2.7 μm C18 packing material (Bruker, Halo, pore size = 90 Å). Peptides were eluted using a 0-50% gradient of Solvent B (80% acetonitrile, 0.15% formic acid) over 60 min and into the mass spectrometer by electrospray ionization. This gradient was followed by 10 min at 100% Solvent B before a 15-min equilibration in 100% Solvent A. The precursor scan (scan range = 360-1700 m/z, resolution = $7.0x10^4$, AGC = 10^6, maximum IT = 100 ms, lock mass=371.1012 m/z) was followed by ten collision-induced dissociation (CID) tandem mass spectra of the top ten ions in the precursor scan (resolution = 3.5×10^4, AGC = 5.0×10^4, maximum IT = 50 ms, isolation window = ±1.6 m/z, normalize collision energy = 26%, dynamic exclusion=30 s). Raw spectra were searched for matches within a forward and reverse mouse proteome (Uniprot, 2011) using SEQUEST,[11,12] requiring tryptic peptides and permitting the following differential modifications: phosphorylation of serine, threonine and tyrosine (+79.9663 Da), oxidation of methionine (+15.9949 Da), and acrylamidation of cysteine (+71.0371 Da). Peptides were filtered by mass accuracy (tolerance = ±4 ppm), cross correlation (XCorr) score (for z=+1, XCorr ≥ 1.8; z=+2, XCorr ≥ 2.0; z=+3, XCorr ≥ 2.2; z=+4, XCorr ≥ 2.4; z=+5, XCorr ≥ 2.6), and unique ΔCorr (≥ 0.15). Proteins were considered identified if 8 or more total spectra were mapped to peptides within that protein across the three replicates.

Bioinformatic analysis.
The number of YXXP motifs per protein in human and mouse sequences were obtained from Scansite (scansite4.mit.edu) as previously described.[9,13] The number of phosphorylated YXXP motifs in select proteins were obtained using a motif search in the Protein Search section of PhosphoSitePlus (phosphosite.org).[12] Clustal Omega was used to create multiple sequence alignments of select proteins across representative vertebrates.[15,16]

RESULTS AND DISCUSSION

CRK and CRKL are known to play important roles in several fundamental developmental processes; however, it is hypothesized that they serve additional roles in signaling pathways that have not yet been described. CRK and CRKL functional domains are highly conserved (**Figure 1A**, **Supplementary Figure 1**), although it remains possible that CRK and CRKL could possess distinct interacting partners, thereby carrying out divergent functions. SH2-mediated interactions between CRK/CRKL and phosphotyrosine residues are typically induced by specific signaling events involving the activation of receptor or non-receptor tyrosine kinases. One way to stimulate general tyrosine phosphorylation in cultured cells is the addition of hydrogen peroxide (H_2O_2) to cell culture medium, simultaneously inhibiting tyrosine phosphatases and activating tyrosine kinases through reactive oxygen species.[17] To identify neuronal SH2-specific binding partners of CRK and CRKL which are regulated by endogenous kinases and phosphatases we either stimulated with H_2O_2 or left untreated N2A cells. Extracts from these cultures were used to conduct a proteomics screen by incubating them with glutathione S-transferase (GST) fusions of the CRK- or CRKL-SH2 domains. Proteins that bound to GST-CRK-SH2 or GST-CRKL-SH2 were separated by SDS-PAGE and subjected to in-gel tryptic digestion. Peptides were subjected to LC-MS/MS leading to protein identification.

Figure 1B shows the successful generation of the fusion proteins via SDS-PAGE in IPTG-induced bacterial extracts and concentrated on glutathione resin. To verify that tyrosine phosphorylation could be induced in N2A cells by H_2O_2, N2A cells were either left untreated or were treated with 8.8 mM H_2O_2 for 15 minutes prior to lysis. N2A extracts were then subjected to SDS-PAGE and Western blotting with a phosphotyrosine antibody (α-pY). Indeed, cells that were treated with H_2O_2 showed a stronger signal in the α-pY blot compared to the untreated controls (**Figure 1C**). Tubulin levels (α-tubulin) served as a loading control. We then tested whether the GST-SH2 fusion constructs could extract proteins containing phosphotyrosine residues from N2A cells. Pulldown assays were conducted by incubating stimulated and unstimulated N2A extracts with GST-CRK-SH2 or GST-CRKL-SH2 resin prior to SDS-PAGE and immunoblotting (α-pY). Resin coated with GST alone was incubated with the same extracts as a control. H_2O_2-treated lanes demonstrate inducible binding of tyrosine phosphorylated proteins to CRK- and CRKL-SH2 fusion proteins, but not to GST (**Figure 1D**). Notably, several phosphotyrosine-containing proteins bound the CRK- and CRKL-SH2 domains in untreated N2A cells, suggesting that several YXXP-containing proteins were phosphorylated in N2A cells prior to H_2O_2 treatment.

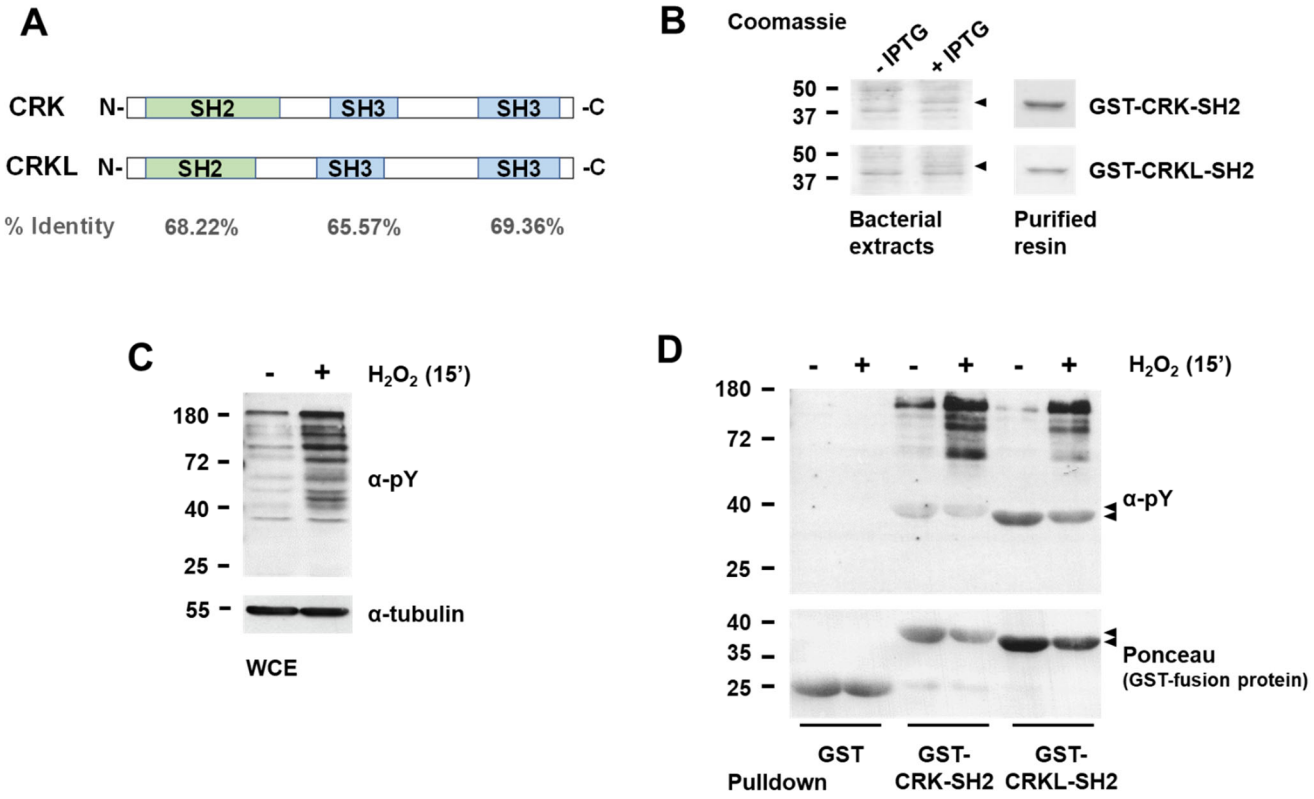

Figure 1. Generation and validation of GST-CRK-SH2 and GST-CRKL-SH2 for pulldown assays in N2A cells. A) Domains structure and conservation of CRK family members. A full alignment of amino acid sequences (ClustalOmega) can be found in **Supplementary Figure 1**. B) Bacterial lysate prior to and following IPTG induction of GST-fusion protein expression. Proteins were separated via SDS-PAGE and stained with Coomassie Brilliant Blue. GST-CRK/CRKL-SH2 expression is visible in the induced lysate (+ IPTG) at 40-45 kDa (indicated with arrows). After incubation with bacterial extracts, glutathione resin was subjected to SDS-PAGE and Coomassie staining, showing successful concentration of the purified GST-fusion protein on the resin. C) N2A cells were either left untreated or were treated with H_2O_2 (8.8 mM) for 15 min prior to lysis. Protein extracts were separated by SDS-PAGE and transferred to a nitrocellulose membrane for immunoblotting. The phosphotyrosine immunoblot (α-pY) shows an induction of tyrosine phosphorylation following H_2O_2 treatment. The α-tubulin blot serves as a loading control. D) Pulldown assays demonstrate functional SH2 domains. N2A extracts from (C) were incubated with GST-alone, GST-CRK-SH2 or GST-CRKL-SH2 prior to SDS-PAGE and Western blotting. The H_2O_2-treated extracts showed an increased phosphotyrosine signal relative to untreated extracts in GST-CRK/CRKL-SH2 pulldowns, while no phosphotyrosine signal was observed in the pulldowns with GST alone. The Ponceau stain shows GST-fusion protein levels around 40 kDa (SH2 fusions are indicated with arrows and background binding of α-pY is observed). GST alone runs at approximately 25 kDa.

To identify the CRK-/CRKL-SH2-interacting phosphoproteins observed in **Figure 1D**, GST-CRK-SH2 and GST-CRKL-SH2 pulldown assays were conducted to analyze via LC-MS/MS. For mass spectrometry assays, pulldowns were conducted as described above in triplicate. An example Coomassie-stained SDS-PAGE gel from one of the GST-CRK-SH2 replicates is shown in **Figure 2A**. Coomassie-stained gels were then cut into four regions by molecular weight (dashed lines in **Figure 2A**), subjected to an in-gel tryptic digest, and extracted peptides were analyzed by LC-MS/MS.

LC-MS/MS analysis of the GST-CRK-SH2 and GST-CRKL-SH2 pulldowns from unstimulated and stimulated N2A cell extracts yielded a total of 135 and 234 binding partners of CRKL-SH2 and CRK-SH2, respectively (**Supplementary Table 2**). Of these, 121 proteins were common interactors of CRK and CRKL, while each SH2 domain exhibited certain unique protein interactors in our study (**Figure 2B**). Spectral counts of proteins induced to bind the CRK- or CRKL-SH2 domain following H_2O_2 treatment (123 in total) are included in Supplementary **Table 3**. To date, no distinct interactor preferences between CRK family members have been described. However, further analysis will be required to determine whether the unique binding partners observed here truly are due to preferential differences between CRK family SH2 domains.

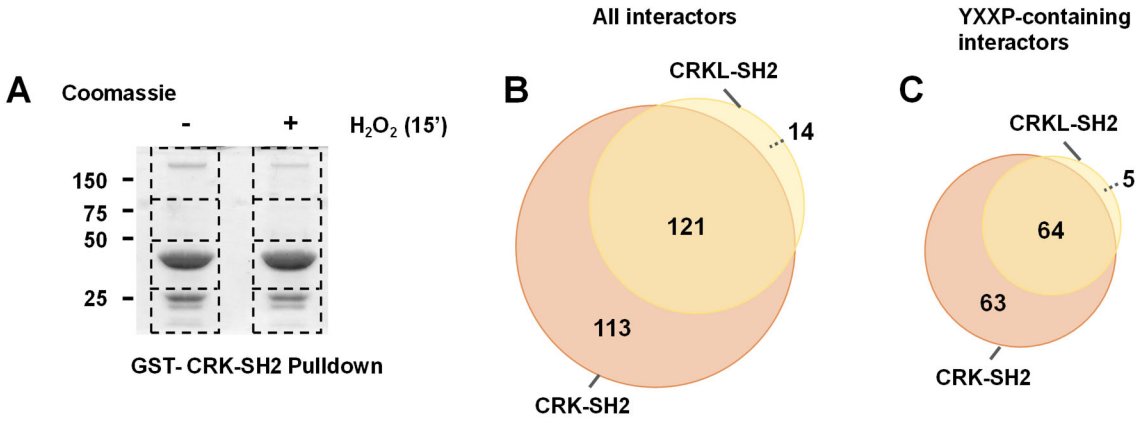

Figure 2. GST-CRK-/CRKL-SH2 pulldown assay for the identification of interactors via LC-MS/MS. A) The Coomassie-stained gel following a GST-CRK-SH2 pulldown from N2A extracts was divided into 4 regions of molecular weight. Each individual sample was subjected to an in-gel tryptic digest and analyzed via LC-MS/MS to identify bound proteins. N2A extracts were precleared with GST alone. RAW files were searched for tryptic matches in a 2011 Uniprot mouse proteome via SEQUEST. Proteins identified by eight or more peptides across three trials were considered SH2-specific interactors. Venn diagrams of all (B) and only YXXP-containing (C) CRK- and/or CRKL-SH2 interactors display the extent of overlapping binding partners identified in N2A cells. Full lists of interactors can be found in **Supplementary Tables 2–4**.

Of the 248 unique proteins identified to interact with the CRK- and/or CRKL-SH2 domain, 132 contain at least one YXXP motif (**Figure 2C**, **Supplementary Table 4**), 77 of which were induced to bind CRK-SH2, CRKL-SH2, or both CRK family members following H_2O_2 treatment (**Table 1**). Ten of the inducible YXXP-containing interactors found in **Table 1** are known to bind to CRK or CRKL (in bold, **Table 1**),[9] although only five of these have previously been shown to bind specifically to the CRK/CRKL-SH2 domain: DOK1, CBL, LASP1, PXN, and DCBLD2 (**Supplementary Table 1**). Importantly, additional known and novel YXXP-containing proteins were found to bind CRK- and/or CRKL-SH2, although they were not specific to the cells treated with H_2O_2 (**Supplementary Table 4**). For example, BCAR1 bound to the SH2 domains of both family members regardless of stimulation, suggesting that BCAR1 YXXP motifs may be highly phosphorylated in N2A cells.

Accession		Gene Symbol	CRK-SH2	CRKL-SH2	# YXXP motifs		# pYXXP IDs	Priority Score
H. sapiens	*M. musculus*				*H. sapiens*	*M. musculus*		*Schmoker, et al. (2018)*
Q99704	**P97465**	**Dok1****	**x**		**6**	**6**	**2886**	**11.5**
P49023	**Q8VI36**	**Pxn****	**x**		**3**	**3**	**2656**	**10.5**
P22681	**P22682**	**Cbl****	**x**		**3**	**3**	**761**	**10**
Q14847	**Q61792**	**Lasp1****	**x**	**x**	**3**	**3**	**517**	**9.5**
Q05397	**P34152**	**Ptk2***	**x**		**5**	**5**	**172**	**8**
Q96PD2	**Q91ZV3**	**Dcbld2****	**x**	**x**	**8**	**8**	**593**	**7.5**
O15357	**Q6P549**	**Inppl1***	**x**		**2**	**2**	**351**	**7**
P19174	Q62077	Plcg1	x		3	3	122	7
Q16555	O08553	Dpysl2	x		2	2	329	6.5
Q9UDY2	Q9Z0U1	Tjp2	x		2	3	943	6.5
Q07157	P39447	Tjp1	x		4	4	355	6.5
Q13813	P16546	Sptan1	x	x	5	5	35	6
O60716	P30999	Ctnnd1	x		3	2	1905	6
Q9UQC2	Q9Z1S8	Gab2	x		5	5	754	6
Q13835	P97350	Pkp1		x	3	3	456	6
Q13671	Q921Q7	Rin1	x		3	3	1074	4.5
P21333	**Q8BTM8**	**Flna***	**x**	**x**	**2**	**3**	**1**	**4**

O75369	**Q80X90**	**Flnb***	**x**	**x**	**4**	**4**	**60**	**4**
Q13191	**Q3TTA7**	**Cblb***	**x**		**3**	**3**	**239**	**4**
Q14203	O08788	Dctn1		x	1	1	0	3.5
P49327	P19096	Fasn	x	x	1	2	95	3.5
Q00610	Q68FD5	Cltc	x	x	5	5	18	3.5
P61160	P61161	Actr2		x	1	1	0	3
P61158	Q99JY9	Actr3		x	1	1	15	3
P52272	Q9D0E1	Hnrnpm		x	1	1	264	3
O43707	P57780	Actn4	x	x	1	1	0	3
P78371	P80314	Cct2	x	x	1	1	25	3
P48643	P80316	Cct5	x	x	1	1	1	3
Q99832	P80313	Cct7	x	x	1	1	0	3
P50990	P42932	Cct8	x	x	1	1	0	3
Q14195	Q62188	Dpysl3	x	x	1	1	3	3
P15924	E9Q557	Dsp	x	x	1	1	0	3
P46940	Q9JKF1	Iqgap1	x	x	1	1	0	3
P55884	Q8JZQ9	Eif3b	x	x	2	2	64	3
P12814	Q7TPR4	Actn1	x	x	3	3	5	3
P13639	P58252	Eef2	x	x	4	4	148	3
P23588	Q8BGD9	Eif4b	x		1	1	63	3
Q8TEW0	Q99NH2	Pard3	x		2	1	9	3
Q9Y490	P26039	Tln1	x		1	1	6	3
P67809	P62960	Ybx1	x		1	1	168	3
Q9Y285	Q8C0C7	Farsa	x		2	2	105	3
P48147	Q9QUR6	Prep	x		2	2	131	3
Q16832	Q62371	Ddr2	x		3	3	92	3
P55196	Q9QZQ1	Mllt4	x		3	4	21	3
P02545	P48678	Lmna		x	1	1	1	3
P61247	P97351	Rps3a		x	1	1	418	3
Q14204	Q9JHU4	Dync1h1		x	7	7	4	3
Q04637	Q6NZJ6	Eif4g1	x	x	2	2	19	0.5
P55072	Q01853	Vcp	x	x	3	3	10	0.5
P26640	Q9Z1Q9	Vars	x	x	5	5	24	0.5
Q14444	Q60865	Caprin1		x	1	1	0	0
P08243	Q61024	Asns	x	x	1	1	0	0
O95817	Q9JLV1	Bag3	x	x	1	1	11	0
Q14008	A2AGT5	Ckap5	x	x	1	1	0	0
P06733	P17182	Eno1	x	x	1	1	4	0
Q92598	Q61699	Hsph1	x	x	1	1	1	0
P11940	P29341	Pabpc1	x	x	1	1	22	0
P62701	P62702	Rps4x	x	x	1	1	0	0

Q8N5H7	Q9QZS8	Sh2d3c	x	x	1	1	1	0
Q13428	O08784	Tcof1	x	x	1	1	1	0
Q8WWM7	Q7TQH0	Atxn2l	x	x	2	2	52	0
P60842	P60843	Eif4a1	x	x	2	2	0	0
Q14240	P10630	Eif4a2	x	x	2	2	0	0
P35637	P56959	Fus	x	x	2	2	0	0
P26599	P17225	Ptbp1	x	x	2	2	1	0
P53396	Q91V92	Acly	x	x	3	3	2	0
A5YKK6	Q6ZQ08	Cnot1	x	x	6	6	8	0
P14868	Q922B2	Dars	x		1	1	1	0
P41250	Q9CZD3	Gars	x		1	1	0	0
P14625	P08113	Hsp90b1	x		1	1	1	0
O95347	Q8CG48	Smc2	x		1	1	0	0
P40939	Q8BMS1	Hadha	x		2	2	2	0
P34932	Q61316	Hspa4	x		2	2	0	0
Q9Y2A7	P28660	Nckap1	x		2	2	0	0
P54577	Q91WQ3	Yars	x		2	2	0	0
Q96F07	Q5SQX6	Cyfip2	x		3	3	0	0
Q9P2J5	Q8BMJ2	Lars	x		5	5	7	0
P62241	P62242	Rps8		x	1	1	18	0

Table 1. YXXP-containing proteins induced to bind CRK-/CRKL-SH2 in H_2O_2-stimulated N2A cells. The number of YXXP motifs (scansite4.mit.edu), the number of experimental identifications of phosphorylated tyrosine residues in YXXP motifs (phosphosite.org) and priority scores from Schmoker, *et al.* (2018) are included for each protein.[9] Known general CRK/CRKL interactors (*) and SH2-specific interactors (**) are indicated. Domain structures and multiple sequence alignments of select potentially novel SH2-specific interactors (underlined gene symbols) are included in **Supplementary Figure 2**. A full list of CRK-/CRKL-SH2 interactors is included in **Supplementary Table 4**.

Interactors in **Table 1** were cross-referenced with predicted CRK/CRKL-SH2 interactors.[7] Schmoker, *et al.* (2018) developed an *in silico* screen to predict and prioritize domain/motif interactions, using the CRK/CRKL-SH2/phospho-YXXP interaction as a model.[9] In that study, priority scores were calculated for each protein using signature characteristics of known interactors, including phospho-motif enrichment parameters, known interacting partners and participation in related signaling pathways.[9] Priority scores calculated by Schmoker, *et al.* (2018) are included for interactors in **Table 1**. Several high-priority novel CRK/CRKL-SH2 interactors were further investigated for their potential to interact with the CRK family of signaling adaptors. Select high-priority interactors involved in developmental processes, particularly those related to neuronal development and cell motility (underlined in **Table 1**), were assayed for conservation of their YXXP motifs across representative vertebrates. Domain structures and multiple sequence alignments of these novel CRK family SH2 interactors are included in (**Supplementary Figure 2**).

Several peptides containing phosphorylated tyrosine residues in YXXP motifs were identified in the pulldown assays. Fragmentation spectra of phosphopeptides were manually validated to confirm localization of the phosphate group on the YXXP tyrosine (**Supplementary Figure 3**). Several of the phosphorylated YXXP-containing peptides were from the known CRK-/CRKL-SH2 interactors BCAR1, DOK1, DCBLD2, and PXN (**Supplementary Table 5**). Phospho-YXXP-containing peptides of eight of the 16 BCAR1 YXXP motifs were identified in both stimulated and unstimulated N2A extracts. It is likely that additional proteins that remain highly phosphorylated in N2A cells, basally, could interact with CRK/CRKL-SH2 in this cell type regardless of H_2O_2 stimulation. Therefore, the list of interactors included in **Table 1** is likely not a complete list of potential phospho-YXXP-dependent CRK-/CRKL-SH2 interactors identified in this study. In addition to these known binding partners, CRMP1 was the only novel phospho-YXXP-containing protein found in complex with CRK- or CRKL-SH2 (**Supplementary Table 5**, **Supplementary Figure 3**). Interestingly, CRMP1 bound to CRK-SH2 regardless of stimulation (**Supplementary Table 4**). Even so, the identification of these phospho-YXXP-containing peptides lends strong evidence toward the interaction of the proteins containing these peptides with CRK/CRKL-SH2 through the identified phospho-YXXP sites (**Supplementary Table 5**).

CONCLUSIONS

In this study, we aimed to identify novel CRK/CRKL-SH2 binding partners that could play important roles in neurodevelopment. A proteomics screen produced 77 inducible CRK/CRKL-SH2 interactors in a neuronal cell line (N2A), with potential to interact specifically via their YXXP motifs (**Table 1**). Given the high conservation of the CRK family SH2 domains (**Figure 1A**, **Supplementary Figure 1**), and the absence of any known unique sequence preferences among these domains, we expected that many of the CRK/CRKL-SH2 interactors identified would overlap. However, we found that although approximately half of the interactors identified were common to CRK-SH2 and CRKL-SH2, each family member possessed a number of unique interactors in N2A cells (**Figure 2B,C**). Although the list of unique CRKL-SH2 interactors was smaller than that of CRK-SH2, this is likely a reflection of the fewer total number of CRKL-SH2 interactors identified (**Supplementary Table 2**). Indeed, a weaker induction of GST-CRKL-SH2 expression prior to purification on glutathione resin (**Figure 1B**) resulted in a lower concentration of fusion protein for use in pulldown assays, relative to GST-CRK-SH2. Despite this, five unique YXXP-containing proteins were identified as unique interactors of CRKL-SH2 (**Figure 2C**), namely, DYNC1H1, PKP1, LMNA, RPS3A, and RPS8. CRK and CRKL are known to play similar roles in developmental processes, however, certain distinctions have been made between CRK family members.[6] Although further studies will be necessary to determine whether the distinct CRK-SH2 and CRKL-SH2 interactors identified here truly are unique to each family member, our findings suggest that certain sequence preferences may exist for CRK family SH2 domains. In addition, several predicted CRK/CRKL-SH2 interactors from our previous *in silico* screen[9] were experimentally validated in this study, providing novel avenues of research regarding CRK family signaling in neuronal development.

ACKNOWLEDGEMENTS

Funding for this project came from the following sources: UVM College of Arts and Sciences and Biology Department; U.S. National Science Foundation IOS grant 1656510; the Vermont Genetics Network through U.S. National Institutes of Health grant 8P20GM103449 from the INBRE program of the NIGMS. The GST-CRK-SH2 and GST-CRKL-SH2 plasmid were kind gifts from Bruce Mayer (U. of Connecticut) and Akira Imamoto (U. of Chicago), respectively.

REFERENCES

1. Park, T.-J. and Curran, T. (2008) Crk and Crk-like play essential overlapping roles downstream of disabled-1 in the Reelin pathway. *Journal of Neuroscience.* 28, 13551-13562. *https://doi.org/10.1523/JNEUROSCI.4323-08.2008*
2. Guris, D. L., Fantes, J., Tara, D., Druker, B. J., & Imamoto, A. (2001). Mice lacking the homologue of the human 22q11.2 gene CRKL phenocopy neurocristopathies of DiGeorge syndrome. *Nat Genet, 27*(3), 293-298. doi:10.1038/85855
3. Park, T. J., Boyd, K., & Curran, T. (2006). Cardiovascular and craniofacial defects in Crk-null mice. *Mol Cell Biol, 26*(16), 6272-6282. doi:10.1128/mcb.00472-06
4. Ballif, B. A., Arnaud, L., Arthur, W. T., Guris, D., Imamoto, A. and Cooper, J. A. (2004) Activation of a Dab1/CrkL/C3G/Rap1 pathway in Reelin-stimulated neurons. *Current biology.* 14, 606-610. *https://doi.org/10.1016/j.cub.2004.03.038*
5. Feller, S. M. (2001) Crk family adaptors–signaling complex formation and biological roles. *Oncogene.* 20, 6348. *https://doi.org/10.1038/sj.onc.1204779*
6. Kobashigawa, Y. and Inagaki, F. (2012) "Structural biology: CrkL is not Crk-like." *Nature chemical biology.* 8, 504. *https://doi.org/10.1155/2014/372901*
7. Ballif, B. A., Arnaud, L. and Cooper, J. A. (2003) Tyrosine phosphorylation of Disabled-1 is essential for Reelin-stimulated activation of Akt and Src family kinases. *Molecular brain research.* 117, 152-159. *https://doi.org/10.1016/S0169-328X(03)00295-X*
8. Aten, T. M., Redmond, M. M., Weaver, S. O., Love, C. C., Joy, R. M., Lapp, A. S., Rivera, O. D., Hinkle, K. L. and Ballif, B. A. (2013) Tyrosine phosphorylation of the orphan receptor ESDN/DCBLD2 serves as a scaffold for the signaling adaptor CrkL. *FEBS letters.* 587, 2313-2318. *https://doi.org/10.1016/j.febslet.2013.05.064*
9. Schmoker, A. M., Driscoll, H. E., Geiger, S. R., Vincent, J. J., Ebert, A. M. and Ballif, B. A. (2018) An *in silico* proteomics screen to predict and prioritize protein-protein interactions dependent on post-translationally modified motifs. *Bioinformatics.* 1, 9. *https://doi.org/10.1093/bioinformatics/bty434*
10. Schmoker, A. M., Weinert, J. L., Kellett, K. J., Johnson, H. E., Joy, R. M., Weir, M. E., Ebert, A. M. and Ballif, B. A. (2017) Dynamic multi-site phosphorylation by Fyn and Abl drives the interaction between CRKL and the novel scaffolding receptors DCBLD1 and DCBLD2. *Biochemical Journal.* 474, 3963-3984. *https://doi.org/10.1042/BCJ20170615*
11. Apweiler, R., Bairoch, A., Wu, C. H., Barker, W. C., Boeckmann, B., Ferro, S., Gasteiger, E., Huang, H., Lopez, R. and Magrane, M. (2004) UniProt: the universal protein knowledgebase. *Nucleic acids research.* 32, D115-D119. *https://doi.org/10.1093/nar/gkh131*
12. Eng, J. K., McCormack, A. L. and Yates, J. R. (1994) An approach to correlate tandem mass spectral data of peptides with amino acid sequences in a protein database. *J Am Soc Mass Spectrom.* 5, 976-989. *https://doi.org/10.1016/1044-0305(94)80016-2*
13. Obenauer, J. C., Cantley, L. C. and Yaffe, M. B. (2003) Scansite 2.0: Proteome-wide prediction of cell signaling interactions using short sequence motifs. *Nucleic Acids Res.* 31, 3635-3641. *https://doi.org/10.1093/nar/gkg584*

14. Hornbeck, P. V., Zhang, B., Murray, B., Kornhauser, J. M., Latham, V. and Skrzypek, E. (2015) PhosphoSitePlus, 2014: mutations, PTMs and recalibrations. *Nucleic Acids Res.* 43, D512-520. *https://doi.org/10.1093/nar/gku1267*

15. Larkin, M. A., Blackshields, G., Brown, N., Chenna, R., McGettigan, P. A., McWilliam, H., Valentin, F., Wallace, I. M., Wilm, A. and Lopez, R. (2007) Clustal W and Clustal X version 2.0. *Bioinformatics.* 23, 2947-2948. *https://doi.org/10.1093/bioinformatics/btm404*

16. Sievers, F., Wilm, A., Dineen, D., Gibson, T. J., Karplus, K., Li, W., Lopez, R., McWilliam, H., Remmert, M. and Söding, J. (2011) Fast, scalable generation of high-quality protein multiple sequence alignments using Clustal Omega. *Molecular systems biology.* 7, 539. *https://doi.org/10.1038/msb.2011.75*

17. Zick, Y. and Sagi-Eisenberg, R. (1990) A combination of hydrogen peroxide and vanadate concomitantly stimulates protein tyrosine phosphorylation and polyphosphoinositide breakdown in different cell lines. *Biochemistry.* 29, 10240-10245. *https://doi.org/10.1021/bi00496a013*

ABOUT THE STUDENT AUTHORS

This work was conducted as part of a course-based undergraduate research experience (CURE) laboratory course at the University of Vermont (UVM) in the spring semester of 2019. The students in this course have since graduated from UVM with the following degrees: Caroline Dumas, B.S. in Neuroscience; Shannon Bennett, B.A. in Biology; Amara Chittenden, B.S. in Biological Sciences; Chelsea Darwin, B.S. in Biological Sciences; Helena Gaffney, B.A. in Biology; Hannah Lewis, B.S. in Biological Sciences; Eliana Moskovitz, B.S. in Biochemistry; Jonah Rehak, B.S. in Biological Sciences; Anna Renzi, B.A. in Anthropology and B.A. in Biology; Claire Rothfelder, B.A. in Biology; Adam Slamin, B.S. in Biological Sciences; Megan Tammaro, B.S. in Biological Sciences.

PRESS SUMMARY

The CRK family of adaptor proteins, composed of CRK and CRKL, play important roles in embryonic brain development. These adaptors facilitate protein-protein interactions by transporting signaling effectors to phosphorylated tyrosine residues near the cell membrane, forming protein complexes required for cell proliferation and migration. This work aimed to identify novel protein interactors of the phosphotyrosine binding domain of CRK family members in a neuronal cell line using mass spectrometry-based proteomics. The screen identified 6 known and 126 novel interactors of the CRK/CRKL phosphotyrosine binding domain, 77 of which were induced to bind in conditions with increased tyrosine phosphorylation. Although approximately half of these interactors were common between family members, several unique CRK or CRKL binding partners were confirmed across experimental replicates. These findings reveal an abundance of novel neuronal CRK/CRKL interactions that could be essential to neuronal development.

Print Edition ISSN 1536-4585
Online Edition ISSN 2375-8732